Controlling Critical Quality Attributes of Therapeutic
Nanoparticles Upon Scale-up Manufacturing

Von der Medizinischen Fakultät
der Rheinisch-Westfälischen Technischen Hochschule Aachen
zur Erlangung des akademischen Grades
einer Doktorin der Theoretischen Medizin
genehmigte Dissertation

vorgelegt von
Maryam Sheybanifard

aus
Kazeroon (Iran)

Berichter: Dr. Josbert M. Metselaar, Ph.D.
Univ.-Prof. Dr. Ing. Laura De Laporte

Tag der mündlichen Prüfung: 28.04.2023

To my dearest family,

for their love, support, and inspiration

Parts of this dissertation have been published in:

Sheybanifard, M*., Beztsinna, N*., Bagheri, M., Buhl, E.M., Bresseleers, J., Varela-Moreira, A., Shi, Y., van Nostrum C.F., van der Pluijm, G., Storm, G., Hennink, W.E., Lammers, T., & Metselaar J.M. Systematic evaluation of design features enables efficient selection of Π electron-stabilized polymeric micelles. *International journal of pharmaceutics.* 2020 Jun 30;584:119409. (*These authors contributed equally).

Sheybanifard, M, Guerzoni L.P.B., Omidinia-Anarkoli, A., De Laporte, L., Buyel, J.F., Besseling, R., Damen, M., Gerich, A., Lammers, T., & Metselaar J.M. Liposome manufacturing under continuous flow conditions: towards a fully integrated set-up with in-line control of critical quality attributes. *Lab on a Chip.* 2023;23(1):182-94.

Contents

List of abbreviations

ATCC	American Type Culture Collection
a.u.	Arbitrary unit
ABCPA	4,4'-Azobis (4-cyanopentanoic acid)
Abs.	Absorbance
ACN	Acetonitrile
ATRP	Atom transfer radical polymerization
BSA	Bovine serum albumin
CC	ChemConnection (a contracted service provider)
cm^2	Square centimeters
CMC	Critical micelle concentration
CPP	Critical packing parameter
CV7000S	Cell Voyager 7000S
DDS	Drug delivery systems
DLS	Dynamic light scattering
DMF	N,N-Dimethylformamide
DMSO	Dimethyl sulfoxide
DMSO-d6	Deuterated dimethyl sulfoxide
DPPC	1,2-dipalmitoyl-sn-glycero-3-phosphocholine
DSPE-PEG 2000	1,2-distearoyl-sn-glycero-3-phosphoethanolamine-polyethylene glycol-2000
EDTA	Ethylenediaminetetraacetic acid
EE	Encapsulation efficiency
EPC	Egg phosphatidylcholine
EPR	Enhanced permeability and retention
FRP	Free radical polymerization
GPC	Gel permeation chromatography
HBS	HEPES buffered saline
HepG2	Human hepatocellular carcinoma cells
HFF	Hydrodynamic flow focusing

HPLC	High performance liquid chromatography
HPMA	N-(2-Hydroxypropyl) methacrylamide
HPMA-Bz	N-(2-Benzoyloxypropyl) methacrylamide
kDa	Kilodalton
LC	Loading capacity
LiCl	Lithium chloride
MeOH	Methanol
mg	Milligram
MHz	Megahertz
mL	Milliliter
Mn	Number average molecular weight
mPEG	Methoxy polyethylene glycol
mV	Millivolt
Mw	Weight average molecular weight
MWCO	Molecular weight cut-off
1H NMR	Proton nuclear magnetic resonance
NFS	NanoFlowSizer
NIR	Near-infrared spectroscopy
NP	Nanoparticles
NTA	Nanoparticle tracking analysis
O/W	Oil in water
PBS	Phosphate buffered saline
PC3	Human prostate cancer cells
PDI	Polydispersity index
PEG	Polyethylene glycol
pH	Potential of hydrogen ions
PM	Polymeric micelles
ppm	Parts per million
PTX	Paclitaxel
RAFT	Reversible addition-fragmentation chain-transfer

RI	Refractive index
RP	Radical polymerization
rpm	Revolutions per minute
RT	Room temperature
TEM	Transmission electron microscopy
TFA	Trifluoroacetic acid
TFF	Tangential flow filtration
TFH	Thin film hydration
THF	Tetrahydrofuran
UPLC	Ultra-performance liquid chromatography
UV-vis	Ultraviolet-visible
Z-ave	Average hydrodynamic diameter
µL	Microliter
µM	Micromolar

1. Introduction

1.1. History of cancer chemotherapeutics

Cancer is recognized as one of the most challenging public health problems worldwide, causing about 10 million deaths in 2020 (Sung et al., 2021). Despite significant advances regarding our understanding of its etiology and the way to treat it, this disease keeps deteriorating the quality of life of many patients and entails numerous physical and psychological impairments (Cleeland et al., 2003), which calls for concerted effort to find new effective therapeutic solutions. So far, the four approaches to treat the disease have been surgery, radiotherapy, immunotherapy, and chemotherapy.

Eight decades ago, the field of cancer chemotherapy emerged with the introduction and approval of nitrogen mustard as the first cancer chemotherapeutic agent. Despite its remarkable outcomes in tumor regression, an utter remedy was not achieved (DeVita and Chu, 2008). The next milestone in cancer chemotherapeutics was achieved in the 1950s with the introduction of methotrexate. Methotrexate became the first chemotherapeutic agent that could result in cancer remission (Li et al., 1958).

Since then, more than 200 different cancer chemotherapeutics have been introduced and used for the treatment of different types of cancer (NCI). Nevertheless, the challenging battle of finding an ultimate treatment to completely eradicate various types of cancer using chemotherapy has remained unresolved. The main reason is that the use of chemotherapeutic agents is limited and inefficient due to several intrinsic and extrinsic barriers. Such barriers arise from the physicochemical properties of the chemotherapeutics (such as poor water-solubility, suboptimal partition coefficient and protein binding, etc.), pharmacokinetics-related factors (poor bioavailability, insufficient target site accumulation, etc.) and pharmacodynamics-related factors (toxicity, narrow therapeutic index, etc.). Altogether, the existence of such barriers results in suboptimal biodistribution, dosing difficulties, adverse effects and suboptimal efficacy. Therefore, there is an increasing demand for improving and maximizing the anticancer effects of the chemotherapeutic agents.

1.2. Drug Delivery Systems: liposomes and micelles

To improve shortcomings related to cancer chemotherapeutics efficacy, various drug delivery systems (DDS) have been designed and evaluated. DDS refer to devices or formulations that are designed to enhance the therapeutic efficacy of the drugs by improving and controlling their bioavailability, release and ultimately their disposition into target tissues (Jain, 2008). Among different types of DDS, nanoparticles (NP) have considerably attracted scientists' attention, owing to a number of technical features and *in vivo* performance characteristics that can improve drug delivery. Two examples are the better accumulation at the target site through enhanced permeability and retention effect (EPR) seen in some forms of cancer as well as the aptitude for surface modifications.

To date, almost 30 different NP have been clinically approved by FDA and/or EMA, among which, 9 NP belong to cancer treatment (Anselmo and Mitragotri, 2021) (Figure 1). Overseeing all NP in the clinic or in clinical trials, it is evident that two nanoparticulate formulations are frontrunners and have particularly been investigated, namely liposomes and (polymeric) micelles (Anselmo and Mitragotri, 2019).

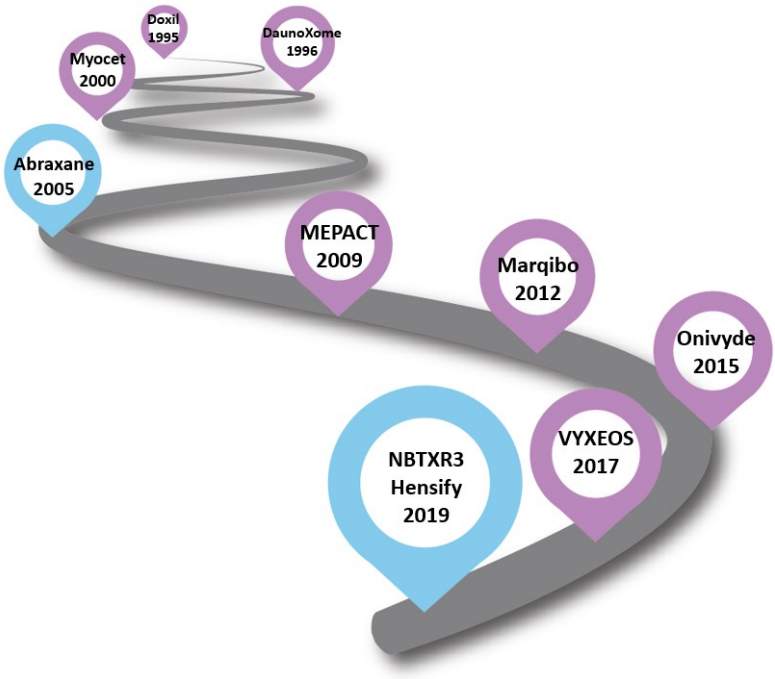

Figure 1. Cancer chemotherapeutic NP that have received the FDA and/or EMA approval. The purple navigation signs represent liposomal formulations and the blue signs represent non-liposomal NP.

Both liposomes and micelles are self-assembled spherical vesicles that are composed of amphiphilic units, with a hydrophilic head and one or more hydrophobic tails (Figure 2). In the process of self-assembly, the key parameter that determines the initiation of colloidal particle formation is known as critical micelle concentration (CMC). CMC refers to the concentration above which the amphiphilic molecules form a colloidal aggregate (Shi et al., 2011). Lowering the concentrations below the CMC results in disassembly of the particles and tilts the balance between the formed colloidal particles and the corresponding monomers towards the latter.

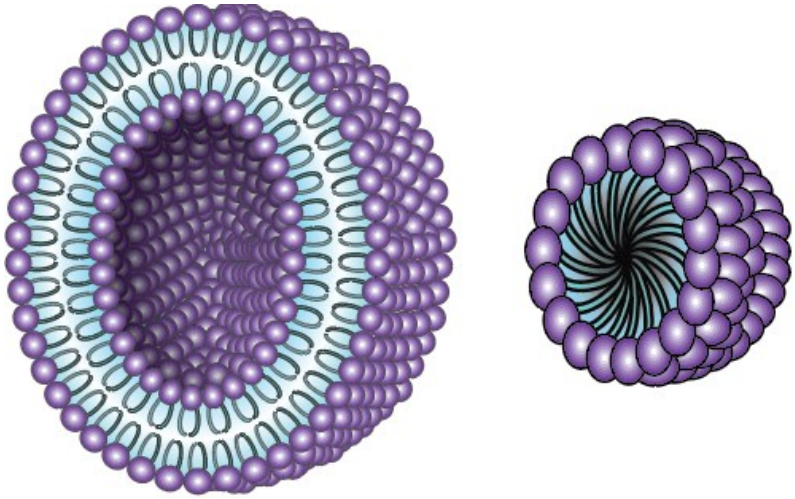

Figure 2. Schematic drawing of a liposome (left) and a polymeric micelle (right). The cross-sectional view is presented for each nanoparticulate system.

Once the concentration of the amphiphilic molecules exceeds the CMC, the particles are formed in a number of different geometries. The main determinant factor that drives the final geometry of the self-assembly is called critical packing parameter (CPP). CPP is a dimensionless parameter that is defined using a formula (Equation 1). In general, the CPP is directly proportional to the volume of hydrocarbon chain and inversely related to the surface cross area of the hydrophilic head and the length of the hydrocarbon chain (Israelachvili et al., 1980). Besides the nature of the amphiphilic molecules, CPP is also dependent on medium conditions including temperature, ionic force, pH, etc. (Bryant et al., 2019).

Analyzing the correlation between the CPP and the geometry of the particles has shown that a CPP of lower than 0.3 results in formation of conical structure of the monomeric units, which eventually results in spherical micelles (Israelachvili et al., 1980; Israelachvili et al., 1976; Lichtenberg et al., 2013). On the other hand, most amphiphilic units that are the building blocks of the liposomes (i.e., phospholipids) have a CPP of between 0.5 to 1. Such CPP values would lead the phospholipids to form a cylindrical shape and eventually, bilayer formation of liposomes.

$$CPP=V\,(SL)^{-1}$$

Equation 1. CPP calculation formula. V represents the volume of hydrocarbon chain; S represents the surface cross area of the hydrophilic head and L represents the length of the hydrocarbon chain.

Altogether, understanding the similarities and the differences between the micellar and liposomal formulations would shed more light into the path of selecting an effective formulation towards cancer treatment.

1.2.1. Polymeric micelles (PM)

After the introduction of PM as a potential drug delivery system in 1980s (Bader et al., 1984; Pratten et al., 1985), they have been extensively used in the delivery of various drugs of interest (Hamaguchi et al., 2005; Kim et al., 2004; Talelli et al., 2010; Yoo and Park, 2001). PM are formed as a result of self-assembly of amphiphilic block copolymers once the concentration of the polymer in aqueous environment exceeds the CMC. Mainly, PM allow for encapsulation of hydrophobic drugs owing to the hydrophobic nature of their inner core. On the other hand, the hydrophilic blocks of the block copolymer congregate on the surface to form the outer shell, thereby improving PM stability in aqueous media (Nasongkla et al., 2006; Shiraishi and Yokoyama, 2013; Soga et al., 2005; Yokoyama, 2014). The main advantages of PM are solubility enhancement and surface modification. The latter can ameliorate blood circulation time, which consequently improves tumor targeting (Deng et al., 2012) through the enhanced permeability and retention (EPR) effect and/or through selective target cell interaction using target-selective ligands (e.g., antibodies, sugar moieties, folate residues, etc.)(Fang et al., 2011; Gothwal et al., 2016; Lu and Park, 2013; Torchilin, 2006).

Several techniques of PM preparation have been employed to effectively encapsulate the drugs of interest. The most commonly used methods for PM preparation include nanoprecipitation (Fessi et al., 1989; Gagliardi et al., 2021), oil in water (O/W) emulsion followed by solvent evaporation (Bodmeier and Huagang, 1990), and the dialysis method (Scholz et al., 1995; Yu and Eisenberg, 1996). Selection of a particular method is determined by the features of the polymer and the cargo, as well as the desired physicochemical properties of the prepared PM (Rao and Geckeler, 2011).

Nanoprecipitation is a single-step technique in which the polymer and the cargo, which in most cases is a hydrophobic drug, are initially dissolved in an organic solvent and then emulsified in an aqueous medium. Upon addition of the polymer/cargo mixture to the aqueous phase, the organic solvent will diffuse into the dispersion media. This causes the polymer concentration to increase above the CMC, which eventually results in the rapid formation of the self-assemblies and entrapping the cargo inside its hydrophobic core (Fessi et al., 1989; Gagliardi et al., 2021; Martínez Rivas et al., 2017). The main advantages of this method are the simplicity of the process and the absence of any extra surfactants in the final product (Almoustafa et al., 2017).

O/W emulsion solvent evaporation is another widely used method of PM preparation, which is based on dissolving the polymer in an organic solvent followed by dispersion in the stabilizer-rich aqueous phase. Emulsification is performed through high-speed homogenization or sonication and at the last step, the organic solvent is removed via evaporation (Gagliardi et al., 2021). In contrast to nanoprecipitation method, the O/W emulsion solvent evaporation technique demands the presence of a surfactant, which is responsible for NP associated toxicity. Moreover, the PM formation is dependent on emulsification methods, which could complicate the preparation process.

Another method of PM preparation is based on dialysis. In this method, the polymer and the drug are dissolved in an organic solvent, placed in a dialysis compartment, and dialyzed against an aqueous phase. The organic solvent inside the dialysis compartment slowly diffuses out of the membrane and is replaced by water. Once the water content inside the membrane is sufficiently high, the polymer spontaneously self assembles to form PM with

the hydrophobic tails converging towards the center and the hydrophilic head affixing outwards (Kesharwani et al., 2019).

1.2.2. Liposomes

Besides PM, liposomal drug formulations are the other widely used and efficient drug delivery system. Despite numerous preclinical studies that are performed on liposomal drug products, only 30 liposomal formulations are currently evaluated in clinical trials (Anselmo and Mitragotri, 2021). Exclusively in the field of cancer therapy, out of 9 FDA and/or EMA approved nanoparticle formulations that has entered the market, 7 are liposomes (Anselmo and Mitragotri, 2021) (Figure 1). Liposomes have gained huge popularity in the field of drug delivery owing to their biocompatibility, biodegradability, relatively simple manufacturing and their unique competence in encapsulating and delivering both hydrophobic and hydrophilic therapeutic agents (Deshpande et al., 2013). To characterize a liposomal formulation, several parameters should be assessed including particle size, polydispersity index, zeta potential, drug encapsulation efficiency, drug to lipid ratio, *in vitro* release, shelf-life stability, etc. These liposome critical quality attributes are heavily dependent on multiple factors including the lipid type, the lipid concentration as well as the preparation method (Akbarzadeh et al., 2013).

To date, several methods have been designed and refined to manufacture liposomes including but not limited to thin film hydration (TFH), solvent dispersion, detergent-depletion, and microfluidic-based methods (Akbarzadeh et al., 2013; Bozzuto and Molinari, 2015). Understanding the process of liposome formation enables a more rational selection of the technique and increases the chance of a successful translation to the manufacturing of clinical batches as well as industrial-scale production.

Thin film hydration (TFH) was a revolutionizing method at the time that was exploited to make the very first liposomal formulation in 1965 (Bangham and Horne, 1964). During the first TFH attempts, lipids were initially dissolved in chloroform, followed by chloroform evaporation under vacuum condition. After formation of the thin lipid film, it was hydrated with an aqueous phase through gentle shaking or sonication, which led to bilayer structure and vesicle formation (Bangham and Horne, 1964). Almost 60 years later, the method is still

intact with the addition of extrusion at the end of the process as the main modifications to obtain small uniform vesicles. The two main drawbacks of this method are the need for post-formation modification processes to obtain monodisperse liposomes as well as the limited capacity to scale up (Wagner and Vorauer-Uhl, 2011).

Soon after the presentation of liposomes using TFH method, another technique of liposome preparation emerged, i.e., the solvent injection method (Batzri and Korn, 1973). Using this technique, lipids are dissolved in an organic solvent (mostly ethanol) and are injected into a large volume of the aqueous phase. The rapid change of the ethanolic environment into water forces the lipids to self-assemble into liposomal vesicles (Akbarzadeh et al., 2013; Bozzuto and Molinari, 2015; Patil and Jadhav, 2014; Wagner and Vorauer-Uhl, 2011). This method is a more simplified technique compared to the TFH method and it eliminates the need for the post modification steps. Nevertheless, the solvent injection method results in a diluted liposome dispersion, which in turn leads to a low concentration of the liposomes and importantly, in a lower drug entrapment efficiency (Akbarzadeh et al., 2013).

The microfluidic manufacturing technique is another method of liposome preparation. This technique employs a mixing device in which lipids are initially dissolved in an organic solvent and under a controlled flow rate, dispersed in the aqueous phase and form self-assemblies. Owing to the unique advantages of this method such as decent reproducibility, straightforward scale up, enhanced control on the key characteristics of the liposomes, and reduced post modification steps, microfluidics is gaining huge popularity (Valencia et al., 2012). Nevertheless, the industrial transition from conventional methods of liposome preparation to microfluidic approaches is expensive and laborious. Moreover, as the name implies, the devices that are employed to produce liposome dispersion (among other NP) are designed in micrometer size (Valencia et al., 2012), which further limits the scale-up possibilities. The latter issue could be addressed by rational design of devices towards millifluidic approaches.

All the above-mentioned techniques are well adapted to small-scale production of liposomal drug products. Therefore, the translation of small-scale to industrial-scale

production of liposomes requires a meticulously designed production setup to overcome challenges that are associated with such a translation.

1.3. Manufacturing of pharmaceutical products: Batch preparation vs. continuous manufacturing

1.3.1. Large-scale production of raw materials: polymeric micelles as an example

Large-scale manufacturing of therapeutic nanoparticles in the pharmaceutical industry must be approached at two levels, one is the industrial-scale production of the raw materials, and the other is the industrial-scale production of the nanoparticles. Regarding the former, we have explored PM as an example. Obtaining the desired raw materials in the desired quantity and quality is the prerequisite for micellar formulation preparation. Therefore, selecting the proper polymer type and polymerization protocol plays a significant role in the quality of the final formulation.

Radical polymerization (RP) is recognized as one of the most popular methods in synthesizing amphiphilic block copolymers for drug delivery purposes. This method is well suited for laboratory-scale production (Moad and Solomon, 2006), owing to its low-cost process as well as its adaptability to different monomers (Hong et al., 2002). Currently, various strategies are employed within the scope of RP to obtain polymers for therapeutic purposes, including atom transfer radical polymerization (ATRP) (Lin et al., 2016), reversible addition fragmentation chain-transfer polymerization (RAFT) (Zhang et al., 2008), and uncontrolled free radical polymerization (FRP) (Soga et al., 2004).

The fundamental requirement for applying any of the RP methods in polymer synthesis is the presence of free radicals in the polymer, which react with monomers in a chain reaction (Greszta et al., 1994). However, monitoring the purity and the reproducibility of the synthesized polymer is more feasible at small scales due to a well-controlled synthesis process that can be achieved in laboratory scale. Nevertheless, large-scale production is always more appealing since it obviates the need for synthesizing multiple batches and thus, reduces the batch-to-batch variation.

Despite the promising results obtained in the laboratory scales, the polymer synthesis transition to industrial scale can be problematic. Main complications that can be encountered are the increased viscosity through preparation and difficulties in heat and mass transfer, which can potentially result in suboptimal quality of the final polymer product (Ilare and Sponchioni, 2020). Such complications appear in different stages of the synthesis, including the monomer synthesis, the macroinitiator synthesis or the final polymerization. Therefore, different impurities (such as undesired homopolymer or unreacted materials) could possibly emerge in the final polymer product and subsequently, disturb the formation of the corresponding PM. A feasible solution to overcome large-scale production problems is changing to continuous synthesis of the polymer. Besides enhancing the quality of the final polymer at industrial scales, continuous synthesis improves the safety, simplifies the synthesis and is more time efficient (Reis et al., 2020).

1.3.2. Large-scale production of nanoparticles: liposomes as a model nanoparticulate system

To explore the large-scale production of raw materials in drug delivery field, polymeric micelles and specifically, polymers as the building blocks were discussed as an example in the previous section. Moving to large-scale production of nanoparticles, we focused on liposomes as a model nanoparticulate system. Going from bench to bedside, several steps are required to obtain a ready-to-use liposomal formulation, namely, liposome formation, drug loading, purification, sterilization and filling. In between these steps, attentive quality controls and characteristic evaluations are required. In this context, to meet the high clinical demand for therapeutic NP in cancer therapy, it is crucial to develop an efficient manufacturing setup for industrial-scale production of liposomes.

Currently, the key industrial-scale technique for liposomal drug product manufacturing is batch-type bulk production (Shah et al., 2020). Typically, in bulk production, multiple steps are conducted discretely, sequentially, and independent of one another to obtain the final formulation from the lipid precursors. Upon successful completion, liposome dispersions are quality controlled, filled in the appropriate containers after which the production line is made ready for the next batch (Lee, 2017; Lee et al., 2015).

Although widely used, there are multiple complications associated with batch production technique. This method suffers from inefficiency and labor-intensiveness, partly as a result of the manufacturing process and its required discrete production steps. Additionally, batch-type bulk production is relatively prone to batch failure at the end of the processing line. Moreover, this technique is sensitive to scalability problems including batch-to-batch variations (Lim et al., 2014; Shah et al., 2020).

To mitigate potential batch-type bulk production problems, continuous flow manufacturing (CFM) can be an elegant solution. CFM is a method in which the aforementioned production steps are conducted in an uninterrupted and coherent setup. Therefore, an end-to-end production line is designed through which the formulation flows, starting as raw materials and ending as a refined liposomal drug product (Allison et al., 2015) (Figure 3).

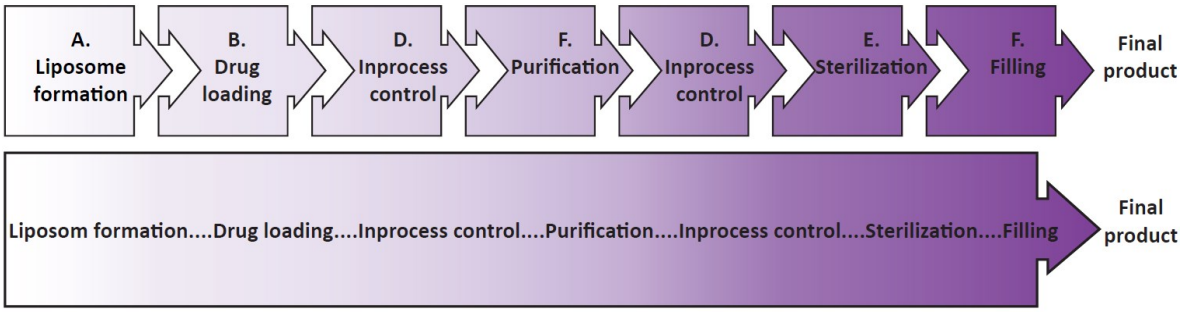

Figure 3. Liposome preparation process. Batch-type bulk preparation is performed through multiple discrete steps (top) while CFM concept hinges on a coherent production line (bottom).

Benefitting from its coherent and uninterrupted setup, CFM is labor-efficient and also more suitable for large-scale production (Costa et al., 2016). Regarding the latter, CFM does not require large manufacturing vessels, which in turn minimizes the risk of temperature variations and mixing problems. Additionally, CFM allows for a better control over the quality of the final product by changing the composition and process parameters while the system is running. This is feasible owing to the CFM potential for implementation of real-time in-line quantification of liposomes' key quality attributes (Chen et al., 2019).

In the context of CFM, microfluidic/millifluidic dispersion techniques to form liposomal particles have been extensively studied (Carugo et al., 2016; Chen et al., 2019; Kastner et al., 2014; Lou et al., 2019). In the early 2000, hydrodynamic flow focusing (HFF) was used

as one of the earliest microfluidic techniques to form liposomal dispersions within CFM setup (Jahn et al., 2004). In this method, the organic solvent containing lipids is confined and focused by the aqueous stream. As a result, the organic phase mixes promptly with the aqueous phase and liposomes will form upon mixing (Rhee et al., 2011).

In general, a microfluidic/millifluidic device consists of T- or Y-shaped channels in which the organic solvent flows through one channel and the aqueous phase is pumped through the other channel(s) of the device. The mixed stream of the organic phase and the aqueous medium can have a laminar flow or turbulent flow fluid dynamics (Tomeh and Zhao, 2020). The type of fluid dynamics depends on the microfluidic/millifluidic channel configuration as well as the fluid characteristics such as fluid velocity, viscosity, etc. Independent of the fluid dynamics, the two fluids mix rapidly and thus, the polarity of the organic solution decreases. This in turn results in lowering its capacity to solubilize the lipids and eventually, liposomes with certain physicochemical characteristics are self-assembled (Shah et al., 2020; Tomeh and Zhao, 2020). To control the main physicochemical characteristics of the produced liposomes, several composition and process parameters are used such as temperature, total flow rate (TFR), flow rate ratio between the organic phase and the aqueous phase, aqueous phase composition, lipid composition and lipid concentration (Costa et al., 2016; Kastner et al., 2014; Lim et al., 2014; Zook and Vreeland, 2010).

From the liposome particle formation as the initial step towards obtaining a final product, several manufacturing processes are performed including the removal of the solvent residues and unencapsulated drug, sterile filtration, filling and quality control of the finished product. Interestingly, numerous studies so far have focused on the primary formation of the nanoparticles using microfluidic/millifluidic devices in a continuous flow manufacturing setup while the integration of aforementioned production steps later in the procedure have not systematically been investigated.

Immediately after liposome formation, the formulation requires to be cleared of the both the organic solvent residues as well as the unencapsulated fraction of the therapeutic agent. To purify the prepared liposome dispersion in a CFM setup, tangential flow filtration (TFF) can be used. TFF method is based on the tangential flow of a solution alongside the

surface of the membrane. Hence, the flow direction of the permeate is perpendicular to the flow direction of the retentate. In comparison to the conventional methods of purification such as centrifugation, filtration or dialysis, TFF is a faster and more efficient method (Maurer et al., 2014). Moreover, unlike the other methods, TFF is more compatible with a CFM setup and can be further improved to maximize the cleaning efficiency (Worsham et al., 2019).

Throughout the formulation process, it is required to ensure the quality of the final product and monitor the characteristics of the liposomes such as particle size, polydispersity index, zeta potential, drug encapsulation efficiency, drug release, and particle stability (Porfire et al., 2019). To evaluate these properties, several instruments have been developed and are being used. Nevertheless, integrating these devices into a CFM setup requires additional provisions to the instruments.

The final step before releasing a liposomal drug formulation is to confirm the sterility of the product. Sterilization of a pharmaceutical product can be achieved via different methods including heat sterilization, radiation sterilization, gas sterilization, filtration and aseptic processing (EMA, 2019). Each of these methods suffer from a particular drawback such as alteration in the physicochemical properties of the NP, complexity of the process, toxicity complications, as well as inconvenient translation to the industrial scale (Delma et al., 2021). Regarding the latter, aseptic processing provides an excellent opportunity to be integrated in large-scale CFM setup. All the above-mentioned steps can be potentially unified and eventually, be translated to the development of an end-to-end manufacturing system for production of parental formulations.

In the context of this doctoral thesis, we aimed to study the formation and characterization of PM and liposomes at laboratory scale as well as industrial scale. We investigated the changes in key critical quality attributes of both PM and liposomes by varying different composition and process parameters. Moreover, we explored the possibility of formulation production in the industrial scale using a continuous flow manufacturing setup.

2. Aims and objectives

Controlling NP critical quality attributes using composition and manufacturing process parameters ensures optimal *in vivo* performance for a defined therapeutic purpose, effective fine-tuning of the NP, and finally, obtaining a more robust industrial-scale production of the NP. The latter is of great importance since successful large-scale production of therapeutic NP is key in meeting their increasing clinical demand. The main aims of the current thesis are as follows:

Objective **(I)**: assessing key composition and manufacturing process parameters of polymeric micelles by focusing on the mPEG-*b*-p(HPMA-Bz) amphiphilic block copolymer starting material. This objective can be split into the following sub-objectives:

A. Establishment of a purification protocol to purify mPEG-*b*-p(HPMA-Bz) polymer that was previously synthesized at an industrial scale using batch processing.
B. Evaluation and characterization of the corresponding polymeric micelles based on the mPEG-*b*-p(HPMA-Bz) polymer with a certain level of purity.
C. Preparation and evaluation of the polymeric micelles based on different mPEG-*b*-p(HPMA-Bz) block copolymers synthesized at laboratory scale via batch processing.

Objective **(II)**: assessing key composition and manufacturing process parameters of liposomes as the leading clinically approved nanoparticle formulation. This objective can be split into the following sub-objectives:

A. Control two main critical quality attributes of liposomes, namely hydrodynamic diameter (size) and polydispersity index (PDI) using several composition and manufacturing process parameters.
B. Design and evaluation of a CFM setup to produce liposomal drug products at large scale from raw materials all the way to a fine dispersion.
C. Integration of post-formation production steps, such as purification.
D. Continuous monitoring and adjustment of the composition and manufacturing process parameters using in-line quality controls of critical quality attributes.

3. Materials and methods

3.1. Materials

Egg phosphatidylcholine (EPC) and 1,2-distearoyl-sn-glycero-3-phosphoethanolamine-polyethylene glycol-2000 (DSPE-PEG 2000) were purchased from Lipoid GmbH (Ludwigshafen, Germany). Cholesterol (99% purity, product of USA) and calcein (product of Japan) were obtained from Sigma-Aldrich. Paclitaxel was purchased from LC laboratories (Woburn, USA). Polysorbate 80 (Tween 80, Fisher Scientific UK, Loughborough, Leicester, UK) and bovine serum albumin (Sigma A-4503) were used as solubilizers of released PTX in the release tests. Phosphate buffered saline (PBS) ready-to-use tablets (ROTI Fair PBS 7.4) were obtained from Carl Roth GmbH (Karlsruhe, Germany). An advanced programmable syringe pump PHD ULTRA was purchased from Harvard Apparatus, (Holliston, USA). Minimate Tangential flow filtration (TFF) cassettes with a MWCO of 100 kDa and a filtration area of 50 cm^2 were acquired from Pall Corporation (Ann Arbor, USA). Hollow fibers with a MWCO of 100 kDa and a filtration area of 193 cm^2 were purchased from WaterSep (USA). Regenerated cellulose MEMBRA-CEL MD10 dialysis tubing (MWCO 14 kDa) was obtained from Viskase (product of USA). Slide-A-Lyzer cassette (MWCO of 10 kDa) was obtained from Thermo-Fisher Scientific and Spectra/Por Float-ALyzer G2 dialysis membranes with MWCO of 100 kDa and 300 kDa were obtained from Spectrum labs (Rancho Dominguez California, USA). All cell labeling reagents and fluorescent dyes were purchased from Thermo Fisher Scientific (Naarden, the Netherlands) unless stated otherwise. Cell medium and supplements were obtained from Gibco BRL Thermo Fisher Scientific (Naarden, the Netherlands). HEPES (99.5%) and NaCl (99%) were purchased from Carl Roth GmbH (Karlsruhe, Germany). Ethylenediaminetetraacetic acid (EDTA) was purchased from Sigma-Aldrich (product of the Netherlands). Ethanol was purchased from Carl Roth GmbH (Karlsruhe, Germany). Tetrahydrofuran (THF, 99.5%), N,N-dimethylformamide (DMF, HPLC), deuterated dimethylsulfoxide (DMSO-d6, 99.8 Atom%D) and dimethylsulfoxide (DMSO) were obtained from Carl Roth GmbH (Karlsruhe, Germany). Gradient grade acetonitrile (ACN, 99.9%) and HPLC grade trifluoroacetic acid (TFA, 99.0%) were obtained from Sigma-Aldrich (product of France). Human hepatocellular carcinoma cells (HepG2) and

human prostate cancer cells (PC3) were obtained from American Type Culture Collection (ATCC). DMEM low glucose medium supplemented with 10% FBS and McCoy's 5A medium supplemented with 10% FBS were purchased from Sigma Aldrich. 96-well μClear black plates (Greiner Bio-One) were used to seed the cells. Cell Voyager 7000S (CV7000S) was obtained from Yokogawa Electric Corporation (Tokyo, Japan). Elplasia 96 microwell plate with a microgrid of 200x200 μm squares in the bottom of each well (Kurarray Co Ltd., Japan) was used for microspheroids generation. Two-lane Mimetas OrganoPlate was obtained from Leiden, the Netherlands and matrigel was purchased from Corning (9.4 mg mL^{-1}).

3.2. Experimental techniques

3.2.1. Standard dynamic light scattering

The average hydrodynamic diameter (Z-ave) and polydispersity index (PDI) of the formulated PM and liposomes (if required) were measured using standard dynamic light scattering (DLS, Nano-s, Malvern Instruments Ltd., UK) using a laser with a wavelength of 633 nm at ambient temperature (24–26 °C). PM were assessed after 10-fold dilution with the corresponding dispersion medium. Liposomes, on the other hand, were assessed without dilution (unless stated otherwise). In the case of liposomes, the refractive index and the viscosity of the solvent was adjusted to account for the presence of ethanol in the medium. Zeta potential of the PM was measured by diluting one volume of PM formulation with nine volumes of a solution of HEPES (10 mM, pH 7.5) and analyzed with Malvern Zetasizer (Nano ZS, Malvern Instruments Ltd., UK).

3.2.2. Spatially resolved dynamic light scattering

Average hydrodynamic diameter (Z-ave) and polydispersity index (PDI) of the liposomes in an in-line or off-line setting was measured using a NanoFlowSizer device (NFS, InProcess-LSP, the Netherlands) unless stated otherwise. The NFS device employs a spatially resolved dynamic light scattering (SR-DLS) technology with low coherence near infrared light and at a center wavelength of 1300 nm. To obtain DLS-type size characterization, backscattered light (180°) that is resolved over approximately 2.5 mm with approximately 3 micron resolution was analyzed (Besseling et al., 2019). Liposome size was assessed using the NFS vial module feature for the off-line measurements and its respective flow-cell module with

1.9 cm inner diameter for the in-line measurements. In the off-line setting, particle characterization results are presented as Z-ave and PDI, which were calculated from the mean of 10 measurements (approximately 10 seconds each). On the other hand, the in-line setting reports individual measurements that are approximately 5 seconds each. All the measurements were performed at ambient temperature (24–26 °C) and the refractive index and viscosity of the solvents were adjusted to the presence of the ethanol in the formulation.

3.2.3. Near-infrared spectroscopy (NIR)

To obtain NIR spectra, a Bruker MPA FT near-infrared spectrometer was used (Bruker, Germany). The device was equipped with a transflectance fiber probe with variable pathlengths and connected to OPUS software (version 6.5). The spectra was obtained between 12,500 and 4,000 cm^{-1} with 16 cm^{-1} optical resolution.

3.2.4. Nanoparticle tracking analysis (NTA)

To visualize liposomes' motion in suspension, a NanoSight instrument was used (Malvern Panalytical PLC, Worcestershire, UK). The NanoSight used in this experiment was equipped with a blue laser (488 nm) and a sCMOS camera. Data was analyzed using NTA software (version 3.2 Dev Build 3.2.16).

3.2.5. Gel permeation chromatography (GPC)

GPC device equipped with two MIXED-D columns (pLgel 5 µm, 300x7.5mm, Agilent technologies) and a pre-column (PLgel 5µm 50x7,5mm, Agilent technologies) was used to assess the weight average molecular weight (M_w), the number average molecular weight (M_n) and the molecular polydispersity index (M_w/M_n) of the polymers. In brief, the column temperature was set at 55 °C and DMF solution supplemented with 10 mM LiCl was used as the eluent at the flow rate of 0.7 mL min^{-1}. To analyze the block copolymers with different levels of purity, 2-3 mg of the desired sample was dissolved in 1 mL of solvent (DMF + 10 mM LiCl) and incubated at 37 °C for 2-3 hours prior to the measurement. Afterwards, each sample was filtered and measured with GPC.

3.2.6. Reversed-phase ultra-high-performance liquid chromatography (UPLC)

An Agilent technologies UPLC system (1260 infinity II, CA, USA) connected to a UV/Vis detector was used to determine the concentration of paclitaxel. The obtained peaks were integrated using chromatographic Openlab CDS software.

Initially a UPLC-UV method was developed and optimized to quantify PTX. An Acquity UPLC BEH C18 column (2.1 mm × 50 mm, 1.7 µm) was used as the stationary phase to separate analytes. An isocratic elution at a flow rate of 0.8 mL min^{-1} was conducted for chromatographic separation using ACN/H2O (40/60 % v/v) and 0.1% TFA as the mobile phase. The injection volume was set at 2 µL and PTX was detected at λ 277 nm with a run time of 3.5 minutes. Different concentrations of PTX were tested to develop a calibration curve, and the change in peak size and area under the curve (AUC) was monitored to validate the PTX peak. The encapsulation efficiency (EE) and loading capacity (LC) of PTX were calculated using equation 2 and 3:

EE%= Encapsulated drug (after filtration)/ initial amount of added drug*100%

Equation 2. Encapsulation efficiency calculation formula. EE represents the encapsulation efficiency in percentage.

LC%= Encapsulated drug (after filtration)/ (initial amount of drug + polymer)*100%

Equation 3. Loading capacity calculation formula. LC represents the loading capacity in percentage.

Here, independent replicates were prepared. Each of the replicates represents an individual formulation which was separately prepared and measured.

3.2.7. Ultraviolet-visible measurement (UV-Vis)

The fluorescent spectrum of calcein dye was recorded using Tecan i-control, infinite 200Pro device. Calcein dye was used as a model hydrophilic compound to assess the effect of counter current flow on the filtration process. A flat-bottom black 96 well plate was used to measure the calcein content before and after applying the counter current. The emission spectrum was recorded at excitation wavelength of λ 480 nm at ambient temperature (24–26 °C).

3.2.8. Transmission electron microscopy (TEM)

TEM analysis was performed on PM formulations to confirm the size ranges obtained by DLS and to visualize their morphology. Samples were allowed to adsorb for 10 minutes on glow discharged formvar-carbon-coated nickel grids (Maxtaform, 200 mesh, Plano, Wetzlar, Germany). Next, a negative staining was implemented using 0.5% uranyl acetate (Science Services GmbH, Munich, Germany). Samples were studied with a TEM LEO 906 (Carl Zeiss, Oberkochen, Germany), operating at an acceleration voltage of 60 kV.

3.3. Large-scale batch process of polymer synthesis

3.3.1. Scale-up production of polymers

The FRP technique was employed for large-scale synthesis of mPEG-*b*-p(HPMA-Bz) polymer at ChemConnection company (ChemConnection BV - Ardena, the Netherlands). During the synthesis process, ABCPA and mPEG were esterified to synthesize PEG-ABCPA-PEG that is used as the macroinitator. Next, DL-1-amino-2-propanol and methacryloyl chloride were reacted to get HPMA. The HPMA-Bz monomers were synthesized by coupling the formed HPMA with benzoyl chloride. Eventually, the monomer and the macroinitiator were dissolved in an organic solvent in a molar ratio of 200:1 and the mPEG-*b*-p(HPMA-Bz) polymer was obtained (Bresseleers et al., 2019).

3.3.2. Purification protocol

Large-scale synthesis of mPEG-*b*-p(HPMA-Bz) polymer requires downstream purification. Purification was preformed using hot-ethanol micelle formation technique (Figure 4). The impure polymer was dispersed in ethanol in a round bottom flask (70 °C, with continuous stirring at 700 rpm) to reach a final concentration of 100 mg mL^{-1} of the polymer in ethanol. After 20 minutes, the ethanol solution was added to the equal volume of Milli-Q water while stirring at 700 rpm for 5 minutes at ambient temperature (24–26 °C). The impurities that did not dissolve in hot ethanol remained as precipitants instead of forming micelles. After micelle formation, the dispersion was placed in a dialysis bag (MWCO of 10-14 kDa) and dialyzed against water for 48 hrs at the ambient temperature (24–26 °C). Next, the sample was centrifuged (at 4,000 rpm for 10 minutes) and the supernatant was collected and filtered through a 0.2 µm filter. The precipitant and the filtered supernatant were freeze-

dried for 2-3 days and the purified polymer was obtained from the filtered supernatant. To calculate the yield, the final mass of the freeze-dried purified polymer (obtained from the supernatant) was divided by the initial amount of the impure polymer (in the beginning of the process). In both cases, the yield was reported as % w/w. To calculate the amount of the impurities, the final mass of the freeze-dried impurity (obtained from the precipitant) was divided by the amount of the impure polymer in the beginning of the process and was reported in w/w percentage.

After purifying the polymer, it was washed with water to further improve its quality. Briefly, one mL of water was added to each 10 mg of the purified polymer. Following this, the sample was vortexed and centrifuged (at 4,000 rpm for 10 minutes) and the supernatant was separated from the undissolved fraction (i.e. the polymer). The washing and centrifuging steps were repeated twice and next, both the supernatant and the polymer were freeze-dried. To calculate the yield, the final weight of the freeze-dried purified and water-washed polymer (obtained from the undissolved fraction) was divided by the initial amount of the purified polymer and the yield was reported in w/w percentage. To calculate the amount of the impurities, the final weight of the freeze-dried impurity (obtained from the supernatant) was divided by the initial amount of the purified polymer and the content was reported in w/w percentage.

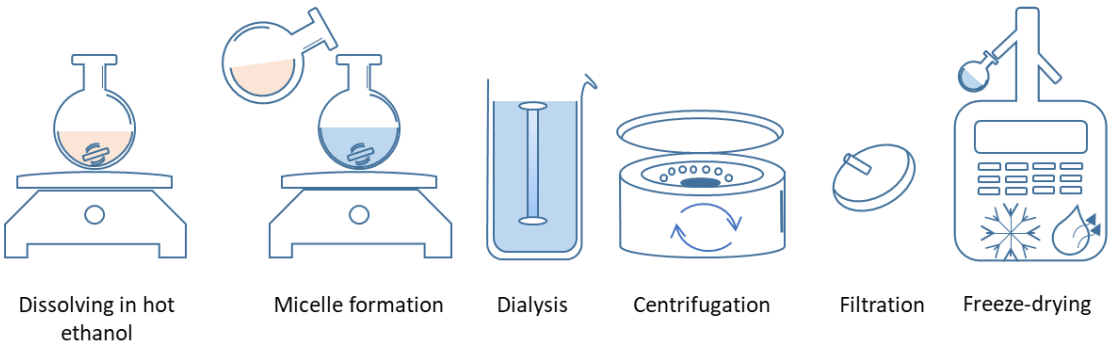

Figure 4. Hot-ethanol micelle formation purification protocol. mPEG-*b*-p(HPMA-Bz) polymer containing impurities was initially dissolved in hot ethanol and added to aqueous phase to form micelles. Subsequently, dialysis was performed followed by centrifugation, filtration and lyophilization to obtain polymer with the desired level of purity.

3.3.3. Preparation of polymeric micelles (THF method)

To prepare non-drug loaded PM using the THF method, 10 mg of the mPEG-*b*-p(HPMA-Bz) polymer was dissolved in 1 mL of THF at ambient temperature (24–26 °C). Next, the organic solvent containing the polymer was added dropwise to 1 mL of Milli-Q water and the colloidal solution was stirred at 1,000 rpm for 1–2 minutes. The formed dispersion was kept under the fume hood overnight to evaporate THF. THF evaporation was followed by the addition of Milli-Q water to restore the volume of the dispersion to 1 mL.

To prepare PTX-loaded PM via the THF method, 1 mg of PTX along with 10 mg of the polymer were dissolved in 1 mL of THF and micelle formation was proceeded as mentioned above. The final formulation of PTX-PM was filtered by passing it through a 0.45 µm filters in order to eliminate the un-encapsulated fraction (precipitations) of the drug.

3.3.4. Assessing the *in vitro* stability of PM using centrifugation method

PM characterization in terms of size, PDI, drug retention stability and polymer recovery was determine by measuring the hydrodynamic diameter of the PM, the PDI, the percentage of remained loaded PTX, and the percentage of remained polymer in the micellar form. After preparation of empty and PTX-loaded PM, one volume of the PM was diluted with five volumes of PBS (pH 7.4) and incubated at 37 °C with mild agitation. After 3 days of incubation, a fraction of the non-drug loaded and PTX-loaded PM was centrifuged at 5,000 g (10 minutes). The leaked fraction of the drug from PTX-loaded PM was precipitated and separated from the PM in the supernatant. To quantify the percentage of the remained loaded drug, the supernatant was further diluted with ACN and measured using UPLC. To assess the stability in size and PDI, after centrifugation, a part of the supernatant was taken from non-drug loaded and PTX-loaded PM and measured with DLS. Changes in average PM size were reported as PM stability in size. To investigate the polymer recovery, a fraction of the supernatant was freeze-dried to remove the aqueous medium. Subsequently, the sample was re-dissolved in DMF supplemented with 10 mM LiCl and incubated at 37 °C for 2-3 hours. To quantify the percentage of the remained polymer in the micellar form, the sample was measured by GPC. Three independently prepared batches of PM were analyzed, and the results were expressed as mean ± standard deviation.

3.4. Polymeric micelle evaluations based on lab-scale polymer synthesis

3.4.1. Preparation of polymeric micelles (ethanol method)

$mPEG_{5k}$-*b*-p(HPMA-Bz) block copolymer with the identical PEG chain length (5 kDa) but different molar feed ratios of macro-initiator to the monomer were synthesized using ethanol method. A total of four polymer were synthesized and used in this study, namely: $mPEG_{5k}$-*b*-p(HPMA-Bz)$_{17k}$, $mPEG_{5k}$-*b*-p(HPMA-Bz)$_{10k}$, $mPEG_{5k}$-*b*-p(HPMA-Bz)$_{5k}$, and $mPEG_{5k}$-*b*-p(HPMA-Bz)$_{3k}$.

To prepare PTX-loaded PM using the ethanol preparation method, different amounts of PTX (1.5, 3 and 4.5 mg PTX) along 30 mg of each polymer were dissolved in 1 mL of ethanol while heating at 60 °C. Maintaining the temperature, the ethanol solution was mixed with 1 mL of HEPES buffered saline (HBS 1x) and the colloidal solution was stirred at 200–400 rpm for 1–2 minutes. After PM formation, the formulations were dialyzed for 48 hrs against HBS using a dialysis cassette (MWCO of 10 kDa) at the ambient temperature (24–26 °C). The final formulation of PTX-PM was filtered through 0.45 µm filters in order to eliminate un-encapsulated fraction (precipitations) of the drug.

3.4.2. *In vitro* stability of the PTX-loaded PM

Stability studies (in terms of size and drug retention) of the different PM formulations were studied by measuring the hydrodynamic diameter, PDI and percentage of remained loaded PTX at different temperatures (7 days at 37 and up to 5 weeks at 25 and 4 °C). After preparation of PTX-loaded PM at different drug to polymer ratios (i.e., 0.05, 0.1, and 0.15 w/w), PM formulations were incubated at the aforementioned temperatures (see above). At each time points, PTX-loaded PM were sampled and centrifuged at 5,000 g for 10 minutes. The leaked fraction of the drug from PM after centrifugation precipitated and is separated from the PM in the supernatant. To quantify the percentage of the remained loaded drug, the supernatant was collected and diluted with ACN followed by UPLC measurement. In this experiment, technical repeats are reported, which were generated by sampling from one formulation incubated at a certain temperature. To assess the stability in size after centrifugation, a fraction of the supernatant was withdrawn and measured with Malvern DLS. Changes in average PM size were reported as the PM size stability. three

independent replicates were prepared, each replicate represents an individual formulation that was independently incubated and measured.

3.4.3. PTX release from PM in the presence of polysorbate 80/PBS and BSA/PBS

To assess PTX release from PTX-PM formulations, the release medium was composed of phosphate-buffered saline (PBS) supplemented with either 4.5% bovine serum albumin (BSA) or 0.2% v/v polysorbate 80. The required volume of the release media that was needed to achieve an excessive amount of polysorbate 80 in the buffer was determined based on the PTX solubility in 0.2% polysorbate 80 in PBS (Abouelmagd et al., 2015). PTX solubility was assessed by adding 0.6, 1.2, and 2.4 mg of PTX powder to 1 mL of the release medium. Samples were incubated at 37 °C for 24 hrs with mild agitating and afterwards, samples were centrifuged for 20 minutes at 10,000 rpm to precipitate the un-dissolved fraction of PTX. Next, one volume of the solubilized PTX in the supernatant was added to 10 volumes of ACN, followed by 10 minutes centrifugation at 5,000 g. A fraction of the supernatant was analyzed by UPLC. To confirm the absence of any mixed micelles, 0.2% polysorbate 80 micelles were incubated at 37 °C with PTX-loaded PM based on $mPEG_{5k}$-*b*-$p(HPMA\text{-}Bz)_{17k}$ polymer (drug to polymer ratios of 0.1 w/w). Samples were checked with Malvern Zeta sizer after 1 hrs, 6 hrs and daily until 7 days.

To evaluate the PTX release from PM, Float-A-Lyzer G2 dialysis membrane (MWCO of 100 kDa or 300 kDa) was used. TO start, PTX-loaded PM were placed in the dialysis bag and submerged in 50 mL of 0.2% polysorbate 80 in PBS. During the 7-day incubation period at 37 °C, samples were gently agitated and the outer medium was frequently refreshed. Samples were collected at different time point from the inside of dialysis membrane. To measure the concentration of the remained encapsulated PTX, the samples were disrupted with at least 2 volumes of ACN and measured by UPLC.

To assess the PTX release from PM in the PBS + BSA medium, 1 volume of the PM was mixed with 2-3 volumes of BSA and placed in the dialysis membrane. The release study was performed as described above. Prior to PTX measurement with UPLC, BSA was removed from the medium by adding 5 volumes of methanol to 1 volume of the samples followed by 15 minutes centrifugation at 4,000 rpm. The supernatant was separated, and the solvent

was dried under the vacuum rotator. After solvent evaporation, PTX precipitants were re-solubilized in ACN and the concentration was measured by UPLC.

3.4.4. Cell culture and Cy-labeled PM preparation

HepG2 cells were cultured in DMEM + 10% FBS and PC3 cells were cultured in McCoy's 5A + 10% FBS and maintained at 37 °C with 5% CO2 and humidified atmosphere. To study the uptake and penetration of the PM, 1–3.3% w/w of either Cy3- or Cy5-conjugated polymer was added to the unlabeled polymer. Synthesis of the dye-conjugated polymer was described previously (Shi et al., 2015) and the PM were prepared as described in Section 3.4.1.

3.4.5. PM uptake in 2D

10,000 cells/well were seeded into 96-well plates and incubated overnight. The next day, the medium was replaced with fresh complete medium and the cells were incubated with the fluorescently labeled PM and imaged live with 60x objective of CV7000s as often and as long as it was required for a particular experiment. Non-treated cells were used as negative control. Organelle labelling was performed according to manufacturing instructions. For the endosomes staining, the cells were incubated for 20 minutes at 37 °C with pHrodo Green Dextran conjugate diluted in complete growth medium to a final concentration of 0.05 mg mL^{-1}. The nuclei was stained with 10 nM Hoechst 33,342 in PBS (100 µL) for 10 minutes at 37 °C. Three independent replicates were prepared. Each of the replicates represents an individual cell-cultured well, which was separately measured.

3.4.6. PM penetration in 3D

For the microspheroid generation, HepG2 cells were seeded in microwell plates (20,000 cells per well) and were randomly dispersed throughout the squares of the microgrid. Individual microspheroids (diameter of 50-120 µm) were established after 3-5 days of culturing (37 °C in 5% CO2 and humidified atmosphere). 10 nM Hoechst 33,342 in full culture medium (100 µL) was used to stain the cell nuclei (1 hrs at 37 °C). Afterward, half of the cell culture medium was replaced with fresh complete medium containing the required amount of fluorescently labeled PM. 20x objective of CV7000s was used to observe the PM penetration in microspheroids. Similarly, non-treated microspheroids as negative controls.

Gel penetrations in 3D was studied using a 384-well microtiter Mimetas OrganoPlate. These plates include 96 microfluidic tissue chips that connect the following neighboring wells: a) a well filled with the mixture of cells and gel (i.e., gel channel, Figure 26), b and c) two wells for providing growth medium (i.e., perfusion channel Figure 26), and d) a well for imaging. In the gel channel, membrane-free capillary pressure barriers (i.e., phase guides) facilitate exchange of nutrients, gases, and waste products between the medium and the gel channel (Wevers et al., 2016).

To study the gel penetration in 3D, HepG2 cells were seeded in Mimetas OrganoPlate (according to the manufacturer protocols). Briefly, harvested and counted cells were centrifuged and the pellet was dissolved in Matrigel (106 cells per mL). Subsequently, 2 µL of gel mixture per chip was placed in the gel channel of the OrganoPlate and incubated for polymerization (30 minutes at 37 °C). Next, the medium inlet was filled with 50 µL of complete growth medium and the perfusion was started by placing the plate on Mimetas rocking platform at 37 °C (Trietsch et al., 2017). After 3-4 days, the nuclei were labeled with 10 nM Hoechst 33,342 in complete medium and incubated for 1 hrs at 37 °C. Next, fresh complete medium with the required amount of PM was added to each chip and the plates were placed on Mimetas rocking platform for continuous gravitational flow (Trietsch et al., 2017). The depth of PM perfusion into the gel channel was measured after 4 or 24 hrs in 5 gel segments using 10x objective of CV7000s (Figure 26). Here, we used chips with non-treated cells as negative controls. In this experiment, independent replicates were prepared. Each of the replicates represents an individual cell-cultured well, which was separately measured.

3.4.7. Image analysis

Image analysis protocols were customized and developed with Columbus Software (U.S. National Institutes of Health, Bethesda, Maryland, USA). Fiji software was used to measure gel penetration depth.

3.5. Continuous flow manufacturing of liposomes

3.5.1. Preparation of liposomes

To prepare liposomes, we have used a millifluidic device with dimensions adapted from a previously developed setup by Costa et al. (Costa et al., 2016). Our microfluidic system consisted of two channels (i.e., inner and outer channels) through which the ethanolic phase containing the lipids and PBS are injected using a syringe pump (Harvard apparatus). More specifically, lipid mixture (consisting DSPE-PEG-2000, EPC, and cholesterol at a molar ratio of 5:60:35 respectively) that was dissolved in ethanol was pumped through the inner channel of the millifluidic device, which has an inner diameter (ID) of 0.6 mm, while PBS, which is used as the aqueous phase, was injected through the outer channel with an ID of 3 mm. At a pre-defined flow rate ratio, the two streams come together, get mixed, and form liposomes which were collected from an outlet that was an extension of the outer channel (Figure 29).

3.5.2. Evaluation of composition and process parameters that influence the size and PDI of the liposomes using Design of Experiment (DoE)

With the help of design of experiment approach (DoE, Design-Expert by Statease), we designed and assessed the effect of several composition and process parameters on the size and PDI of different liposome dispersions. These parameters include total flow rates (TFRs), lipid concentrations, and ethanol content. TFR values varied from 5-70 mL min^{-1}, which resulted in Reynolds numbers in the range of 14-214 (depending on the formulation preparation condition). The injected concentration of lipids in ethanol ranged from 10-100 mM total lipids, and the ethanol content at the point of liposome formation was set to either 30 or 50% v/v ethanol. Within a D-optimal cubic model, 39 to 45 experimental runs (i.e., liposomal formulations) were designed and evaluated. Liposomes were prepared with various lipid concentrations and TFRs. To achieve the desired lipid concentration as defined by the DoE design, a concentrated stock solution of lipids in ethanol (100 mM) was prepared and mixed with pure ethanol using a static mixer. Next, the flow rates of the organic solution and aqueous phase were set according to the run specifications in DoE and the ethanolic lipid solution was directed into the inner channel while the aqueous phase (i.e., PBS) was

led into the outer channel of the millifluidic device. Depending on the run specifications, the flow rates of each phase was adjusted. The final ethanol content was set at 50% v/v and 30% v/v, which resulted in the flow rate ratios of 1 and 0.43 (organic phase to the water phase). After formation, the liposomes were evaluated in terms of size and PDI. Non-significant terms ($p > 0.05$) were removed from the design model with exceptions that were essential to preserve the hierarchy of the design and to generate a response surface model. Heatmap plots were generated with the aid of DoE software, to demonstrate the relationship between the process parameters (lipid concentration and TFR) and the responses (size and PDI).

3.5.3. Size adjustment using the residence time of the liposomes in high ethanol environment

3.5.3.1. Changes in liposome size over time as measured by NFS and NTA

A solution of 100 mM lipids in ethanol was prepared and mixed with pure ethanol using a static mixer to obtain a 70 mM ethanolic lipid solution. Using the millifluidic device, liposome dispersions were formed by mixing the ethanolic lipid solution with PBS in a one to one flow rate ratio with a final TFR of 62 mL min^{-1}. Thus, the obtained liposomal formulation contained 50% v/v ethanol. Right after formation, the sample was fractioned and aliquoted into 3 different vials for various downstream analyses. To the first portion, a one to one mixture of PBS and ethanol was added in order to dilute the dispersion 10,000 times for NTA analysis. The concentration of particles in the dispersion (expressed as the number of the particles per mL) and videos of the particle movements were recorded for 60 min using the NTA device. The second fraction of the sample was continuously quantified for 90 minutes with respect to the mean size and PDI using the NFS instrument. The last fraction of the dispersion was diluted 10 times with PBS at predefined time points for 90 minutes (i.e., 0, 1, 2.5, 5, 10, 20, 30, 60, 90 min after particle formation to fix particle size). After completion of the continuous measurement of the second fraction, the diluted and size-fixed samples were measured by NFS instrument. Three independent replicates were prepared and analyzed.

3.5.3.2. Defining the required ethanol content for liposome size growth

Liposomes were prepared as described in section 3.5.3.1. Right after formation, the dispersion was diluted 1.25-, 2.5-, 5-, and 10-fold with PBS to reduce the ethanol content from 50% to 40, 20, 10, and 5% v/v ethanol respectively. Next, the size and PDI of each sample were continuously measured for 60 minutes using NFS device. For this experiment, three independent replicates were prepared.

3.5.4. Effect of different dilution methods on liposome characteristics

Liposomes were prepared as described in section 3.5.3.1. Immediately after formation liposome dispersions were diluted inline using a syringe pump to reduce the ethanol content from 50% v/v to 5% v/v (10x dilution). The dilution process was performed using either a standard medical three-way connected to the tubing or using a static mixer. The hydrodynamic diameter and PDI of the liposomes were measured using a standard DLS device (Materials and methods section 3.2.1).

3.5.5. Tangential flow filtration (TFF)

To clear the liposome dispersion from residual ethanol, a TFF system was used. A filtration unit was connected to a peristaltic pump while disconnecting the retentate outlet from the pump reservoir to convert it from the standard recycling configuration into a one-time-only flow through configuration through which the dispersion passes along the filtration unit. To evaluate the changes in pressure, two pressure gauges were positioned, one before and one after the filtration unit. Two filtration units with filtration areas of 50 cm^2 and 193 cm^2 were tested (see materials section for more details). To assess the effect of pressure at the inlet and outlet on the filtration efficiency, various pressures were tested. Regarding the inlet pressure, we changed the pump speeds to obtain inlet pressures from 21 to 207 kilopascal (kPa). With respect to the outlet pressure, we varied the filter outlet diameter to obtain pressures from 14 to 52 kPa. The efficiency of TFF in removing ethanol was expressed as the waste volume fraction. To calculate this parameter, the filtrate volume was divided by the sum of the filtrate and retentate volumes. Three independent replicates were prepared.

3.5.5.1. Utilizing a counter current flow for enhancing the ultrafiltration

In the absence of liposomes, a solution of 0.5 mM calcein in PBS was prepared and passed through the cleaning unit from an inlet and left the unit from the outlet. A clean stream of PBS was flushed into the cleaning unit in the opposite direction (i.e., the counter current, Figure 37). To investigate the effect of the counter current flow rate on sample purification, the flow rate of the calcein solution (herein referred as TFF flow rate) was fixed at 65 rpm, and the flow rate of the counter current was varied (60, 30, 15, and 7.5 rpm). On the other hand, to investigate the effect of sample flow rate on the purification process, the counter current flow rate was fixed at 60 rpm, and the TFF flow rate was varied (32, 65, and 120 rpm). In both cases, the sample was collected from the outlet and the calcein content was measured using the UV spectrophotometry (Materials and methods section 3.2.7). The fluorescence intensity of the calcein in the outlet was normalized to the fluorescence intensity of the calcein in the inlet and expressed as the relative calcein intensity in percentages.

3.5.6. Real-time measurements of the liposome size, PDI and ethanol content

Prior to the in-line measurements of the ethanol content, we sought to evaluate the effect of liposomes on ethanol quantification using NIR. To this end, liposomes were prepared using 70 mM of total lipid in ethanol and at 62 mL min^{-1} TFR. Right after preparation, samples were dialyzed for 3 days against PBS (1L PBS per each mL of the ethanol/day), followed by addition of known quantities of ethanol to the dispersions (i.e., 0.5, 1, and 5% v/v ethanol). Ethanol content of the dispersions was quantified with NIR in an off-line setting using the NIR probe module.

Liposomes were prepared as described in section 3.5.3.1. Immediately after formation, the liposome dispersion was diluted with PBS in an in-line setup utilizing a three-way connector. After dilution, the liposome dispersion was directed to enter a flow-cell module of the NFS instrument for real-time in-line quantification of the mean size and PDI. Next, using tubing connections, the sample entered a vessel for ethanol quantification using an NIR probe. The input sample was measured for 4 minutes, and the measurements were 5 seconds apart.

Once the syringes containing the concentrated lipid, ethanol and PBS were emptied of the materials, we continued to measure the size and PDI of the remained sample in the flow cell in an off-line flow-cell module. Here three independent replicates were prepared.

3.6. Statistical Analysis

Statistical analysis on non-DoE graphs was performed using GraphPad prism software (Prism 9 for Windows 64-bit, Version 9.1.1) and statistical significance was defined at an alpha threshold of < 0.05.

4. Results

4.1. Batch process: large-scale synthesis of polymer

mPEG$_{5k}$-*b*-p(HPMA-Bz) block copolymer was previously synthesized at large scale at ChemConnection company (Bresseleers et al., 2019). Previous experiments with PM based on this batch of polymer demonstrated instability in particle size and drug retention. Therefore, it was required to characterize this polymer and remove any possible impurities.

4.1.1. Characteristics of impurities

To assess the purity of the large-scale synthesized mPEG-*b*-p(HPMA-Bz) polymer, NMR and GPC analyses were conducted. GPC analysis revealed one peak appearing with two fade shoulders (Figure 5A). Characterizing the peak showed an M_w of 27 kDa and a PD of 1.55 (Table 1).

Table 1. Characterization of the impure mPEG-*b*-p(HPMA-Bz) polymer. GPC Analysis of the large-scale synthesized mPEG-*b*-p(HPMA-Bz) block copolymer revealed a PD of 1.5 and M_w of around 27 kDa.

M_p	M_n	M_w	M_z	M_{z+1}	M_v	PD
27835	17668	27299	36606	44570	25905	1.54511

In the obtained NMR spectrum of the polymer, multiple low-intensity peaks appeared at different chemical shifts of the spectrum (Figure 5B). Nevertheless, integration of the peak at 5 ppm, which corresponds to the relative number of monomer units in the polymer, was showed approximately 50 monomers per polymer chain.

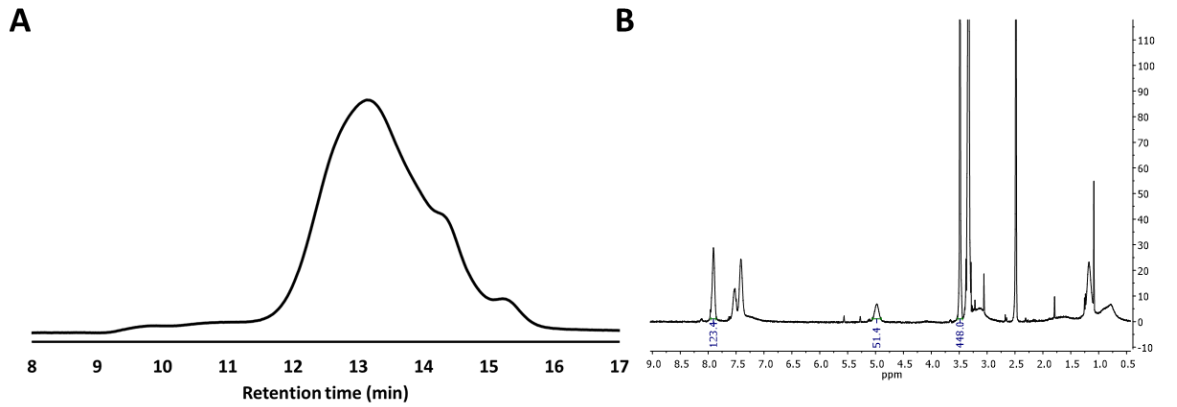

Figure 5. Characterization of impure mPEG-*b*-p(HPMA-Bz) polymer. A) GPC chromatogram and B) ^{1}H NMR spectrum (DMSO-d6, 400 MHz).

To verify the impurities, we initially analyzed ethanol- and water-insoluble precipitants from the impure polymer using GPC and NMR (Figure 6A and 6B). We observed that 3.2 ± 0.4 % w/w of the impure polymer was the ethanol- and water-insoluble impurities. In the GPC analysis of this fraction, two large-molecular weight peaks with M_w of above 1,000 kDa and above 100 kDa appeared before the peak corresponding to the residues of the polymer (Figure 6A and Table 2). Such large-sized impurities in the ethanol-insoluble fraction could be corresponding to the presence of the homopolymer.

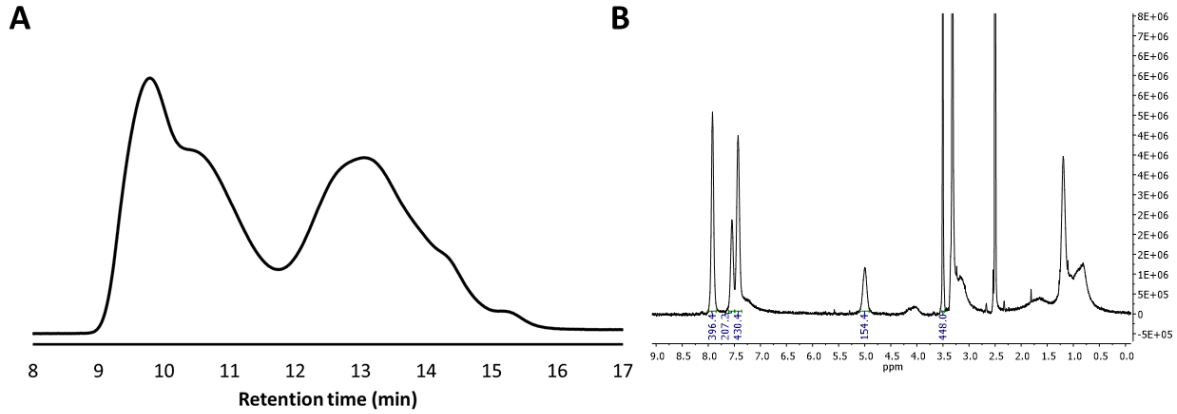

Figure 6. Characterization of ethanol-insoluble and water-insoluble impurities. A) GPC chromatogram and B) ^{1}H NMR spectrum (DMSO-d6, 400 MHz).

Table 2. Characterization of ethanol- and water-insoluble impurities. GPC Analysis show two large-molecular weight peaks with M_w above 100 kDa.

Peak	M_p	M_n	M_w	M_z	M_{z+1}	M_v	PD
1	1170752	996828	1287309	1705604	2191936	1234272	1.29141
2	105194	104763	104766	104769	104772	104765	1.00003
3	28251	20498	28552	35791	41655	27431	1.39292

After purification, the purified polymer was washed with water to eliminate any water-soluble impurities and the collected impurities were analyzed with GPC and NMR (Figure 7A and 7B). After the water wash, it was revealed that the purified (and not water washed) polymer contained 9.8 ± 0.6 % w/w water-soluble impurities.

In the GPC analysis of such impurities, 3 peaks emerged in the chromatogram with M_w of 35.2 kDa, 9.5 kDa and 4.4 kDa (Table 3 and Figure 7A). The first peak possibly corresponds to the polymer residues. However, the molecular weights of the second and the third peaks are in concurrence with the molecular weights of the macroinitiator and PEG respectively (Table 3), which both are water soluble.

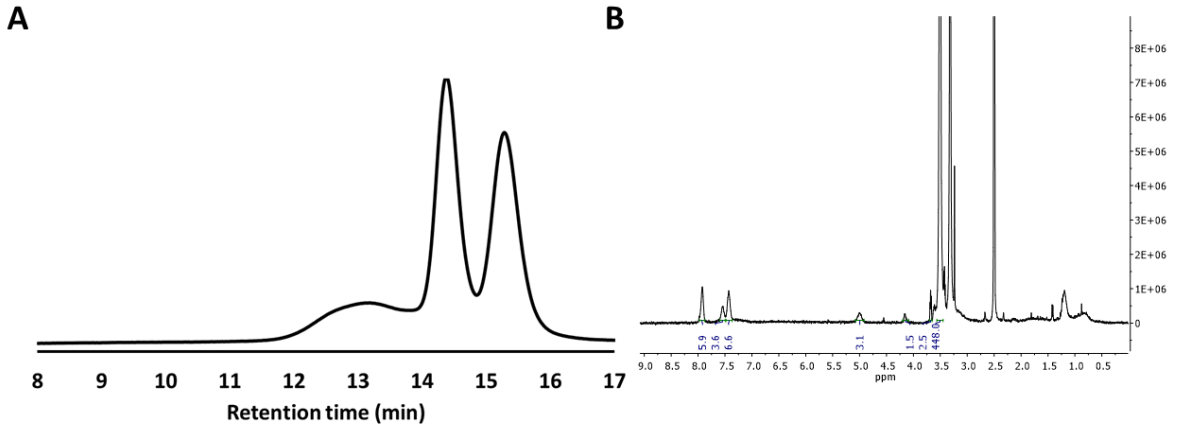

Figure 7. Characterization of water-soluble impurities. A) GPC chromatogram and B) ^{1}H NMR spectrum (DMSO-d6, 400 MHz).

Table 3. Characterization of water-soluble impurities. GPC Analysis show three peaks with M_w that possibly correspond to the residues of the polymer, the macroinitiator and PEG respectively.

Peak	M_p	M_n	M_w	M_z	M_{z+1}	M_v	PD
1	31456	32351	35242	38256	41210	34798	1.08936
2	9570	9398	9550	9702	9855	9527	1.01617
3	4510	4350	4434	4516	4596	4421	1.01931

4.1.2. Characteristics of the purified polymer

Following the purification protocol, a purification yield of 68.4 ± 5.8 % w/w was obtained. GPC chromatogram of the purified polymer showed only one peak, with two fade shoulders (Figure 8A). The peak had a similar M_n and M_w to that of the impure polymer (M_w of 28 kDa and PD of 1.6, Table 4).

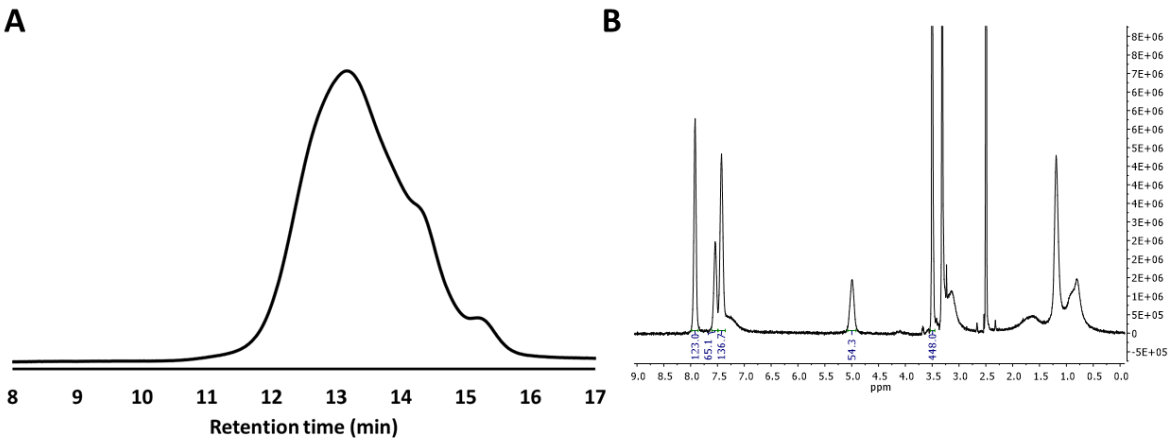

Figure 8. Characterization of the purified polymer. A) GPC chromatogram and B) ^{1}H NMR spectrum (DMSO-d6, 400 MHz).

Table 4. Characterization of the purified polymer as determined by GPC Analysis. GPC Analysis of the purified mPEG-*b*-p(HPMA-Bz) block copolymer revealed a PD of 1.6 and M_w of around 28 kDa.

M_p	M_n	M_w	M_z	M_{z+1}	M_v	PD
27019	17194	27876	39933	54396	26241	1.62126

In the obtained NMR spectrum, however, almost all the low-intensity excess peaks were removed from the spectrum and approximately 54 monomers per polymer chain were obtained (Figure 8B).

To further improve the purification quality, the purified polymer was washed with water. After washing, 82.7 ± 3.0 % w/w of the polymer was recovered (purified and water-washed). As a result of washing, the GPC spectrum revealed a single peak with no additional shoulders (Figure 9A). This peak had an M_w of 29 kDa with an improved PD of 1.5 (Table 5 and Figure 9A).

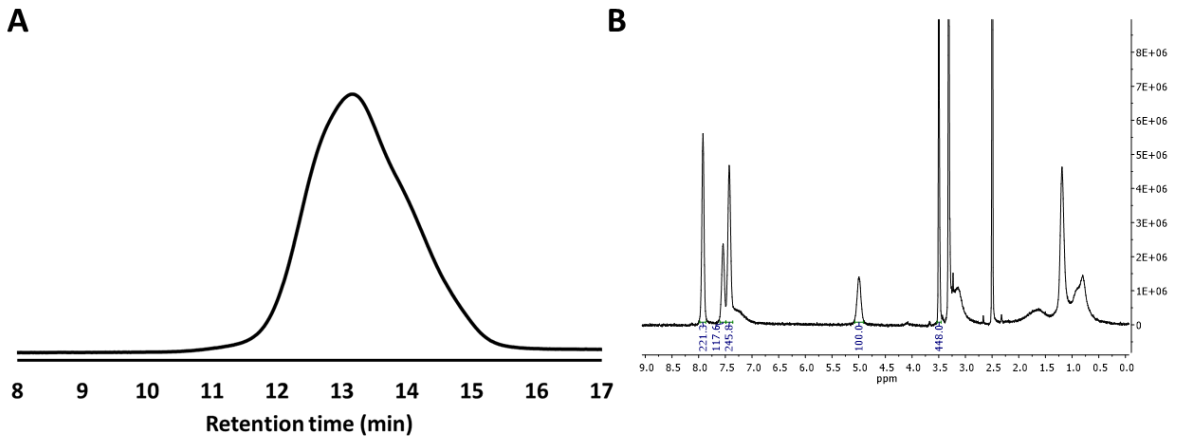

Figure 9. Characteristics of the purified and water-washed polymer. Representative A) GPC chromatogram and B) 1H NMR spectrum (DMSO-d6, 400 MHz).

According to NMR analysis of the rinsed polymer, each polymer chain contained approximately 100 monomers (Figure 9B).

Table 5. Characteristics of the purified and water-washed polymer as determined by GPC Analysis. GPC Analysis of the purified mPEG-*b*-p(HPMA-Bz) block copolymer revealed a PD of 1.5 and M_w of around 30 kDa.

M_p	M_n	M_w	M_z	M_{z+1}	M_v	PD
27019	19741	29277	40812	56061	27763	1.48306

4.1.3. Characterization of the micelles based on different polymers

4.1.3.1. *In vitro* stability of non-drug loaded PM based on polymers obtained from different purification method

To assess the stability of non-drug loaded PM-based formulations, the mean size (presented as hydrodynamic diameter), the size distribution (presented as PDI), and the PM integrity (presented as polymer recovery) was monitored after 3 days at 37 °C. Results show that the stability of PM (in terms of size and PDI) didn't depend on the presence of polymer impurities (Figure 10 A to D). However, PM based on the impure polymer demonstrated the largest mean size of all (approximately 80 nm). Other PM based on the purified polymer, the purified and water-washed polymer as well as the lab-scale synthesized polymer had sizes of approximately 60 nm with PDIs around and below 0.1 (Figure 10 B to D). Data obtained from GPC show that almost 100% of the polymer was recovered in all PM based on polymers with different levels of purity (Figure 10E).

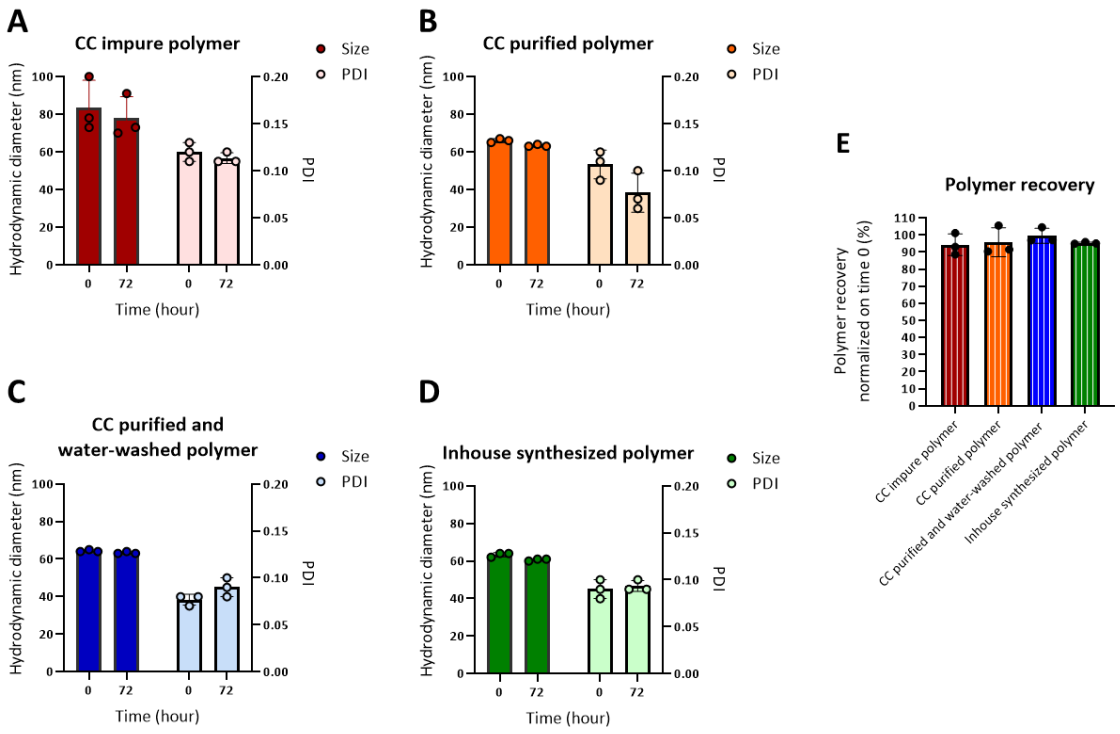

Figure 10. Evaluation of PM stability by monitoring the changes in PM size and PDI (A, B, C, and D) and polymer recovery (E) during storage at 37 °C for 3 days. In this condition, the size and PDI changes were monitored for A) CC impure polymer, B) CC purified polymer, C) CC purified and water-washed polymer and

D) Laboratory-scale (inhouse) synthesized polymer. Data are presented as mean ± SD of independent replicates (n = 3).

4.1.3.2. *In vitro* stability of PTX-loaded PM based on polymers obtained with an alternative purification method

After thoroughly studying the properties of non-drug loaded PM and given that the addition of drugs might possibly alter PM physicochemical properties, we sought to better understand the behavior of the drug-loaded PM. To this end, PTX-loaded PM based on mPEG-*b*-p(HPMA-Bz) polymer with different purity levels were prepared and evaluated with respect to the mean size (presented as hydrodynamic diameter), the size distribution (presented as PDI), the PM integrity (presented as polymer recovery), and drug retention during storage at 37 °C for 3 days. The results demonstrate that all PM based on polymers with different levels of purity show a hydrodynamic diameter of around 70 nm. After 3 days of storage of PTX-loaded PM at 37 °C, the size and PDI of the PM did not change drastically across the studied groups (Figure 11 A, B, D and E). It should be noted that, two technical repeats in the PM based on purified polymer and purified-water-washed polymer were outliers resulting in an elevation in size and PDI (Figure 11B and 11D). In all the PM based on polymers with different purity levels, almost 100% of the polymer was recovered after 3 days of incubation (Figure 11C).

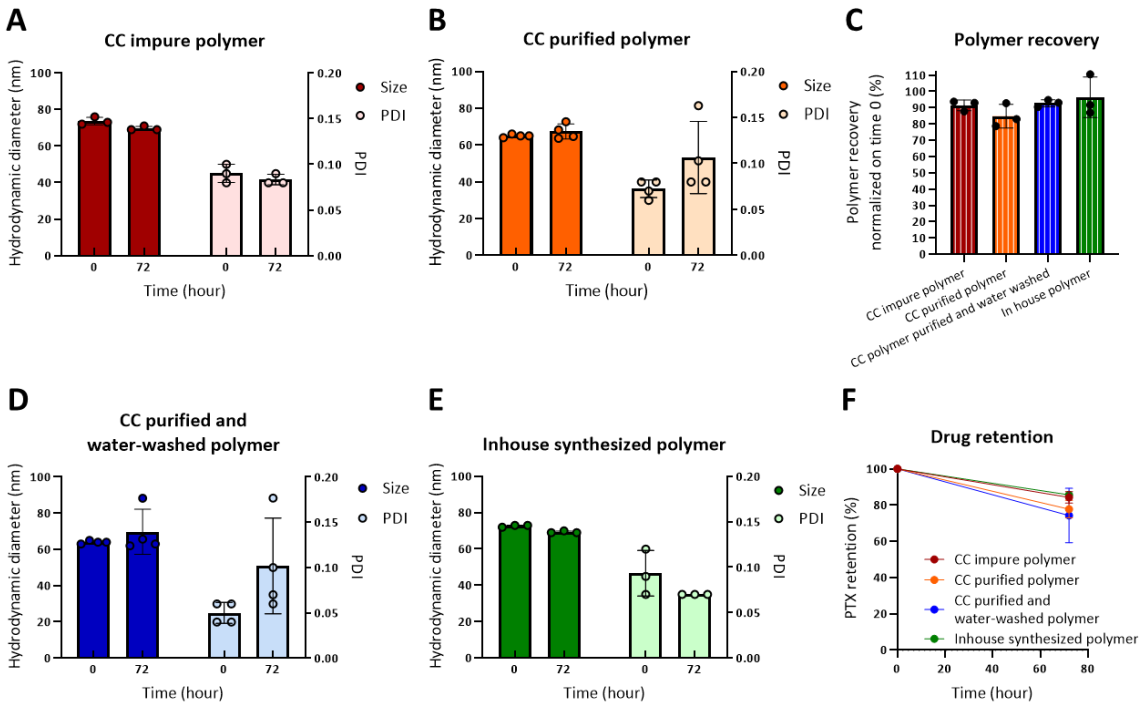

Figure 11. Evaluation of PTX-loaded PM stability during storage at 37 °C for 3 days. PM were monitored regarding the changes in PM size and PDI (A, B, D, and E), polymer recovery (C) and PTX retention in PM (F). In this condition, changes in the size and PDI were monitored for A) CC impure polymer, B) CC purified polymer, D) CC purified and water-washed polymer and E) Laboratory-scale (inhouse) synthesized polymer. Data are presented as mean ± SD of independent replicates (n ≥ 3).

For the PM based on polymers with different purity levels, the encapsulation efficiencies (%) were comparable and all were above 75% (Table 6).

Table 6. Encapsulation efficiency (%) of PM based on four mPEG-*b*-p(HPMA-Bz) block copolymers. The polymers differed in their level of purity and the micelles were prepared at a drug to polymer ratio of 0.1 (1 mg PTX and 10 mg polymer, n ≥ 3).

Polymers with different level of purity	EE (%)
CC impure polymer	77 ± 1
CC purified polymer	92 ± 11
CC purified and water-washed polymer	81 ± 9
Inhouse synthesized polymer	77 ± 1

To evaluate the drug retention during storage in the drug-loaded PM formulations, PTX-loaded PM were prepared with the initial preparation drug to polymer ratio of 0.1 and incubated at 37 °C for 3 days. Results show that regardless of the polymer's purity level, all PM revealed a relative stability in terms of drug retention. Here, more than 70% of the drug was retained in the different PM formulations after 3 days of incubation (Figure 11F).

4.2. Batch process: Lab-scale synthesis of polymers

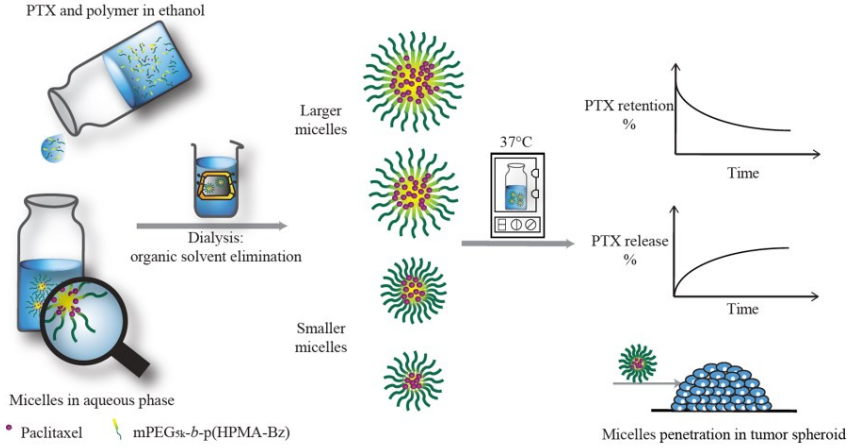

Figure 12. Preparation and evaluation of polymeric micelles based on four different mPEG$_{5k}$-b-p(HPMABz) block copolymers. PM are prepared via nanoprecipitation and dialyzed against aqueous phase to remove the organic solvent. PM were obtained with different characteristics and show specific drug retention, drug release and penetration in tumor spheroids (Sheybanifard et al., 2020).

4.2.1. Characterization of small-scaled synthesized mPEG$_{5k}$-*b*-p(HPMABz) PM

mPEG$_{5k}$-*b*-p(HPMA-Bz) block copolymers were previously synthesized at laboratory scale with four different molecular weights of the pHPMA-Bz as the hydrophobic blocks (i.e., 3, 5, 10 and 17 kDa) and with an identical molecular weight of PEG (i.e., 5 kDa). The GPC and NMR analysis of the lab-scale synthesized polymers showed that all variants of the polymer have a very low PD (Table 7).

Table 7. Characterizing the lab-scale synthesized mPEG$_{5k}$-*b*-p(HPMA-Bz) block copolymers. ^{1}H NMR and GPC analysis was used to determine the M_n and M_w of the polymer (Sheybanifard et al., 2020).

Polymer	MI:M	M_n by ^{1}H-NMR (kDa)	M_n by GPC (kDa)	M_w by GPC (kDa)	Polydispersity (M_w/M_n) (GPC)
mPEG$_{5k}$-*b*-p(HPMA-Bz)$_{17k}$	1:200	22.1	15.8	20.7	1.31
mPEG$_{5k}$-*b*-p(HPMA-Bz)$_{10k}$	1:100	15.0	13.2	17.5	1.32
mPEG$_{5k}$-*b*-p(HPMA-Bz)$_{5k}$	1:50	10.2	10.8	14	1.30
mPEG$_{5k}$-*b*-p(HPMA-Bz)$_{3k}$	1:25	7.7	8.9	11	1.24

Following the preparation and characterization of empty PM based on these polymers (Bagheri et al., 2018), we sought to evaluate PTX-loaded PM formulations based on the aforementioned polymers. As indicated in Tables 8-10, we assessed the encapsulation efficiency (EE), loading capacity (LC), particle size, size distribution and zeta potential of the different PM. The obtained data show that on the one hand, the hydrodynamic diameter (Z-ave) and polydispersity index (PDI) of the PM of a given polymer was independent of the PTX loading percentage. On the other hand, decreasing the hydrophobic block size (from 17 to 3 kDa) and consequently the hydrophobic/ hydrophilic ratio of the polymer, resulted in a decrease in the average size of the PM (from 53 to 38 nm). A slightly negative zeta potential (between −1.6 and −3.5 mV) was observed for all variants. With respect to the EE of PTX, data show a range of approximately 40-70% (with the exception of the last formulation in Table 10 where the EE was 21%). Such EE resulted in LC's ranging from approximately 2–9% (Tables 8-10).

Table 8. Physicochemical properties of PM with a drug to polymer ratio of 0.05 (1.5 mg PTX and 30 mg polymer). PM were prepared based on four different mPEG$_{5k}$-*b*-p(HPMA-Bz) block copolymers. Data are presented as mean ± SD of independent replicates (n = 4) (Sheybanifard et al., 2020).

Polymer	Z-ave (nm)	PDI	Zeta potential*, (mV)	EE (%)	LC (%)

$mPEG_{5k}$-*b*-p(HPMA-Bz)$_{17k}$	52 ± 1	0.05 ± 0.03	-2.8 ± 1.4	56.6 ± 3.3	2.7 ± 0.2
$mPEG_{5k}$-*b*-p(HPMA-Bz)$_{10k}$	51 ± 1	0.04 ± 0.03	-2.7 ± 1.2	51.3 ± 11.6	2.4 ± 0.6
$mPEG_{5k}$-*b*-p(HPMA-Bz)$_{5k}$	40 ± 1	0.06 ± 0.05	-3.5 ± 0.9	56.8 ± 3.9	2.7 ± 0.2
$mPEG_{5k}$-*b*-p(HPMA-Bz)$_{3k}$	39 ± 3	0.13 ± 0.06	-3.4 ± 1.0	45.1 ± 8.7	2.2 ± 0.4

Table 9. Physicochemical properties of PM with a drug to polymer ratio of 0.1 (3 mg PTX and 30 mg polymer). PM were prepared based on four different $mPEG_{5k}$-*b*-p(HPMA-Bz) block copolymers. Data are presented as mean ± SD of independent replicates (n = 4) (Sheybanifard et al., 2020).

Polymer	Z-ave (nm)	PDI	Zeta potential* (mV)	EE (%)	LC (%)
$mPEG_{5k}$-*b*-p(HPMA-Bz)$_{17k}$	53 ± 1	0.05 ± 0.01	-2.1 ± 0.4	52.6 ± 6.7	4.9 ± 0.6
$mPEG_{5k}$-*b*-p(HPMA-Bz)$_{10k}$	51 ± 1	0.04 ± 0.02	-3.2 ± 1.9	53.9 ± 7.9	5.0 ± 0.6
$mPEG_{5k}$-*b*-p(HPMA-Bz)$_{5k}$	40 ± 1	0.05 ± 0.03	-3.3 ± 0.7	42.7 ± 8.9	3.9 ± 0.8
$mPEG_{5k}$-*b*-p(HPMA-Bz)$_{3k}$	38 ± 1	0.10 ± 0.03	-3.1 ± 1.2	43.4 ± 9.2	4.0 ± 1.0

Table 10. Physicochemical properties of PM with a drug to polymer ratio of 0.15 (4.5 mg PTX and 30 mg polymer). PM were prepared based on four different $mPEG_{5k}$-*b*-p(HPMA-Bz) block copolymers. Data are presented as mean ± SD of independent replicates (n = 4) (Sheybanifard et al., 2020).

Polymer	Z-ave (nm)	PDI	Zeta potential*, (mV)	EE (%)	LC (%)
$mPEG_{5k}$-*b*-p(HPMA-Bz)$_{17k}$	53 ± 2	0.07 ± 0.03	-1.6 ± 0.7	67.0 ± 20.1	8.7 ± 2.6
$mPEG_{5k}$-*b*-p(HPMA-Bz)$_{10k}$	51 ± 2	0.04 ± 0.01	-1.7 ± 0.6	69.4 ± 22.1	9.0 ± 2.9

$mPEG_{5k}$-*b*-p(HPMA-Bz)$_{5k}$	40 ± 1	0.04 ± 0.03	-1.6 ± 1.2	62.2 ± 18.4	8.1 ± 2.4
$mPEG_{5k}$-*b*-p(HPMA-Bz)$_{3k}$	40 ± 3	0.14 ± 0.04	-2.1 ± 2.0	21.2 ± 9.6	2.8 ± 1.3

* Zeta potential was measured in a solution of HEPES (10 mM, pH 7.5).

4.2.2. Size stability evaluation of unloaded PM based on different polymer types

We started evaluating the size stability of the PM in the absence of the drug. To this end, non-drug loaded PM based on all four polymer variants were prepared and stored either at 4 °C or 25 °C for 5 weeks. Results show maximal size stability when the non-drug loaded PM were stored in these conditions (Figure 13).

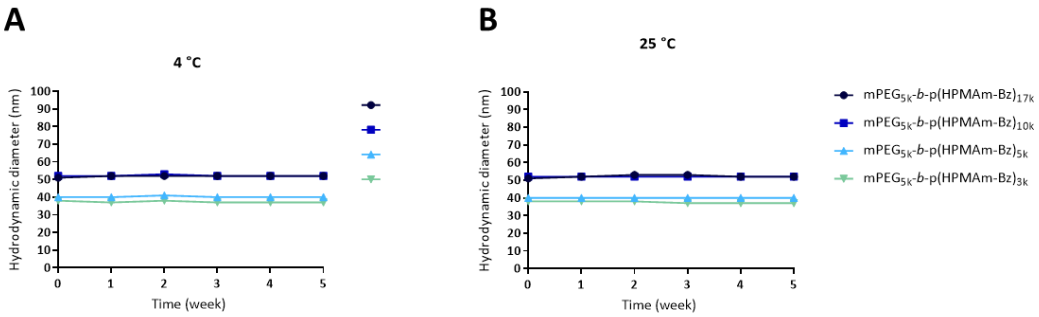

Figure 13. Alteration in PM size after storage at A) 4 °C and B) 25 °C. PM show maximum stability with no substantial change in size over the tested period (Sheybanifard et al., 2020).

To further mimic the physiological condition, the same experiment was conducted on PM that were incubated at 37 °C for 7 days. As shown in Figure 14A, PM from all four polymer variants showed stability in size up to 7 days. TEM images of these PM showed no obvious aggregation and further confirmed the observed stability of the PM as demonstrated by DLS analysis (Figure 14B).

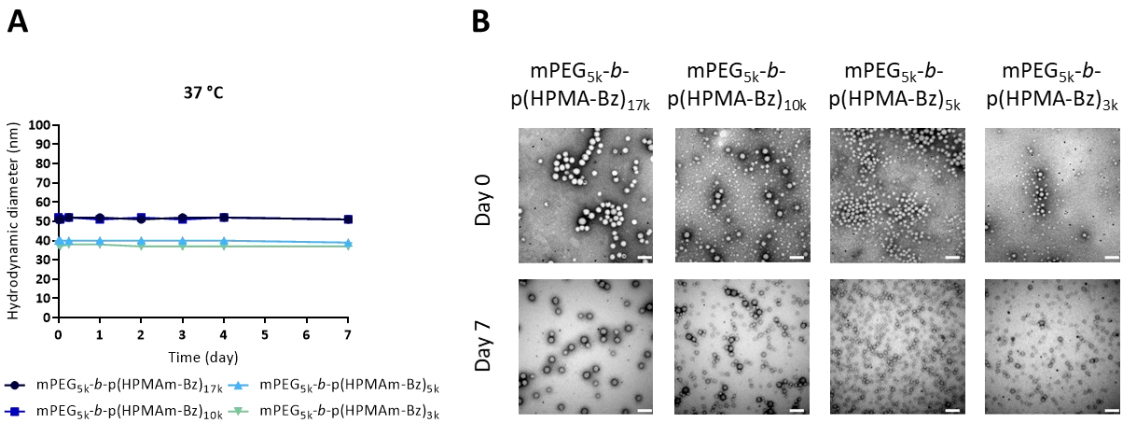

Figure 14. Stability in size of PM based on four polymer types after storage at 37 °C. A) Hydrodynamic diameter variations obtained by DLS, and B) TEM images of empty PM immediately after preparation and after 7 days of storage at 37 °C (size bar is 100 nm) (Sheybanifard et al., 2020).

4.2.3. Evaluating the effect of drug to polymer ratio on drug leakage and size stability of PM based on different polymer types

To evaluate the drug retention during storage in the drug-loaded PM formulations, PTX-loaded PM were prepared and incubated at 37 °C for 7 days. The obtained results demonstrate that PM based on the polymer with the shortest hydrophobic block (i.e., $mPEG_{5k}$-*b*-$p(HPMA\text{-}Bz)_{3k}$) was by far the leakiest under all drug to polymer ratios (Figures 15A, 15C and 16A). After 6 hours of incubation, only 40% of the drug was retained in the PM with an initial drug to polymer ratio of 0.1. After 24 hrs, only 20% of PTX was retained inside these PM. At this time point, PM based on the polymer with the longest hydrophobic block size (i.e., $mPEG_{5k}$-*b*-$p(HPMA\text{-}Bz)_{17k}$) retained almost 80% of PTX. On the other hand, PM formulations based on $mPEG_{5k}$-*b*-$p(HPMA\text{-}Bz)_{10k}$ and $mPEG_{5k}$-*b*-$p(HPMA\text{-}Bz)_{5k}$ showed an intermediate PTX retention; with relatively more PTX leakage from PM prepared of $mPEG_{5k}$-*b*-$p(HPMA\text{-}Bz)_{5k}$ polymer (i.e., the polymer with shorter hydrophobic block size) (Fig 16A).

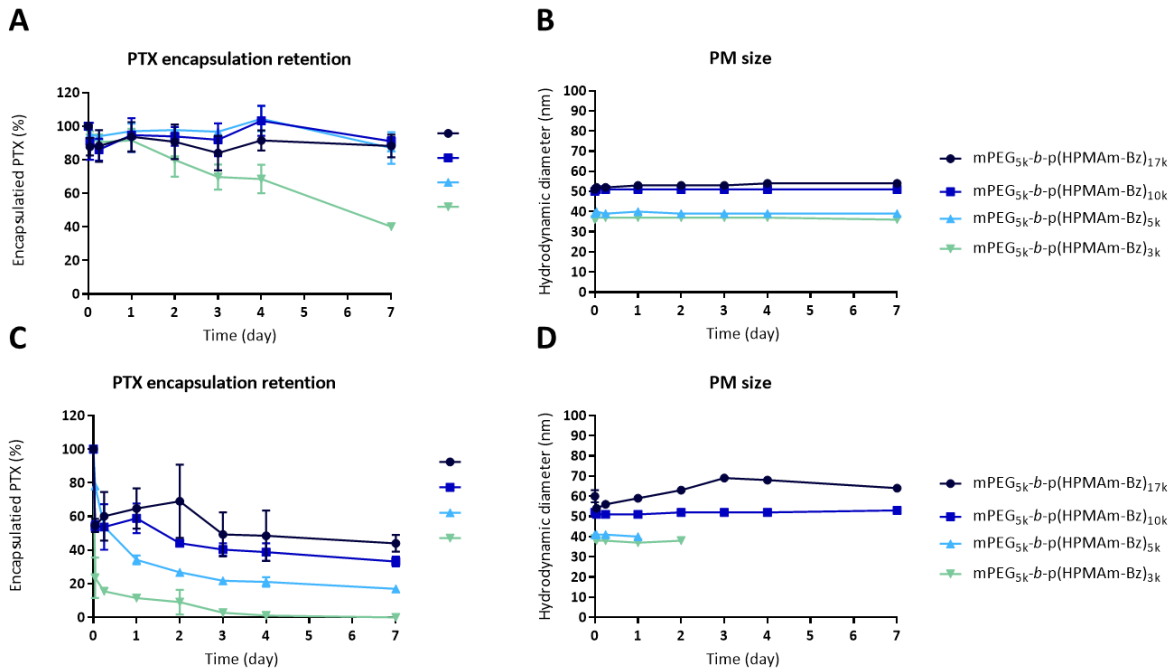

Figure 15. Changes in encapsulation retention and mean size (presented as hydrodynamic diameter) of PM. PM were prepared based on all four mPEG$_{5k}$-*b*-p(HPMA-Bz) block copolymer with drug to polymer (w/w) ratios of 0.05 (A and B) and 0.15 (C and D). Samples were stored at 37 °C for 7 days (Sheybanifard et al., 2020).

The drug retention as a function of the initial drug to polymer ratio was assessed in the most and the least stable PM (i.e., PM based on mPEG$_{5k}$-*b*-p(HPMA-Bz)$_{17k}$ and mPEG$_{5k}$-*b*-p(HPMA-Bz)$_{3k}$ respectively). Results show that irrespective of the PM type, a higher drug retention was obtained at a lower initial drug to polymer ratio (Figures 16B and 16C). Similar findings were observed with the set of PM based on mPEG$_{5k}$-*b*-p(HPMA-Bz)$_{17k}$, where drug retention was more than 80% for PM with initial drug to polymer ratio of 0.05 and 0.1 (i.e., 5 and 10% w/w PTX loading) after 7 days of incubation (Figure 16B). Meanwhile, at this time point, PM with higher initial drug to polymer ratio of 0.15 (i.e., 15% w/w PTX loading) showed the highest drug leakage (44% of PTX retention). Of all the prepared PM with different drug to polymer ratio and based on different polymer variants, PM based on mPEG$_{5k}$-*b*-p(HPMA-Bz)$_{3k}$ with initial drug to polymer ratio of 0.15 (i.e., 15% PTX loading) was the least stable with almost no drug remained encapsulated at the end of the incubation period. At this time point, around 13% and 40% of PTX was retained in PM with initial drug

to polymer ratio of 0.1 (i.e., 10% PTX loading) and 0.05 (i.e., 5% PTX loading), respectively (Figure 16C).

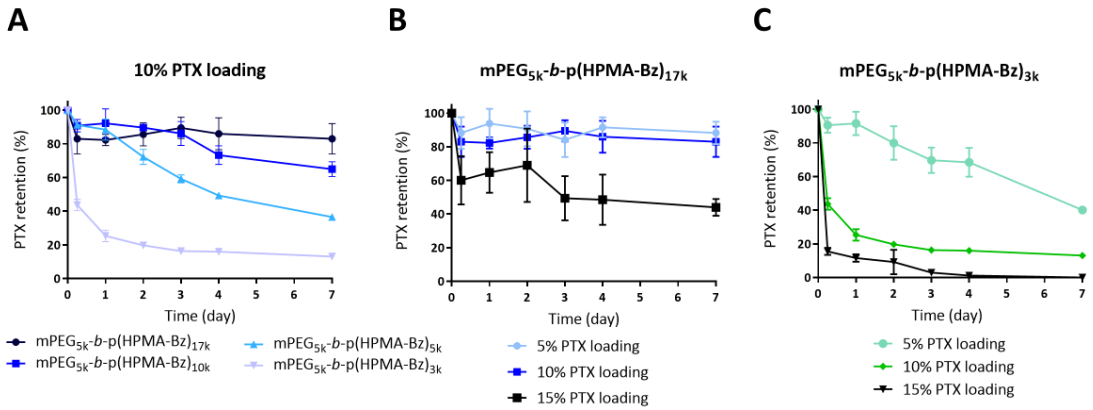

Figure 16. PTX retention in PM during 7 days of storage at 37 °C in HBS medium. A) PM were generated based on different variants of mPEG$_{5k}$-*b*-p(HPMA-Bz) at a drug to polymer ratio of 0.1, B) PM based on mPEG$_{5k}$-*b*-p(HPMA-Bz)$_{17k}$ polymer with initial drug to polymer (w/w) ratios of 0.1, 0.15, and 0.45 and C) PM based on mPEG$_{5k}$-*b*-p(HPMA-Bz)$_{3k}$ polymer with initial drug to polymer (w/w) ratios of 0.1, 0.15, and 0.45. Results are presented as mean ± SD of three technical repeats (n = 3) (Sheybanifard et al., 2020).

Besides the drug retention, we also evaluated the stability of PM regarding the mean size (presented as hydrodynamic diameter), light-scattering intensity (presented as derived count rate) and size distribution (presented as PDI) during 7 days of storage at 37 °C. For all the aforementioned analyses, PM showed a high stability at the initial drug to polymer ratio (w/w) of 0.1 (Figure 17 A to C). Moreover, TEM images of the PM based on different polymer variants showed no obvious aggregation, which further confirms the observed stability of the PM as demonstrated by DLS analysis (Figure 17).

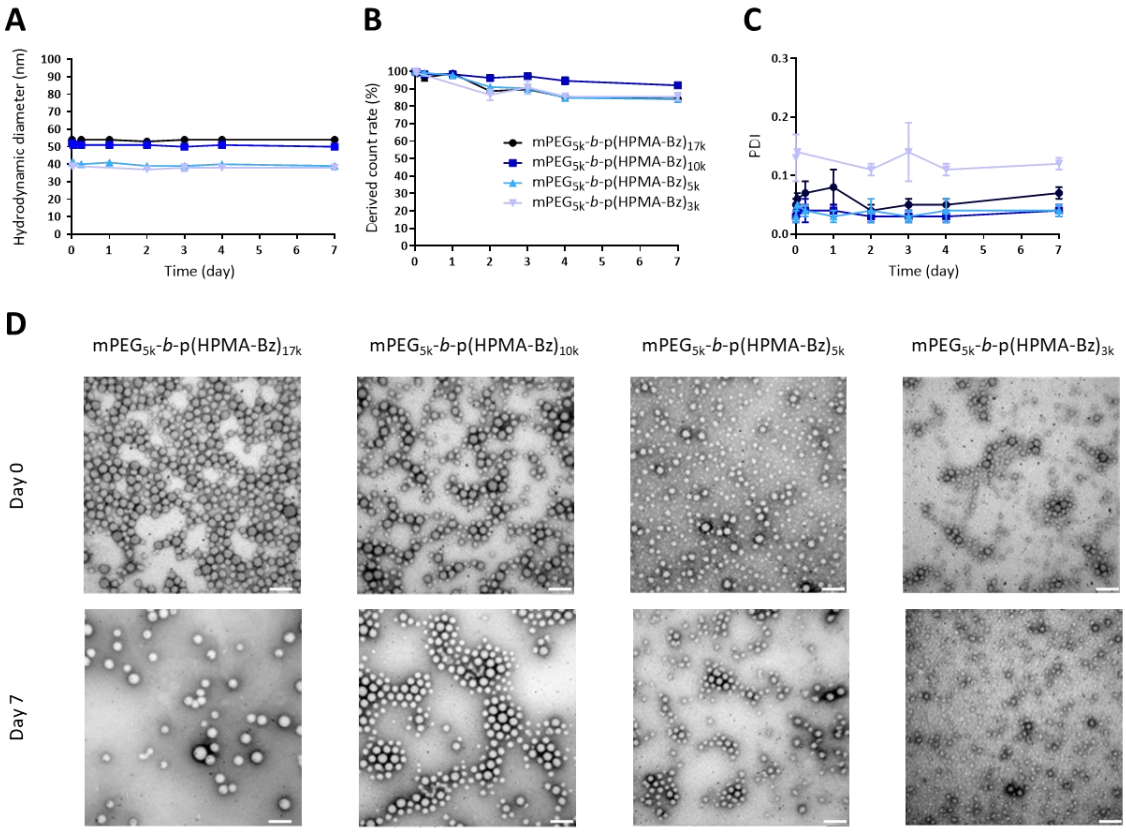

Figure 17. Stability of the PTX-loaded PM based on different mPEG$_{5k}$-*b*-p(HPMA-Bz). PM were prepared with initial drug to polymer ratio of 0.1 and stored at 37 °C for 7 days to evaluate A) Mean size, B) Derived count rate, C) PDI, and D) Morphology (size bar is 100 nm). In Figures A, B and C, data are presented as mean ± SD of three independent replicates (n = 3) (Sheybanifard et al., 2020).

The stability of PTX-loaded PM were also examined at two other temperatures, namely 25 and 4 °C for 5 weeks (Figures 18 A to J). The obtained results point to a higher PM stability in terms of both drug retention and mean size once they are stored at 4 °C. At this temperature, PM were most stable with the polymer type or drug to polymer ratio slightly affecting PTX stability (Figures 18B, 18D, 18F). Storing the PM at 25 °C show an intermediate stability in comparison to 4 and 37 °C. At 25 °C, the overall drug retention of the PM based on the polymer with the shortest hydrophobic block (i.e., mPEG$_{5k}$-*b*-p(HPMA-Bz)$_{3k}$) was inferior compared to the PM based on the longest hydrophobic block (i.e., mPEG$_{5k}$-*b*-p(HPMA-Bz)$_{17k}$) (Figure 18G). In terms of mean size, however, only the PM based on the longest hydrophobic block (i.e., mPEG$_{5k}$-*b*-p(HPMA-Bz)$_{17k}$) showed a relatively stable profile

over the 5 weeks of storage whereas PM based on the other 3 variants of the polymer showed instability after to 2-3 weeks of storage (Figure 18I).

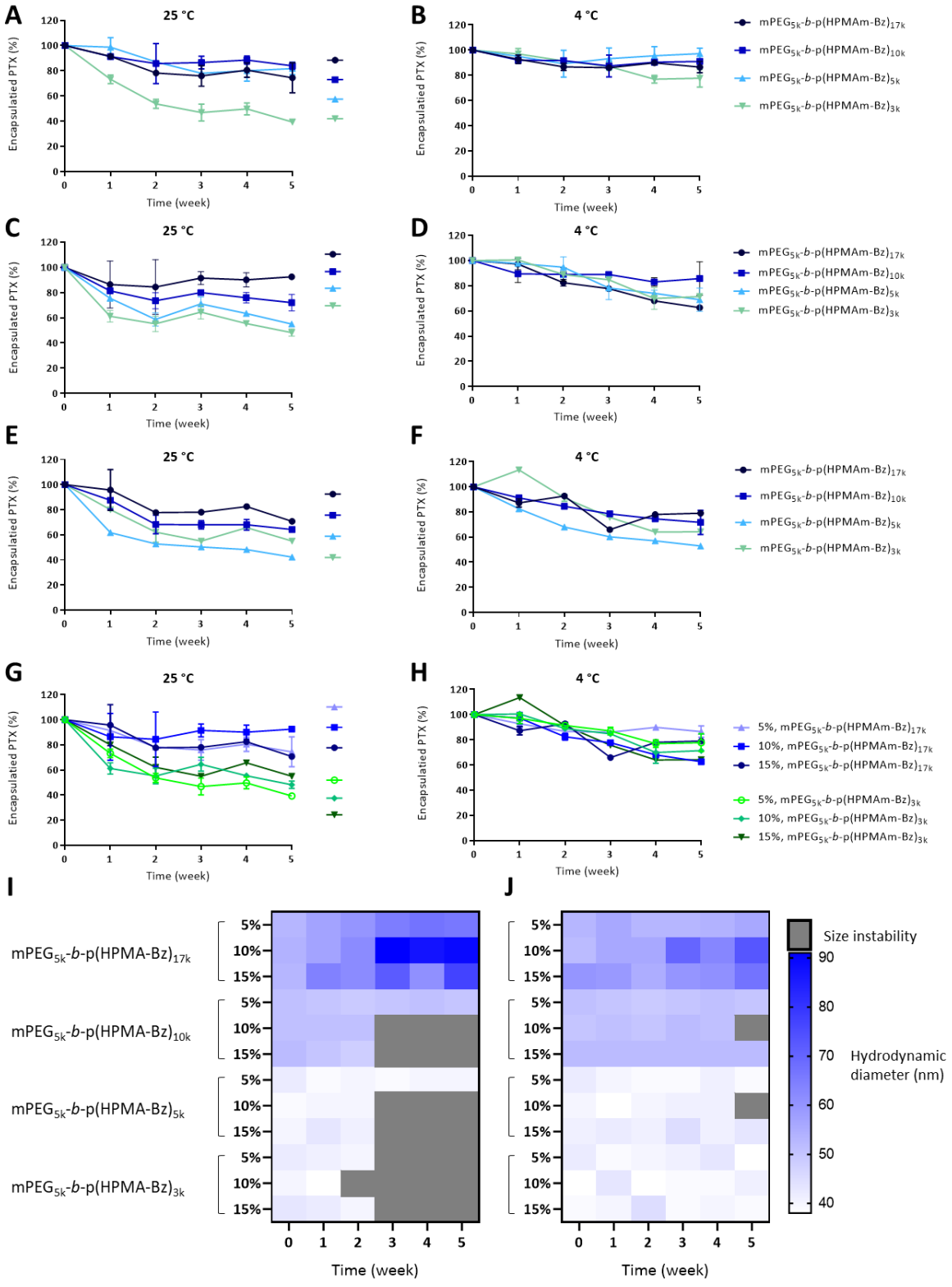

Figure 18. Changes in drug retention and size of PM when stored at 25 and 4 °C for 5 weeks. PM of all four

polymers were stored at 25 °C while loaded with A) 5%, C) 10%, and E) 15% PTX or stored at 4 °C with B) 5%, D) 10%, and F) 15% PTX loading. The PTX retention of the PM with different initial drug to polymer ratios were compared for the PM based on polymer $mPEG_{5k}$-*b*-$p(HPMA\text{-}Bz)_{17k}$ and $mPEG_{5k}$-*b*-$p(HPMA\text{-}Bz)_{3k}$ at G) 25 °C and H) 4 °C. Heatmaps represents changes in PM size during 5 weeks of storage at I) 25 °C and J) 4 °C (Sheybanifard et al., 2020).

4.2.4. *In vitro* release evaluation of PTX-loaded PM in presence of polysorbate 80 and BSA

We studied the drug release of PTX-loaded PM in 0.2% polysorbate 80 micelles or 4.5% BSA dispersion mediums. Polysorbate 80 micelles can interact with PTX and albumin captures PTX with high protein binding (more than 90%) (Eiseman et al., 1994; Kumar et al., 1993). Therefore, including polysorbate 80 micelles or BSA in the release media improves our understanding of the *in vivo* drug release kinetics. The surfactant nature of polysorbate 80 results in formation of micelles in aqueous media. To validate the absence of any mixed micelles formed during incubation between polysorbate 80 and mPEG-*b*-p(HPMA-Bz), we incubated PM with 0.2 v/v % polysorbate 80 micelles for 7 days and evaluated the dispersion using Malvern DLS. Data show two peaks, one corresponding to polysorbate 80 micelles (mean size of around 10 nm) and the other corresponding to PM (mean size of around 60 nm) (Figure 19). Results obtained with DLS confirmed the absence of any mixed micelles between polysorbate 80 and PM based on mPEG-*b*-p(HPMA-Bz) polymer, indicating that the polysorbate 80 micelles do not disturb the PM based on mPEG-*b*-p(HPMA-Bz) polymer. Moreover, PTX can be captured by the polysorbate micelles only upon its release from the PM.

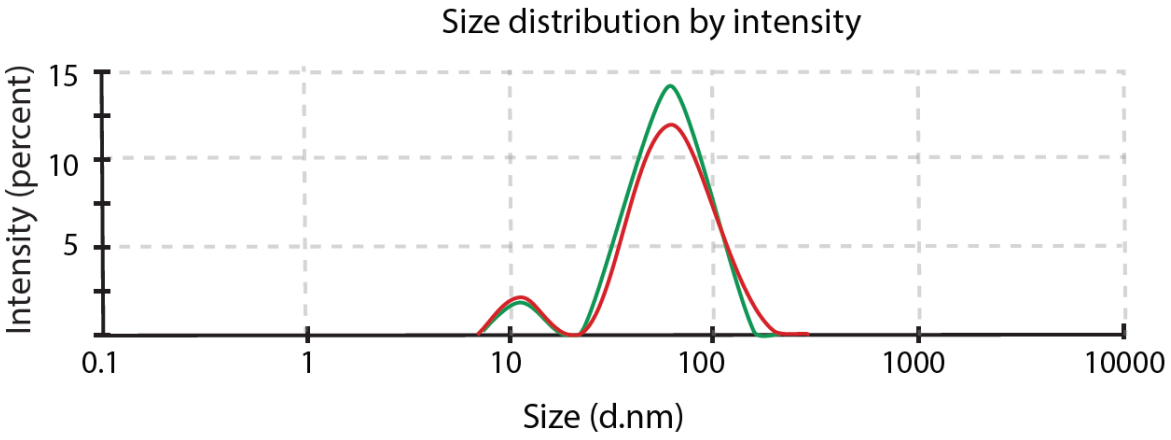

Figure 19. Intensity-based size analysis of the PM based on mPEG$_{5k}$-*b*-p(HPMA-Bz)$_{17k}$ polymer that was incubated with 0.2% polysorbate 80 micelles for 7 days at 37 °C. Two individual peaks were observed that indicate the presence of micelles from polysorbate 80 and PM based on mPEG$_{5k}$-*b*-p(HPMA-Bz) polymer and confirms the absence of mixed micelles (Sheybanifard et al., 2020).

The same experiment was also conducted with PM incubated with PBS/BSA 4.5% w/w. Similar to the results obtained with polysorbate 80, DLS analysis showed two peaks, indicating that the BSA did not disrupt the PM (Figure 20).

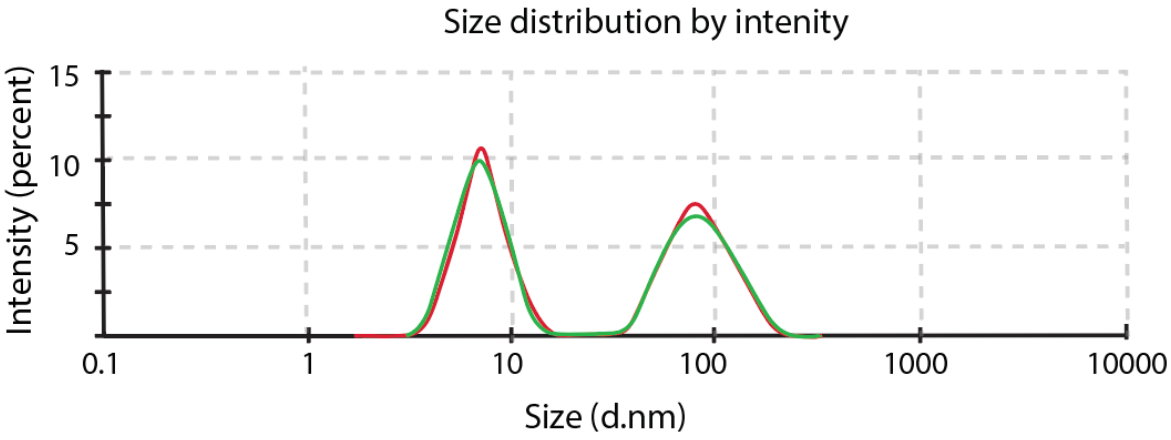

Figure 20. Intensity-based size analysis of the PM based on mPEG$_{5k}$-*b*-p(HPMA-Bz)$_{17k}$ polymer that was incubated with 4.5% PBS/BSA for 7 days at 37 °C. Two individual peaks were observed that indicate the presence of BSA and PM based on mPEG$_{5k}$-*b*-p(HPMA-Bz) polymer.

We started the PTX-release evaluation by preparing PM at initial drug to polymer ratio of 0.1. Independent of the media, we observed a prompt release of PTX from PM within the

first 4 hours (PTX release was between 36 to 69%, depending on the PM variant). Such fast release was followed by a steady release during the following 7 days (Figure 21). In either media, PM based on the shortest hydrophobic blocks size (i.e., mPEG$_{5k}$-*b*-p(HPMA-Bz)$_{3k}$) showed the fastest release. However, once the molecular weight of the hydrophobic block was increased, we observed a slower drug release. Specifically, it was observed that after 7 days of incubation, 72-78% of the loaded PTX was released from PM based on mPEG$_{5k}$-*b*-p(HPMA-Bz)$_{17k}$ and mPEG$_{5k}$-*b*-p(HPMA-Bz)$_{10k}$ while 81-90 % of the loaded-PTX was released from PM based on mPEG$_{5k}$-*b*-p(HPMA-Bz)$_{5k}$ and mPEG$_{5k}$-*b*-p(HPMA-Bz)$_{3k}$ (Figure 21).

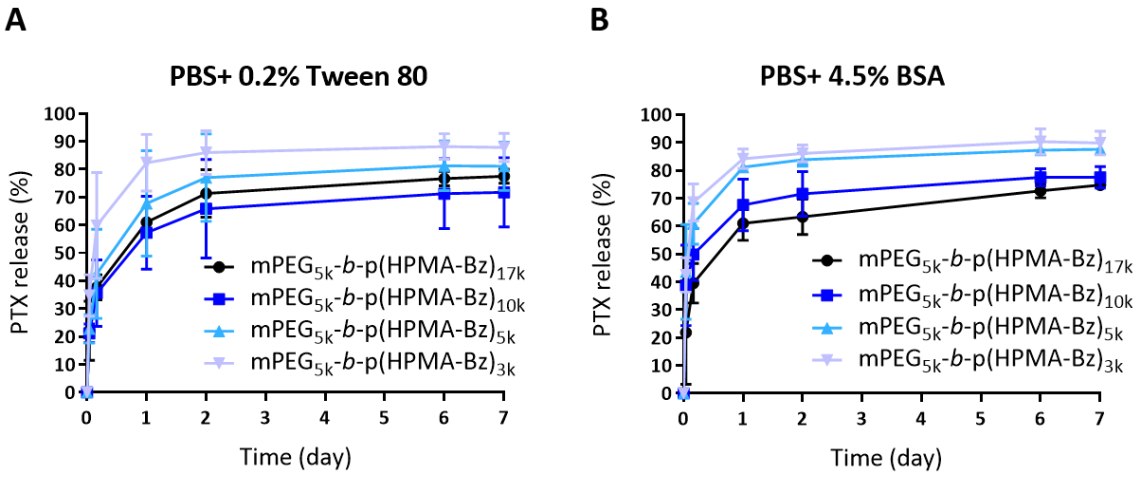

Figure 21. Evaluation of the PTX release from PM based on different mPEG$_{5k}$-*b*-p(HPMA-Bz) variants at 37 °C (initial drug to polymer ratio of 0.1). The release was assessed in A) PBS with 0.2% polysorbate 80 micelles or B) PBS with 4.5% BSA. Data are presented as mean ± SD of three independent replicates (Sheybanifard et al., 2020).

Besides evaluating the PTX release in different media, we studied the effect of the initial drug to polymer ratio (w/w) on the drug release profile of PM. To this end, we prepared PTX-loaded PM based on different polymer variants and investigated the release in the presence of 4.5% BSA containing medium (7 days at 37 °C). The drug release was compared for the PM based on polymers with the longest and the shortest hydrophobic blocks at drug to polymer ratio of 0.05, 0.1, and 0.15. The obtained data indicated the independency of PTX release from the initial drug to polymer ratio in both formulations (Figures 22).

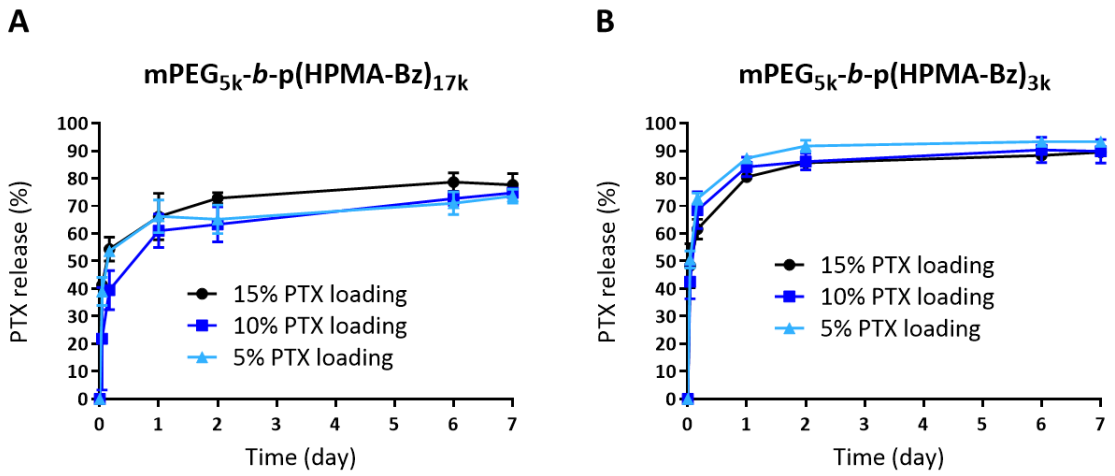

Figure 22. Evaluation of PTX release from PM with varying initial drug to polymer ratios in PBS with 4.5% BSA medium (37 °C for 7 days). The release was performed for PM based on A) $mPEG_{5k}$-*b*-$p(HPMA\text{-}Bz)_{17k}$ and B) $mPEG_{5k}$-*b*-$p(HPMA\text{-}Bz)_{3k}$ variants. Data are presented as mean ± SD of three independent replicates (Sheybanifard et al., 2020).

4.2.5. Evaluation of the effect of PM mean size on the uptake by tumor cells cultured in 2D

We investigated the effect of Cy3-labeled PM mean size on their uptake by cancer cells. To this end, we cultured monolayer-grown PC3 prostate cancer cells and HepG2 hepatocellular carcinoma cells and used PH Rodo dextran green to label the endosome. As depicted in Figure 23, after two hours of incubation, both cell types internalized the PM based on $mPEG_{5k}$-*b*-$p(HPMA\text{-}Bz)_{17k}$ (PM were partially co-localized with the endosomal staining). There were minor differences in the uptake of the differently sized PM in PC3 cells (Figure 23). Interestingly, HepG2 cells, showed a relatively higher PM uptake compared to PC3 cells. This was more pronounced with PM based on the polymer with the short hydrophobic block (i.e., $mPEG_{5k}$-*b*-$p(HPMA\text{-}Bz)_{5k}$ and $mPEG_{5k}$-*b*-$p(HPMA\text{-}Bz)_{3k}$).

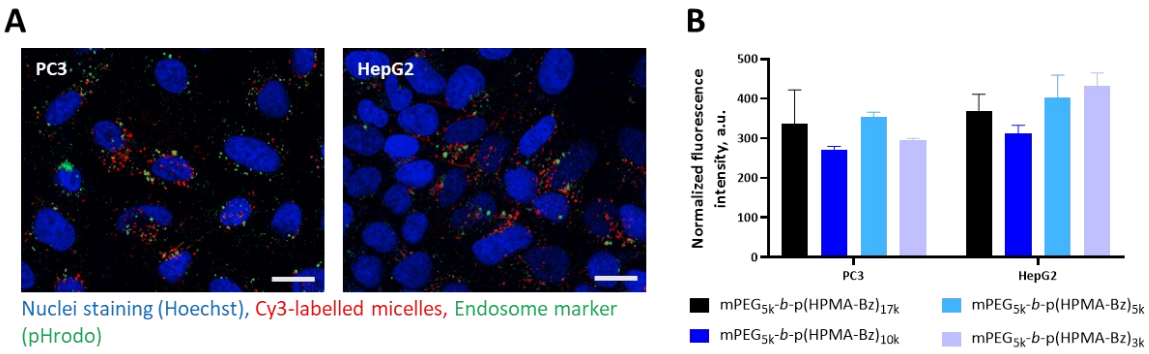

Figure 23. In vitro uptake of PM by PC3 and HepG2 cells in 2D culture. A) Examples of attained confocal microscopy images after 2 hours of incubation of Cy3-labeled PM based on mPEG$_{5k}$-*b*-p(HPMA-Bz)$_{17k}$ with PC3 and HepG2 cells; Red: PM label, blue: nuclei stained with Hoechst 33342, and green: endosomes labeled with pHrodoTM green; size bar 10 µm. B) Fluorescence intensity associated with PC3 and HepG2 cells after incubation with PM based on four different mPEG$_{5k}$-*b*-p(HPMA-Bz) block copolymers for four hours. Fluorescence intensity was normalized by subtraction of baseline fluorescence of non-treated cells. Data are presented as mean ± SD of independent replicates (n = 3) (Sheybanifard et al., 2020).

4.2.6. Evaluation of the effect of PM mean size on their penetration into 3D cultured tumor tissue

In order to investigate the effect of mean size of mPEG$_{5k}$-*b*-p(HPMABz) PM on tumor tissue penetration, we prepared two different culture media with different degree of complexity: a) microspheroids from HepG2 cells that were grown in low attachment Elplasia microplate and b) hydrogel embedded HepG2 3D cultures in OrganoPlate.

To study the PM penetration into the microspheroids, we incubated PM based on four different mPEG$_{5k}$-*b*-p(HPMA-Bz) block copolymers with HepG2 microspheroids (approximate diameter of 50-100 µm) and imaged with confocal microscopy. Evaluating the PM penetration into the tumor microspheroids after 4 hours of incubation showed minor differences in the penetration of PM based on four polymer variants and with different mean size. In general, we observed a relatively higher PM penetration in case of PM based on the polymers with longer hydrophobic block sizes (i.e., mPEG$_{5k}$-*b*-p(HPMA-Bz)$_{17k}$ and mPEG$_{5k}$-*b*-p(HPMA-Bz)$_{10k}$). Furthermore, we investigated the penetration kinetics for the PM based on mPEG$_{5k}$-*b*-p(HPMA-Bz)$_{17k}$ using live imaging over time. Data show a deeper

penetration of the PM in microspheroids over time (Figure 24). Here, the periphery of the microspheroid was the major contributor of the fluorescence intensity signal in the first 1-2 hours. After 4, 8, and 16 hours of incubation, however, most of the fluorescence intensity signal was originated in the central parts of the micro spheroid.

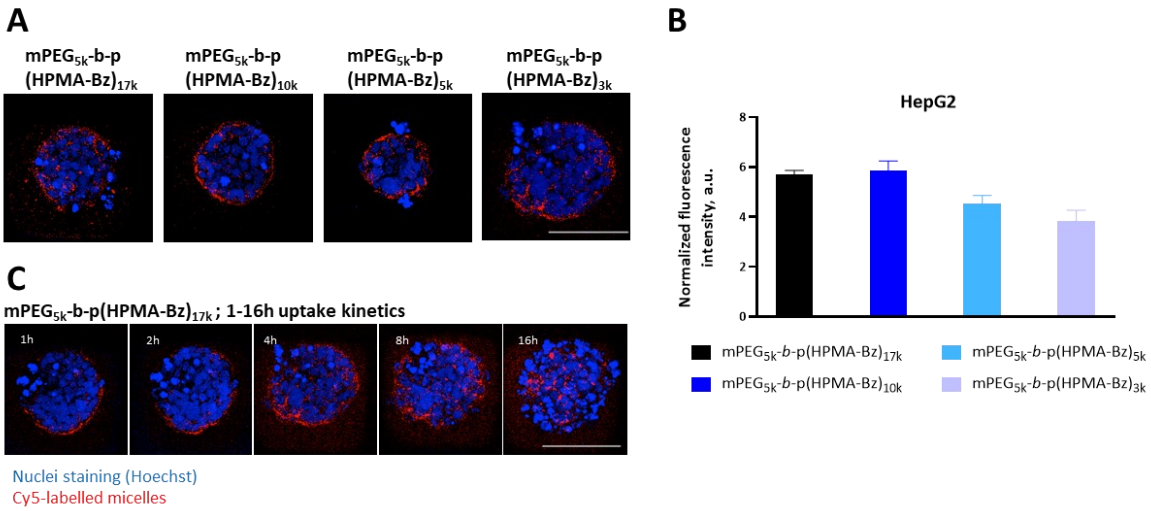

Figure 24. PM penetration into HepG2 microspheroids. A) Representative examples of maximum projection images of acquired Z stacks showing the penetration of Cy5-labeled PM into the HepG2 microspheroids (after 4 hours of incubation at 37 °C). B) Cy5 fluorescence intensity detected in the microspheroids that is normalized by subtraction of baseline fluorescence of non-treated wells (microspheroids were incubated with PM for 4 hours). Data are presented as mean ± SD of independent replicates (n = 3); C) Penetration kinetics of PM based on mPEG$_{5k}$-*b*-p(HPMA-Bz)$_{17k}$ polymer (representative images); Red: PM label, blue: nuclei stained with Hoechst 33342, size bar 100 µm (Sheybanifard et al., 2020).

To evaluate the ability of PM to penetrate into the extracellular matrix surrounding tumor cells, we used the hydrogel embedded HepG2 3D cultures in OrganoPlate. PM based on all four variants of the polymer were prepared and incubated with HepG2 cells seeded in OrganoPlate and confocal microscopy imaging was performed after 4 hours and 24 hours of incubation with cells (Figure 25, representative images for each formulation).

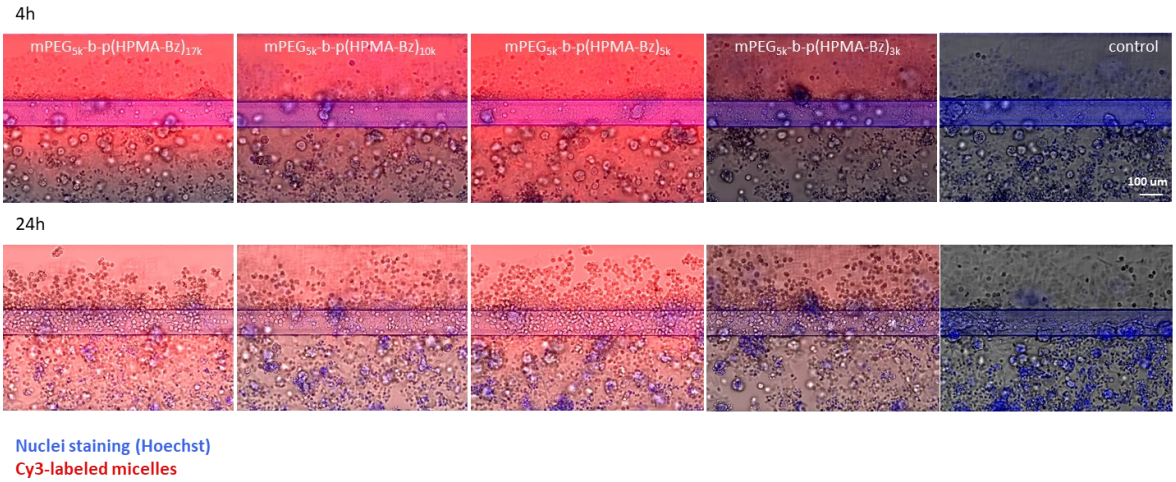

Figure 25. Cy3-labeled PM penetration into 3D cultured gel embedded HepG2 in OrganoPlate. Representative examples of confocal microscopy images after 4 hours (top) and 24 hours (bottom) of incubation. It shows channels geometry of the OrganoPlate and image fields used for Cy3 intensity analysis. Red: PM label, blue: nuclei stained with Hoechst 33342, size bar 100 µm (Sheybanifard et al., 2020).

The obtained data show that after 4 hours of incubation, PM based on mPEG$_{5k}$-*b*-p(HPMA-Bz)$_{5k}$ present the highest fluorescence signal at the deepest gel layers (400 and 500 µm). After 24 hours, the differences were minimal and PM formulations based on all polymer variants showed approximately the same gel penetration behavior. Here, PM based on mPEG$_{5k}$-*b*-p(HPMA-Bz)$_{3k}$ showed minimal gel penetration at all depths and at both time points (Figure 26).

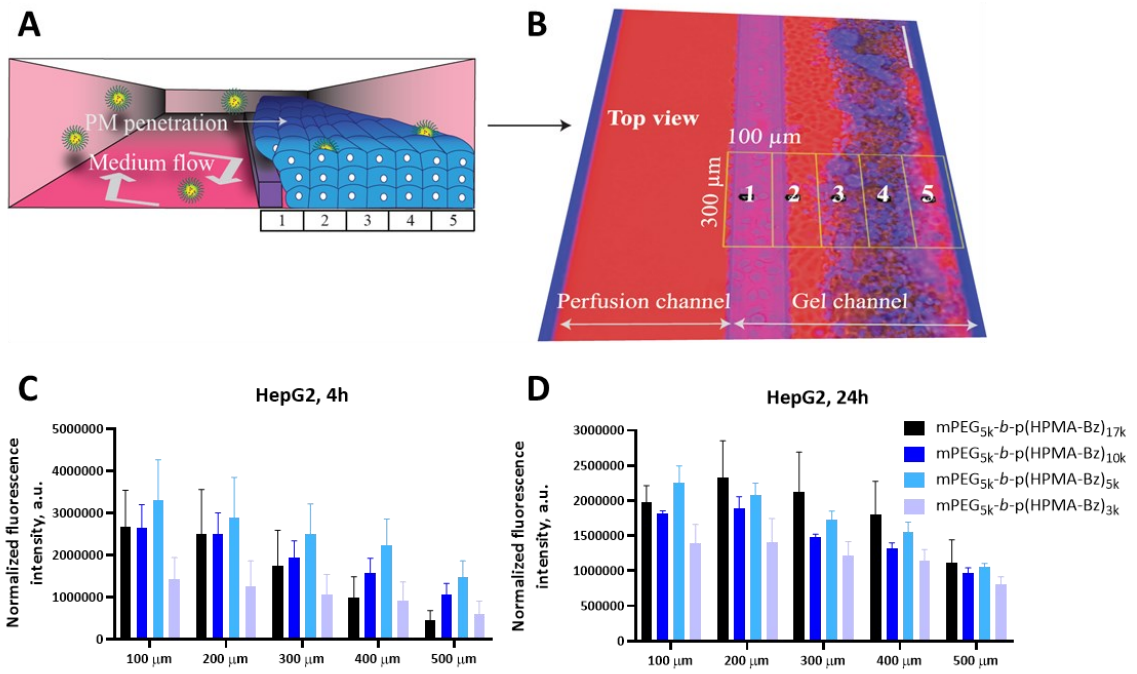

Figure 26. PM penetration into 3D cultured gel embedded HepG2. A) A schematic view of PM penetration in HepG2 cells seeded in OrganoPlate. B) Top view of the PM penetration. A representative confocal microscopy image of gel embedded HepG2 in OrganoPlate in the presence of Cy3-labeled PM in 5 depth layers (after 4 hours of incubation). Red: PM label, blue: nuclei stained with Hoechst 33342, size bar 200 µm. C) and D) Normalized Cy3 fluorescence intensity detected in the 300 µm by 100 µm regions of the gel after C) 4 and D) 24 hours of continued perfusion of PM through the medium channel. Data are normalized by subtraction of baseline fluorescence of non-treated cells and presented as mean ± SD of independent replicates (n = 3) (Sheybanifard et al., 2020).

4.3. Continuous flow manufacturing of liposomes

After successful synthesis and purification of the mPEG$_{5k}$-*b*-p(HPMA-Bz) PM polymer building block and having elucidated the key physicochemical characteristics of the polymer building block that determine critical quality attributes of PM, in the following section we focus more on the overall nanoparticle composition and on key process parameters during manufacturing, both of which are equally important in controlling the critical quality attributes. For this assessment we evaluated another nanoparticle type, namely liposomes. To better understand the key composition and manufacturing process parameters that

determine the final liposome critical quality attributes, we designed and tested a novel continuous flow manufacturing setup (Figure 27).

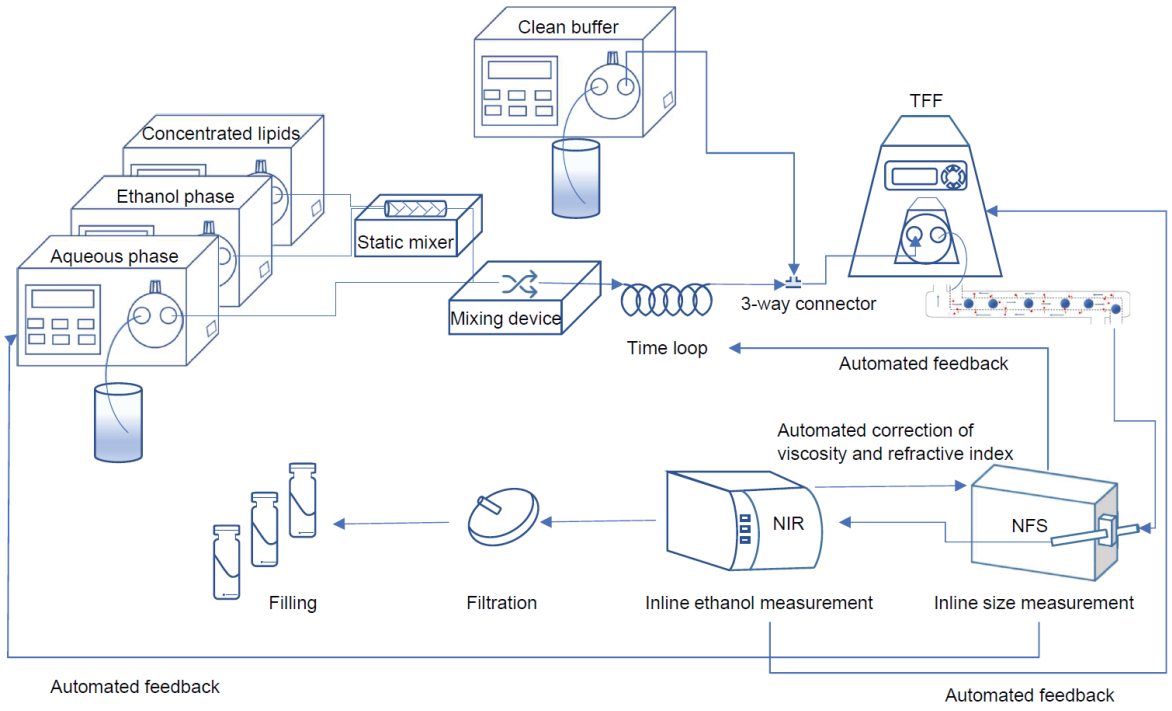

Figure 27. Continuous flow manufacturing of therapeutic nanoparticles. Liposomes were prepared using a millifluidic device and processed for purification, characterization and in-line control of critical quality attributes in a coherent continuous system. Reproduced from Ref. (Sheybanifard et al., 2023) with permission from the Royal Society of Chemistry.

The initial step in CFM manufacturing of liposomal drug products is to actually form the liposomes. Liposomes were formed using DSPE-PEG-2000, EPC, and cholesterol at a molar ratio of 5:60:35 respectively (Materials and methods section 3.5.1). We chose a millifluidic device to produce the liposomes in an uninterrupted approach. After formation, the dispersion requires rapid alcohol clearance and removal of unencapsulated drug. To this end, we chose a purification unit (i.e., a tangential flow filtration (TFF) unit). To assess and control the product's quality, it is crucial to continuously monitor critical quality attributes of the liposomes (e.g., particle mean size and residual ethanol content) in real time while the system is running. Ultimately, a parenteral liposomal product requires sterilization as the final step (Figure 27).

4.3.1. Design and production of a millifluidic device: PTFE tubing fixed by polydimethylsiloxane lithography

As mentioned above, the actual liposome formation is the first step in the manufacturing of a final liposomal product. To form liposomes, a millifluidic mixing device was assembled roughly in line with a previous study (Costa et al., 2016) that connected two channels with predefined dimensions (Materials and methods section 3.5.1). The first device we designed was made using polydimethylsiloxane (PDMS) lithography method (Figure 28).

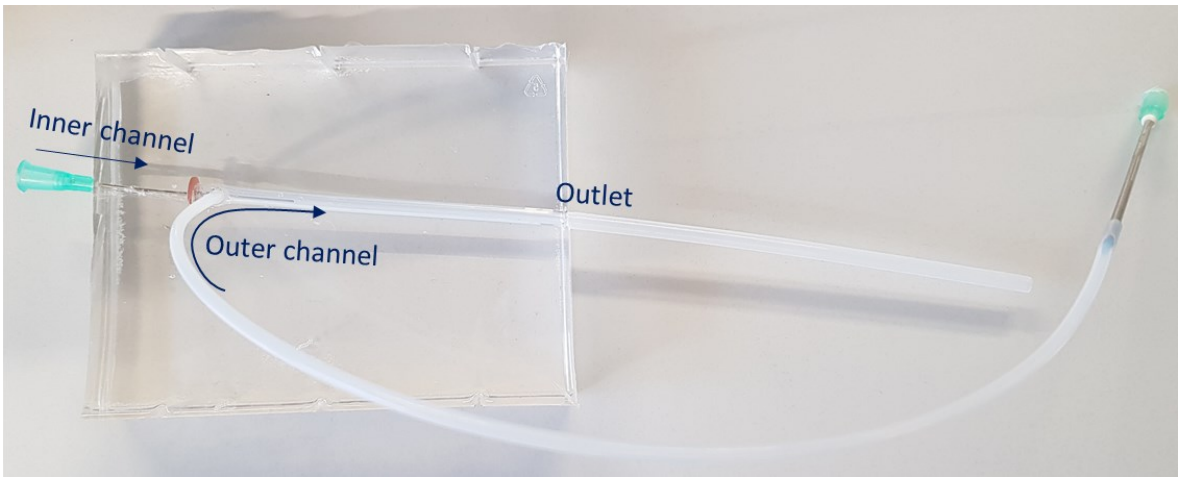

Figure 28. Liposome forming millifluidic device made by PDMS lithography method. Lipids that are dissolved in the organic phase would flow through the inner channel (the needle inserted in PDMS) and the aqueous phase flows through the outer channel (made from PTFE tubing). Formed liposome dispersion leaves the device from an outlet which is the extension of the outer channel.

Over time, however, we observed leakage of materials from the intersection of the inner channel (the needle) and the outer channel (the PTFE tubing). Therefore, the device required to be repaired and/or modified. Nevertheless, liposome dispersions were prepared and assessed with the device to check the effect of composition and process parameters on their characteristics after removal of the organic solvent.

4.3.2. Design and production of a millifluidic device: PTFE tubing fixed by a supporting structure

Using the same dimensions (Costa et al., 2016), the millifluidic device was modified with the addition of a concrete structure to support the channels (Figure 29). With the newly

assembled device, we aimed to evaluate the impact of composition and process parameters on the liposome key quality attributes in the presence of the ethanol as the organic solvent. To achieve this aim, we prepared a range of liposomal dispersions.

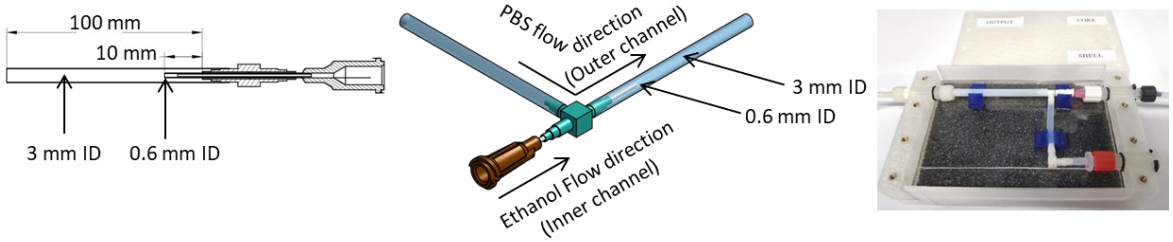

Figure 29. Liposome forming millifluidic device made by PTFE tubing fixed by a supporting structure. Lipids that are dissolved in the organic phase would flow through the inner channel (the needle) and PBS flows through the outer channel (PTFE tubing). Formed liposome dispersion leaves the device from an outlet which is the extension of the outer channel. Reproduced from Ref. (Sheybanifard et al., 2023) with permission from the Royal Society of Chemistry.

4.3.3. Effect of composition and process parameters on liposomes characteristics. Part I: evaluation of the liposome dispersions in the presence of the organic solvent

Liposome dispersions were formed and the mean particle size and PDI were measured before removal of the organic solvent using a spatially resolved dynamic light scattering device (i.e., NanoFlowSizer device). As shown in Figure 30, the liposome mean size decreased upon using high TFRs and low lipid concentrations. By decreasing the TFRs and increasing lipid concentration, liposome mean size increased from below 100 nm to above 150 nm (Figure 30A, blue area). Across this range, liposomes were fairly monodisperse with PDIs below 0.25 (Figure 30B blue/green areas). Further decreasing the TFR and increasing lipid concentrations resulted in PDIs above 0.25 (Figure 30B green/red areas). In this range, intensity-based graphs of NFS showed multiple populations of particles in the dispersion (data not shown). The obtained models from the DoE software were significant (p-value < 0.0001) with R^2 of 0.89 (for size) and 0.92 (for PDI) (Table 11).

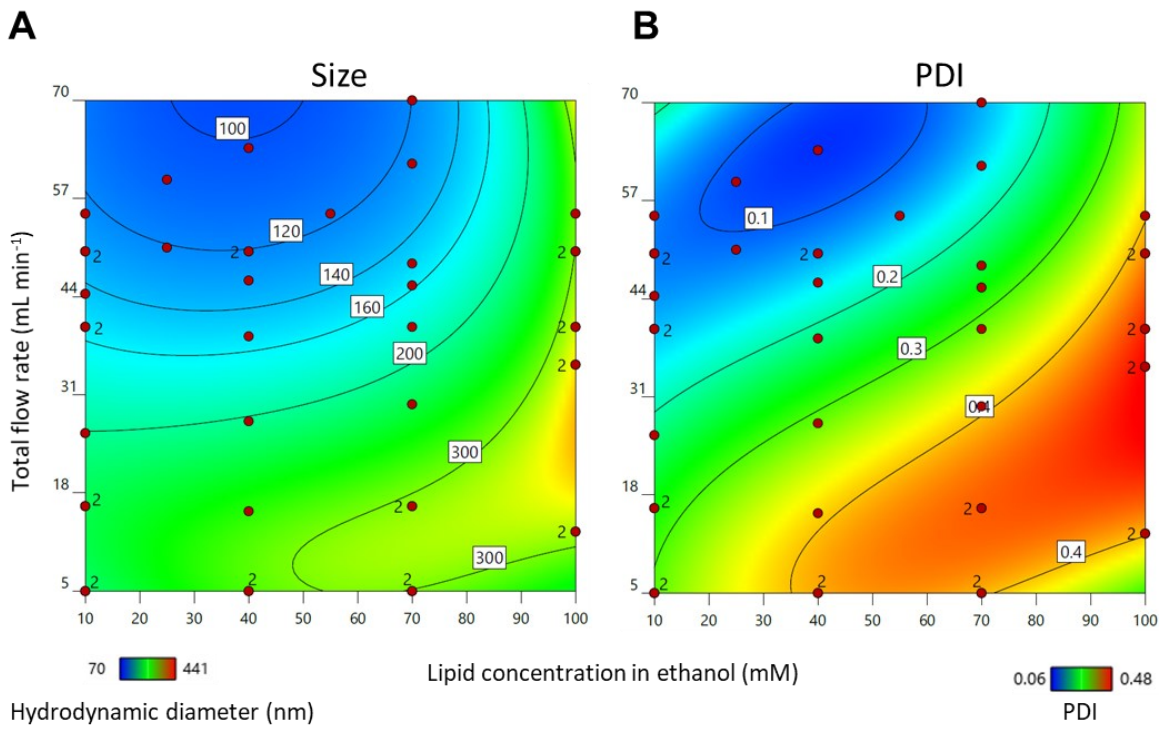

Figure 30. Heatmaps of response surface model obtained from liposome dispersions that were prepared by millifluidic device made by PTFE tubing fixed by a supporting structure and in the presence of the organic solvent. Panel A) Presents the mean size (hydrodynamic diameter in nm) and B) Presents the PDI of the liposomes in relation to the lipid concentration (x axis) and the total flow rate (y axis). The ethanol content as a composition parameter was fixed during this experiment and set at 50% v/v ethanol at the point of mixing. In each graph, each red dot represents the results of an individual liposomal formulation. Reproduced from Ref. (Sheybanifard et al., 2023) with permission from the Royal Society of Chemistry.

Table 11. ANOVA analysis for the size and PDI responses corresponding to the heatmap models shown in Figure 30. Data were obtained from liposome dispersions that were prepared with the millifluidic device made by PTFE tubing fixed by a supporting structure and in the presence of the organic solvent (i.e., 50% v/v ethanol at the point of mixing). Reproduced from Ref. (Sheybanifard et al., 2023) with permission from the Royal Society of Chemistry.

ANOVA	Size (50% v/v ethanol)	PDI (50% v/v ethanol)
R^2	0.8885	0.9192
Adjusted R^2	0.8641	0.8984

Predicted R^2	0.8117	0.8538
Lack of fit (p-value)	0.0103	0.0962
Model	Reduced cubic	Reduced cubic
Model significant?	Yes, p-value < 0.0001	Yes, p-value < 0.0001

4.3.4. Effect of composition and process parameters on liposomes characteristics. Part II: evaluation of the liposome dispersions after the removal of the organic solvent

In the previous section, the size and PDI of the liposomes were assessed in the presence of the ethanol and immediately after liposome formation. Prior to initiating subsequent steps, knowing this information enables immediate interventions and early parameter corrections if necessary. However, it is also essential to assess the effect of composition and manufacturing process parameters on liposome size and PDI in the final formulation and after the removal of the ethanol. Therefore, we evaluated these characteristics using a standard Malvern DLS device after dialyzing the liposomes against PBS to remove the residues of the organic solvent. As shown in Figure 31, our results confirm the effect of TFR and lipid content on liposome size and PDI in the absence of the ethanol. Similar to the previous experiment, the liposome dispersions with mean sizes from below 110 nm to above 150 nm were monodisperse with PDIs below 0.15 (Figure 31). The obtained models from DoE software were significant (p-value < 0.0001) with R^2 of 0.71 (for size) and 0.69 (for PDI) (Table 12).

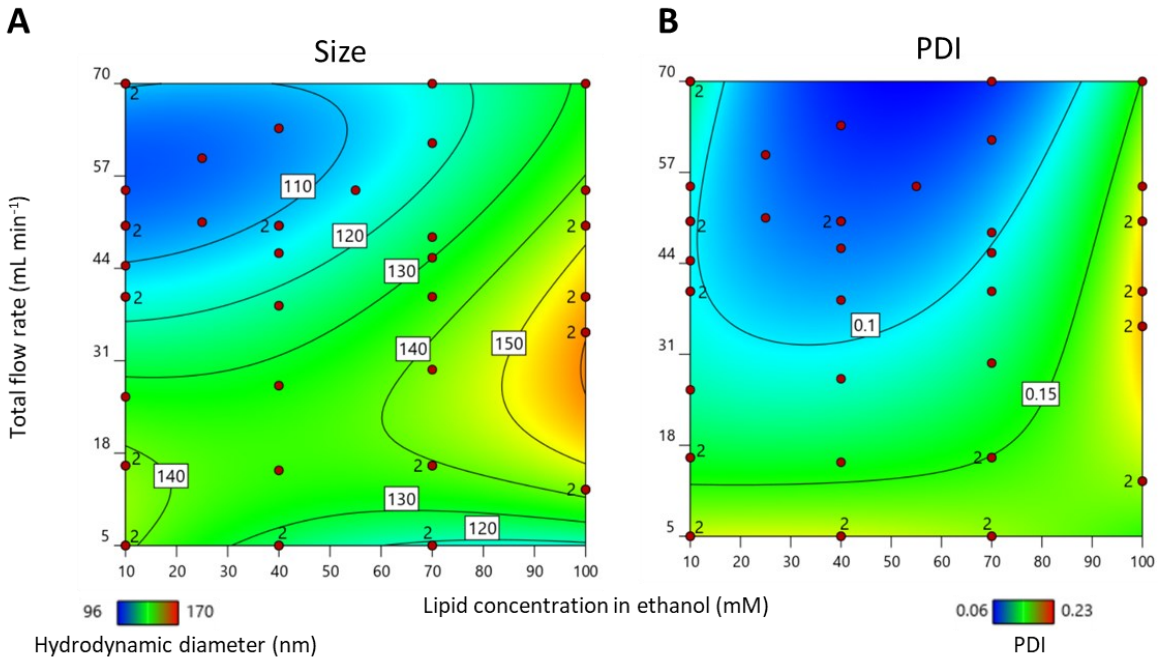

Figure 31. Heatmaps of response surface model obtained from liposome dispersions that were prepared by millifluidic device made by PDMS lithography method and after removal of the organic solvent. Panel A) Presents the mean size (hydrodynamic diameter in nm) and B) Presents the PDI of the liposomes in relation to the lipid concentration (x axis) and the total flow rate (y axis). The ethanol content as a composition parameter was fixed during this experiment and set at 50% v/v ethanol at the point of mixing and the measurements were performed after 2 days of dialysis using standard DLS. In each graph, each red dot represents the results of an individual liposomal formulation.

Table 12. ANOVA analysis for the size and PDI responses corresponding to the heatmap models shown in Figure 31. Data were obtained from liposome dispersions that were prepared by millifluidic device made by PDMS lithography method and after removal of the organic solvent with 50% v/v ethanol at the point of mixing.

ANOVA	Size (50% v/v ethanol)	PDI (50% v/v ethanol)
R^2	0.7112	0.6866
Adjusted R^2	0.6546	0.6442
Predicted R^2	0.5351	0.5240
Lack of fit (p-value)	0.9608	0.0706

Model	Reduced cubic	Reduced cubic
Model significant?	Yes, p-value < 0.0001	Yes, p-value < 0.0001

4.3.5. Evaluation of changes in the liposome size and PDI by changing the ethanol concentration at the point of liposome formation

So far, we have evaluated the critical quality attributes of the liposomes by changing one composition and one process parameter, namely lipid concentration and total flow rate, respectively. In the next experiment, another influential parameter is evaluated, i.e., the ethanol concentration at the point of liposome formation.

Liposome dispersions were prepared at a fixed TFR of 50 mL min^{-1} and fixed final lipid concentration of 25 mM. The ethanol percentages at the point of mixing, however, was unique for each formulation through changing the flow rate of the ethanol stream relative to the aqueous phase stream. As a result, by changing the ethanol concentration at the point of mixing, the flow velocity ratio (FVR) between ethanol and water was altered as well. As shown in Figure 32A, liposome size is at its maximum (i.e., hydrodynamic diameter of 317 nm) when the ethanol percentage at the point of formation is very high (i.e., 76.23% v/v). By decreasing the ethanol concentration at the point of the mixing and consequently decreasing the FVR, smaller liposomes were obtained with a hydrodynamic diameter of around 120 nm (i.e., at 50% v/v and 46.1% v/v of ethanol). Decreasing the ethanol percentage beyond this point led to an increase in size again (hydrodynamic diameter of 136 nm and 210 nm for 23.8% v/v and 18.2% v/v respectively). Analyzing the results regarding the size and PDI revealed that the minimum size and PDI of the liposomes were obtained from the 50% v/v ethanol at the point of mixing (Figure 32).

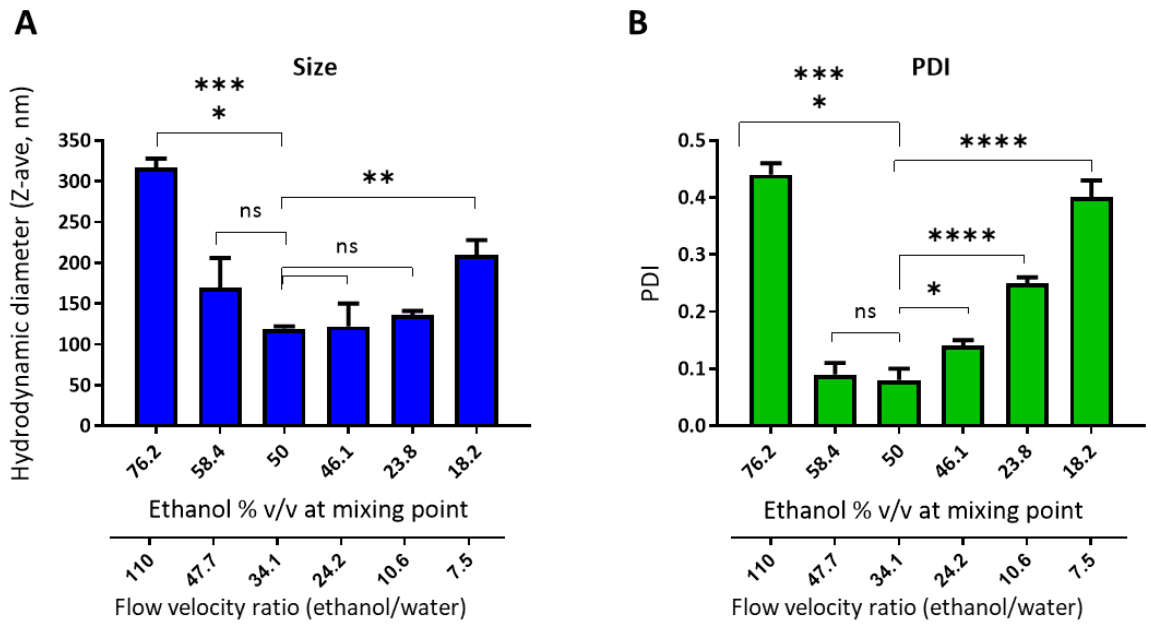

Figure 32. The effect of ethanol content at the point of mixing on A) Liposome size and B) PDI. Liposomes that were prepared with 50% v/v ethanol at the point of mixing demonstrated the minimum size and PDI. Data sets that are significantly different are shown at different levels: * p<0.05, ** p<0.01, *** p<0.001, and ****<0.0001 and data sets that are deemed not significantly different are shown with ns (p>0.05). The liposomal dispersions are prepared at a fixed lipid concentration and a fixed TFR with different ethanol concentrations at the point of formation. Reproduced from Ref. (Sheybanifard et al., 2023) with permission from the Royal Society of Chemistry.

Similar to 50% v/v, the obtained size and PDI at 23.8% and 46.1% v/v ethanol were also promising. Therefore, we selected 30% v/v ethanol as an intermediate value and repeated the same DoE in this condition. Liposomal particles were formed with similar composition and process parameters as described in the previous sections, except for the ethanol content at the point of mixing. In contrast to the previous experiments, we decreased the ethanol content from 50% v/v to 30% v/v (Figure 33). As shown in Figure 33A, the resulting liposome size and PDI were controlled by the lipid concentration and TFR similar to what was shown before. Nevertheless, liposomes that were prepared in lower ethanol percentage condition (i.e., 30% v/v ethanol at the point of mixing) show larger sizes in comparison to their counterparts which were formed at a higher ethanol percentage (e.g., 100 nm in 30% v/v ethanol vs. 80 nm in 50% v/v ethanol). Another major difference

between the two sets is that almost all of the liposomes that prepared with 30% v/v ethanol at the point of mixing show polydispersity with PDI values between 0.2 and 0.5 (Figure 33B). Moreover, the obtained PDIs did not correlate to the changes in TFR and lipid concentrations (Figure 33B). The obtained model for the size graph was significant (p-value < 0.0001) with R^2 of 0.74. Regarding the PDI plot, the model was not significant (Table 13).

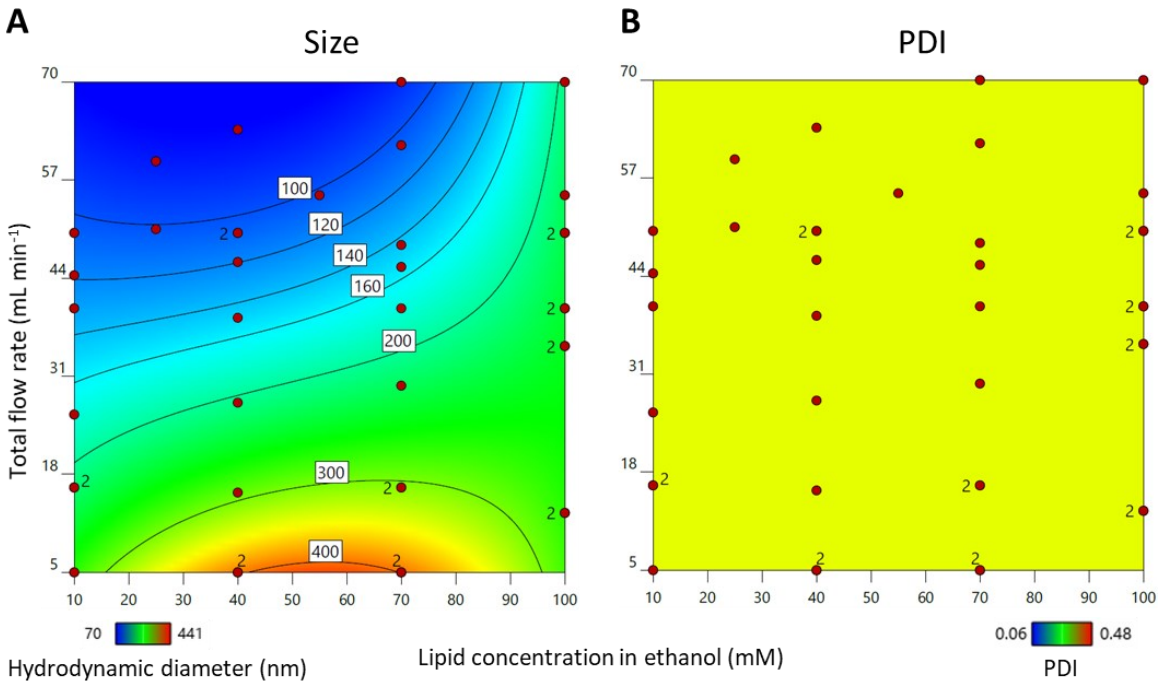

Figure 33. Heatmaps of response surface model obtained from liposome dispersions that were formed with 30% v/v ethanol at the point of mixing. Panel A) Presents the mean size (hydrodynamic diameter in nm) and B) Presents the PDI of the liposomes in relation to the lipid concentration (x axis) and the total flow rate (y axis). The ethanol content as a composition parameter was fixed during this experiment and set at 30% v/v ethanol at the point of mixing. Measurements were performed before removal of the organic solvent using NFS device and in each graph, each red dot represents the results of an individual liposomal formulation. Reproduced from Ref. (Sheybanifard et al., 2023) with permission from the Royal Society of Chemistry.

Table 13. ANOVA analysis for the size and PDI responses corresponding to the heatmap models shown in Figure 32. Data were obtained from liposome dispersions that were prepared by millifluidic device made by PTFE tubing fixed by a supporting structure and in the presence of the organic solvent (30% v/v ethanol at the

point of mixing). Reproduced from Ref. (Sheybanifard et al., 2023) with permission from the Royal Society of Chemistry.

ANOVA	Size (30% v/v ethanol)	PDI (30% v/v ethanol)
R^2	0.7364	0.0000
Adjusted R^2	0.6939	0.0000
Predicted R^2	0.5828	-0.1652
Lack of fit (p-value)	0.2234	0.0056
Model	Reduced cubic	Mean
Model significant?	Yes, p-value < 0.0001	-

4.3.6. Evaluation of changes in the liposome size and PDI as a result of prolonged residence time of the liposome dispersions in high ethanol environment

Interestingly, during our experiments we observed that liposomes size increased over time once they remain in contact with high percentages of ethanol after particle formation and before dialysis. In order to further explore the effect of high ethanol environment on liposome quality attributes, liposomes were formed with 70 mM lipid in ethanol and TFR was set at 62 mL min^{-1} while having 50% v/v ethanol at the point of mixing. Liposomes were kept exposed to this high ethanolic environment for a certain period of time while the size and PDI were continuously monitored. Initially and right after formation, the liposome hydrodynamic diameter was recorded as 83 nm (i.e., at zero time point). As time passed, the size gradually increased until it reached 150 nm after 90 min (Figure 34A). Although the liposome size gradually increased, the PDI remained constant and even modestly decreased (below 0.2). This suggests the presence of a single population of particles in the formulation and that excludes the presence of large aggregates (Figure 34B). We hypothesize that sudden decrease of ethanol concentration halts the growing process. To this end, samples were taken from the dispersion at different arbitrary time points and were diluted with PBS to decrease the ethanol concentration to a very low content (i.e., we attempted to lower

the ethanol concentration down to 5% v/v, Figure 34, black data points). We observed that the liposome size remained unchanged upon dilution. Therefore, we confirmed that the growth in size of the liposomes was a result of their presence in high ethanol environment.

The next step was to systematically evaluate and identify the exact critical ethanol concentration below which no size growth is observed. As shown in Figure 34C, decreasing ethanol concentration resulted in a slower size increase. The maximum increase in size was observed with liposomes prepared with 50% v/v ethanol at zero time point. Once the ethanol content was reduced to 40% v/v at the time point zero, liposome hydrodynamic diameter increased from 86 nm to 110 nm within 60 minutes. At 20% v/v (or less) ethanol at the time point zero, liposome size remained unchanged.

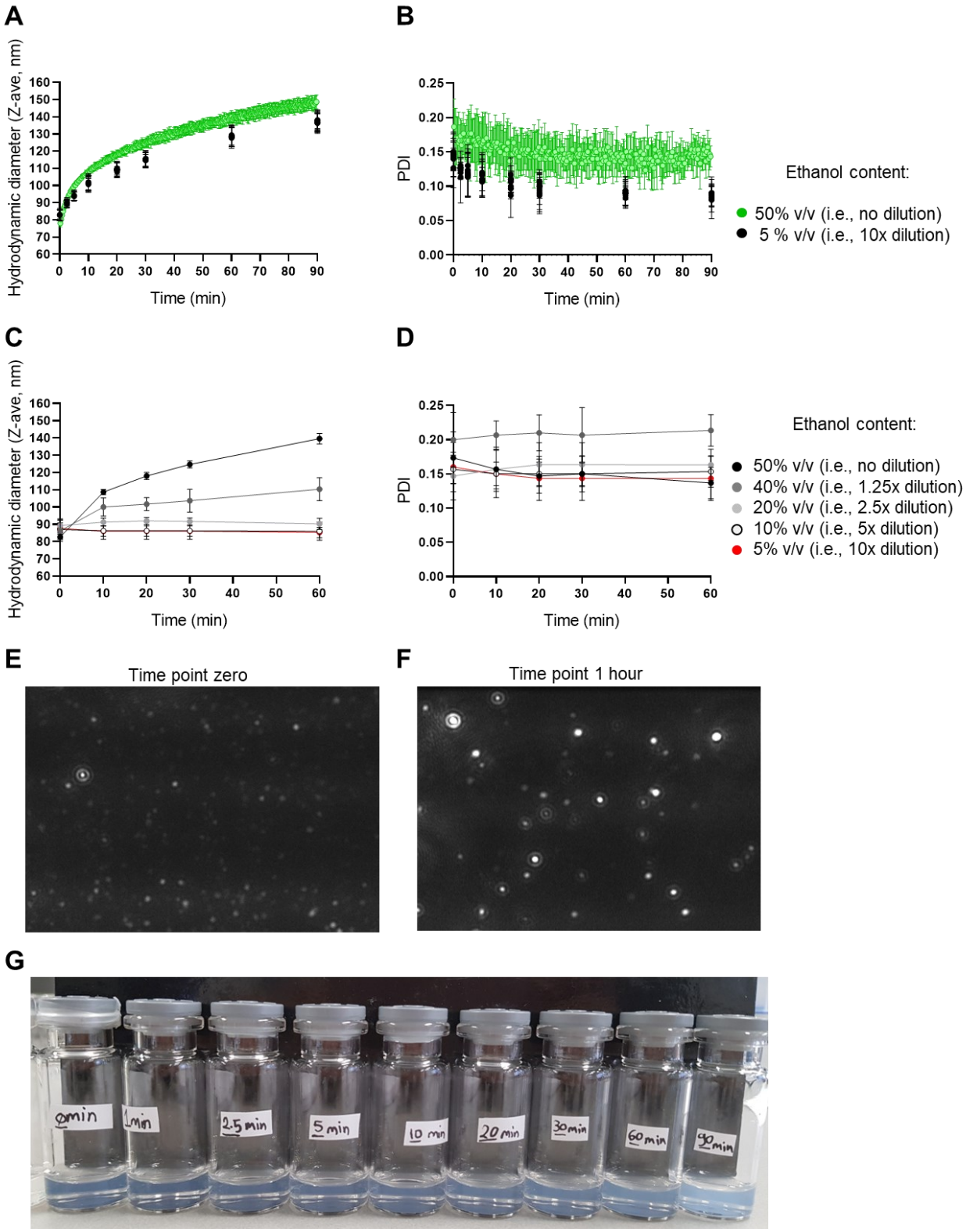

Figure 34. The effect of residence time of the liposomes in high ethanol environment on size and PDI as critical quality attributes. A) Hydrodynamic diameter (size, nm) and B) PDI of liposomes in the presence of 50% v/v ethanol at the time point zero (green dots) and after decreasing the ethanol content to 5% v/v at a

defined time point (black dots). C) Hydrodynamic diameter (size, nm) and D) PDI of liposomes as a result of 1 hour incubation with different initial ethanol concentrations (i.e., 50% v/v to 40, 20, 10, and 5% v/v at the time point zero). E) Time point zero and F) Time point 1-hour representative images of incubating liposomes in high ethanol environment (i.e., 50% v/v). G) Representative image of liposome dispersions depicting the changes in turbidity of the formulation through time. Liposomes were formed with 70 mM lipid in ethanol while the TFR was set at 62 mL min^{-1} (n=3). Reproduced from Ref. (Sheybanifard et al., 2023) with permission from the Royal Society of Chemistry.

To better understand the mechanism behind liposome size growth, an NTA device was used to record the number of the particles in a one-hour video. Liposomes were formed and incubated for one hour in a medium containing 50% v/v ethanol. The obtained results during this hour show that the number of particles decreased over time (Figure 35).

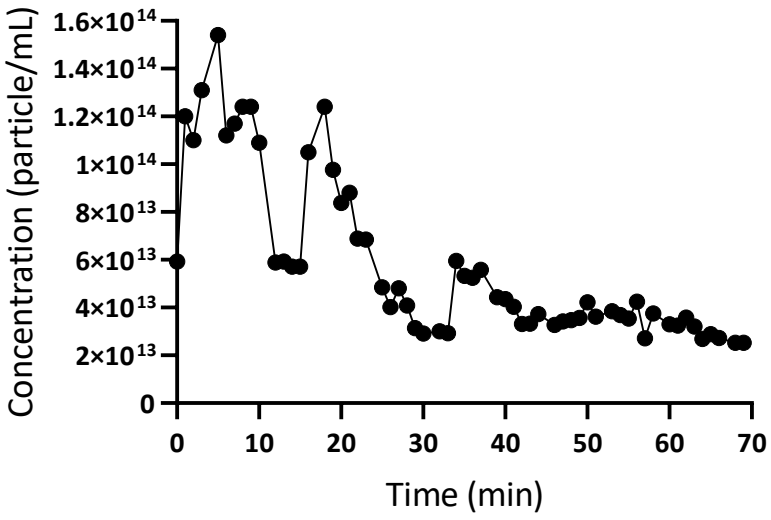

Figure 35. Changes in the concentration of liposomes over time as a result of incubation at high ethanol environment (i.e., 50% v/v ethanol). Liposomal dispersions were diluted 10,000 times with a mixture of PBS and ethanol (one to one ratio) before NTA analysis. Reproduced from Ref. (Sheybanifard et al., 2023) with permission from the Royal Society of Chemistry.

Although understanding the exact mechanism behind the increase in liposome size merits further investigations, based on the obtained results from NFS and NTA, we hypothesize

that a type of vesicle annealing process happens that might be driven by Ostwald-ripening or coalescence mechanism.

4.3.7. Effect of different dilution methods on liposome characteristics

Before the dispersions enters the tangential flow filtration unit, liposome dispersions must be diluted with clean dispersion buffer (PBS in our case). The way by which this dilution is performed may have an impact on the eventual particle characteristics. To assess this possible effect, we tested the liposome size and PDI before and after dilution using a regular three way or a static mixer. The obtained results show that the hydrodynamic diameter of liposomes in both approaches are similar and close to 80 nm (Figure 36A). However, the un-diluted samples showed slightly larger particle sizes after 1 day of dialysis. With regard to the PDI, all samples were monodisperse as indicated by a PDI around or smaller than 0.1 (Figure 36B).

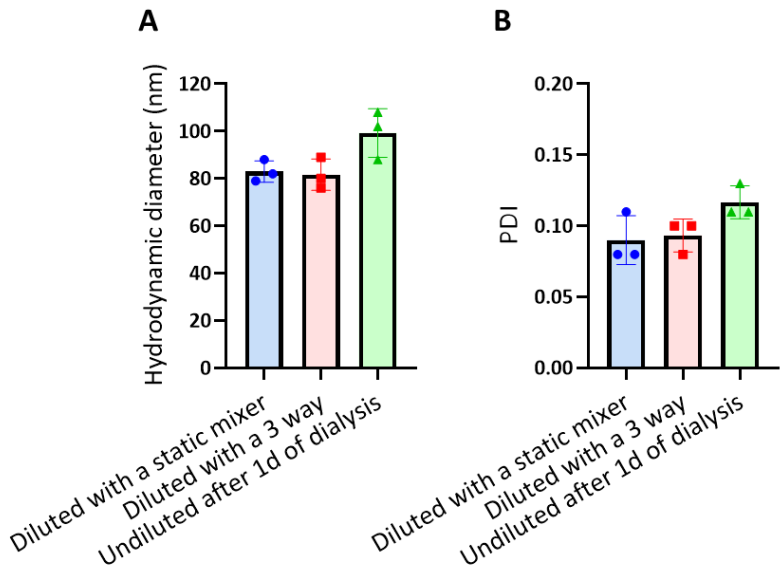

Figure 36. The effect of dilution method on the liposome A) Hydrodynamic diameter (nm) and B) PDI. Liposomes were obtained with similar characteristics regardless of the dilution method. However, the undiluted liposomes show slightly larger particle size. Liposomes were formed with 70 mM lipid in ethanol while the TFR was set at 62 mL min^{-1} and samples were diluted 10 times (n=3).

4.3.8. Removal of the organic solvent using tangential flow filtration

After identifying the key composition and process parameters that determines the liposome critical quality attributes, we sought to explore methods of removing the residual organic solvent and the un-encapsulated drug within the CFM setup. To reach this goal, a tangential flow filtration (TFF) unit was used, and liposome dispersions were purified (Figure 37).

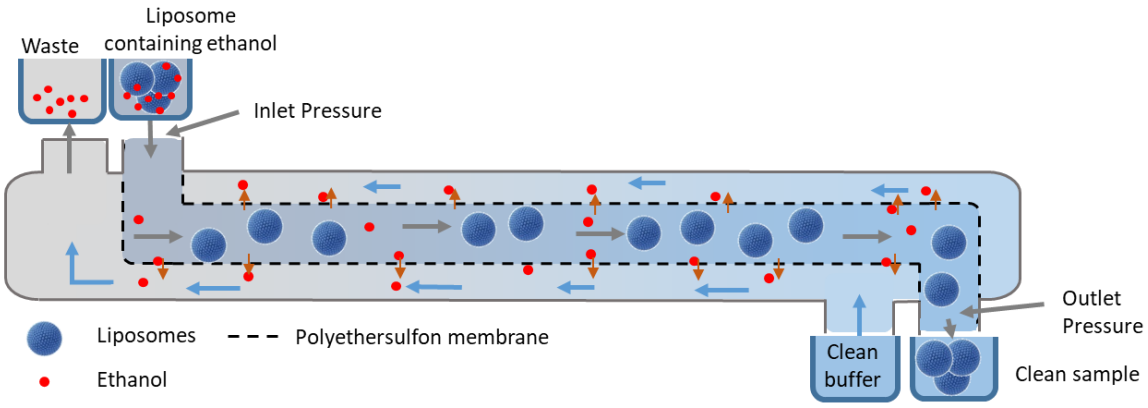

Figure 37. Schematic view of a filtration cassette to purify the liposome dispersion using TFF. Dispersion containing ethanol enters the membrane through an inlet and clean sample leaves the cassette through an outlet. In case a counter current flow is used, a clean buffer flows in an opposite direction and enters the cassette through an inlet that is positioned close to the dispersion's outlet and the counter current leaves the cassette from an outlet that is positioned adjacent to the dispersion's inlet. Reproduced from Ref. (Sheybanifard et al., 2023) with permission from the Royal Society of Chemistry.

4.3.8.1. Utilizing a counter current flow for enhancing the filtration

To study how we could most effectively utilize the TFF device and purify our samples in a CFM setup, we first tested the effect of having a counter current flow in the filtration unit on the purification efficiency of our samples. As depicted in Figure 38, despite our attempts to vary the sample flow rate and the counter current flow rate, the experiment was not successful and almost all the calcein dye was recovered in the outlet under different conditions (Figure 38). Therefore, to improve the purification efficiency, we removed the countercurrent flow and went on with changing other factors such as the pressure and the

surface area of the filtration unit. These experiments are further outlined in the sections below.

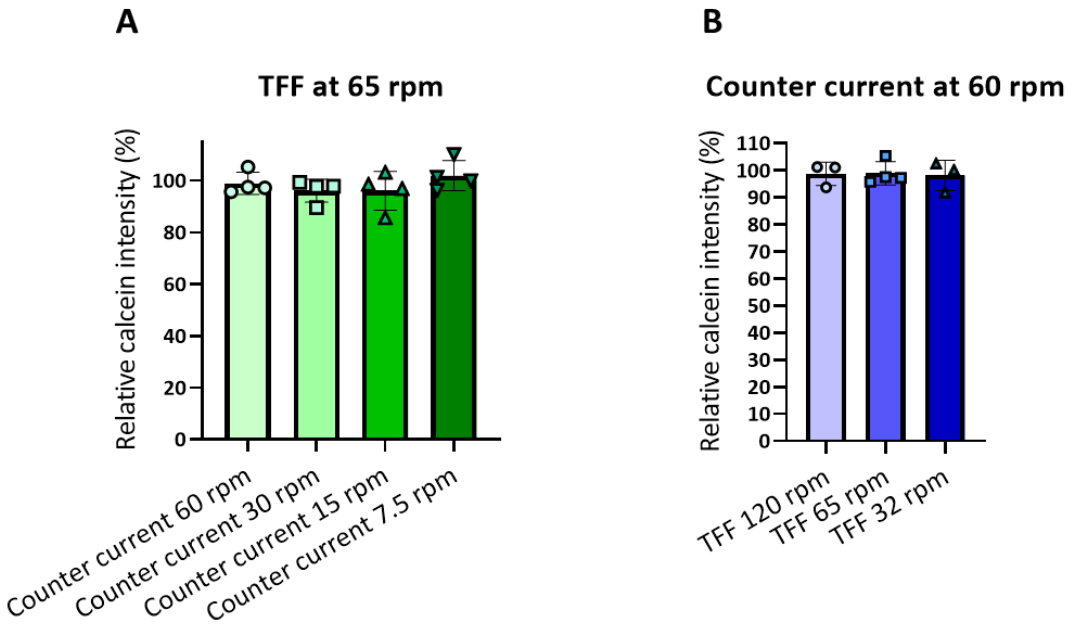

Figure 38. The presence of a counter current of a clean buffer could not improve the filtration efficiency. A) Relative calcein intensity as a function of counter current flow rates. B) Relative calcein intensity as function of sample flow rates.

4.3.8.2. Effect of liposome presence and the filtration unit's surface area on the dispersion purification

To better understand the impact of liposomes on the efficiency of the cleaning process, we first passed water through the filtration unit. As shown in Figure 39, the filtration efficiency of water sample with the smaller surface area (i.e., 50 cm^2) was 14% at the minimum inlet pressure (i.e., 21 kPa) and slightly increased upon increasing the inlet pressure and reached 15% at the maximum tested inlet pressure (i.e., 207 kPa, Figure 39A, light blue bars). When the filtration unit with a larger surface area (i.e., 193 cm^2) was used, the waste volume fraction was 41% at the minimum inlet pressure (i.e., 21 kPa) and 46% at the maximum tested inlet pressure (i.e., 207 kPa, Figure 39A, dark blue bars). Here, the average filtration efficiency of the sample using the surface of 193 cm^2 was 44%. The obtained results show

that in the absence of liposomes, the filtration efficiency of the water sample is significantly increased by increasing the filter surface area while slightly increased by increasing the inlet pressure.

The next step was to evaluate the effect of the presence of liposomes on the filtration efficiency and on the waste volume fraction. As shown in the Figure 39B, with the smaller surface area filtration unit (i.e., 50 cm^2) the waste volume fraction produced from liposome dispersion sample was 9% at the minimum inlet pressure (i.e., 21 kPa) and 5% at the maximum tested inlet pressure (i.e., 207 kPa, Figure 39B, light green bars). When the filtration unit with a larger surface area (i.e., 193 cm^2) was used, the waste volume fraction was 14% at the minimum inlet pressure (i.e., 21 kPa) and 6% at the maximum tested inlet pressure (i.e., 207 kPa, Figure 39B, dark green bars). Similar to the water samples, in the presence of the liposomes, increasing the filter surface area enhanced the filtration efficiency. However, the mere presence of liposomes strongly reduced the filtration efficiency (Figure 39B).

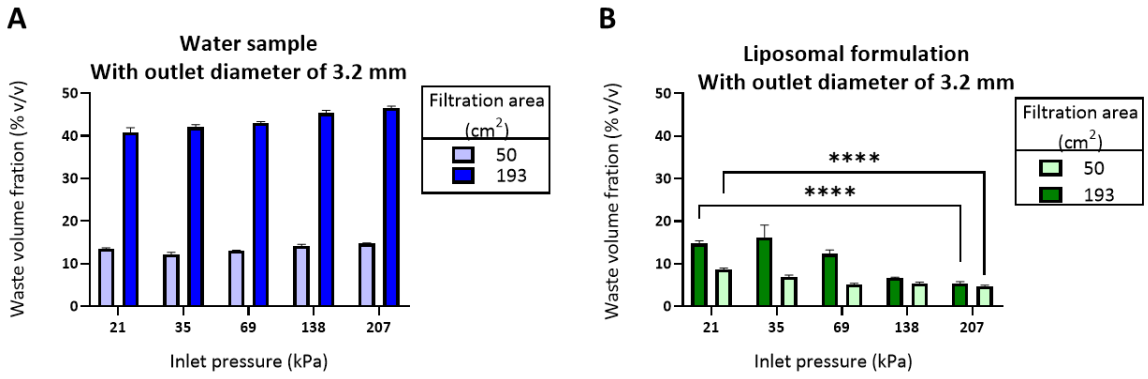

Figure 39. The effect of liposome dispersion, surface area and inlet pressure on filtration efficiency using an open TFF system. A) Effect of surface area and inlet pressure on the waste volume fractions of water B) Effect of surface area and inlet pressure on the waste volume fractions of liposomal dispersion. Data sets that are significantly different are shown at different levels: * p<0.05, ** p<0.01, *** p<0.001, and ****<0.0001 and

data sets that are deemed not significantly different are shown with ns ($p>0.05$, $n=3$). Reproduced from Ref. (Sheybanifard et al., 2023) with permission from the Royal Society of Chemistry.

4.3.8.3. Effect of outlet pressure on liposome purification

So far, the two process parameters that apparently promote the filtration efficiency are large surface area and a minimal inlet pressure. As the next step, we evaluated the effect of the outlet pressure on the filtration efficiency. To this end, we started our experiments by keeping the outlet diameter as is (i.e., 3.2 mm) and measured the outlet pressure. As shown in Figure 40A, the pressure gauge at the outlet diameter of 3.2 mm was recording outlet pressures of 0 kPa, which resulted in having no bars corresponding to the outlet diameter of 3.2 mm in the Figure 40A. In this condition, the waste volume fractions were 15, 16 and 12% for the inlet pressures of 21, 35, and 69 kPa respectively (Figure 40B). Next, we decreased the outlet diameter to 0.5 and 0.2 mm and as a result, the outlet pressure was increased (Figure 40A). At the smallest outlet diameter tested (i.e., 0.2 mm), and at an inlet pressures of 21, 35, and 69 kPa, the outlet pressures increased to 14, 21, and 52 kPa respectively (Figure 40A, dark orange bars). When an inlet pressure of 21 kPa and a 0.2 mm outlet diameter was used, the outlet pressure was 14 kPa resulting in obtaining the maximum waste volume fraction (i.e., 36%). This value is comparable to the corresponding value of water samples in Figure 39A and thus seems to minimize the impact of the presence of liposomes on the filtration efficiency (Figure 40B). Overall, decreasing the outlet diameter increased the outlet pressure, which apparently leads to a more evenly distributed pressure throughout the filtration unit and consequently, results in a higher waste volume fraction. Collectively, the three main parameters that can maximize the filtration efficiency are low inlet pressures, large filtration surface area and adjusted outlet pressure to distribute the pressure equally along the entire filter surface area.

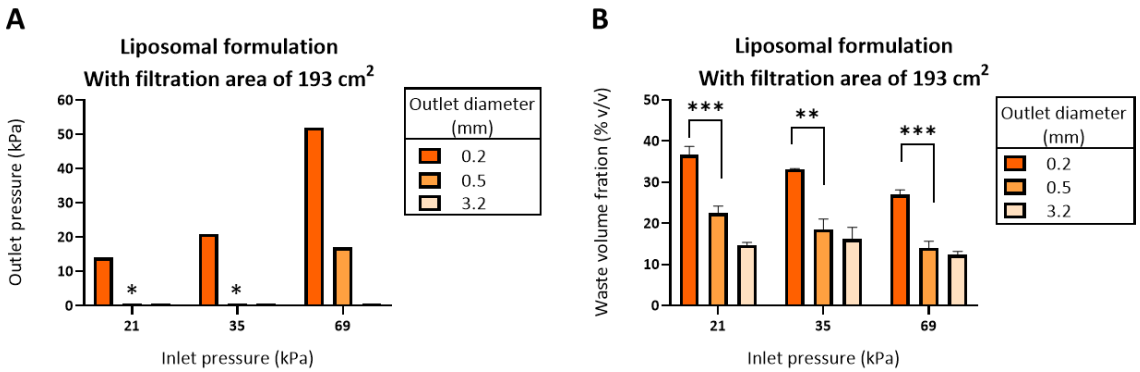

Figure 40. The effect of outlet pressure on filtration efficiency using an open TFF system. A) Outlet pressure of the filtration unit as a function of inlet pressures obtained at different outlet diameters. B) Waste volume fraction as a function of outlet pressures and inlet pressures assessed in liposomes. Data sets that are significantly different are shown at different levels: * p<0.05, ** p<0.01, *** p<0.001, and ****<0.0001 and data sets that are deemed not significantly different are shown with ns (p>0.05). Pressures with a star sign on top of them in panel A) were out-of-range measures (n=3). Reproduced from Ref. (Sheybanifard et al., 2023) with permission from the Royal Society of Chemistry.

4.3.9. In-line measurement of liposome characteristics, size, PDI and ethanol content

4.3.9.1. Probe-based calibration plots of ethanol using NIR spectroscopy

In-line real-time quantification of the liposome properties leads to avoiding batch-to-batch variations and ensures the quality of the finished product. In the current thesis, the key properties that were monitored in real-time were the ethanol content of the formulation, the liposome size and PDI. To measure the ethanol content in-line, an NIR instrument was used. Initially, we confirmed the accuracy and precision of the NIR device in detecting ethanol using a probe by preparing samples of PBS/ethanol with different ethanol contents. Partial least squares multivariate calibration plots were generated using second derivative of NIR absorbance. The obtained calibration curves in both sets of ethanol standards (i.e., from 0.156 to 5% v/v and from 1.56 to 50% v/v ethanol in PBS), showed a very good correlation between the actual ethanol content and the predicted outcomes. Here, the R^2 was 0.998 and 0.999 for the calibration curves obtained from low range and high range of the ethanol standards respectively (Figure 41).

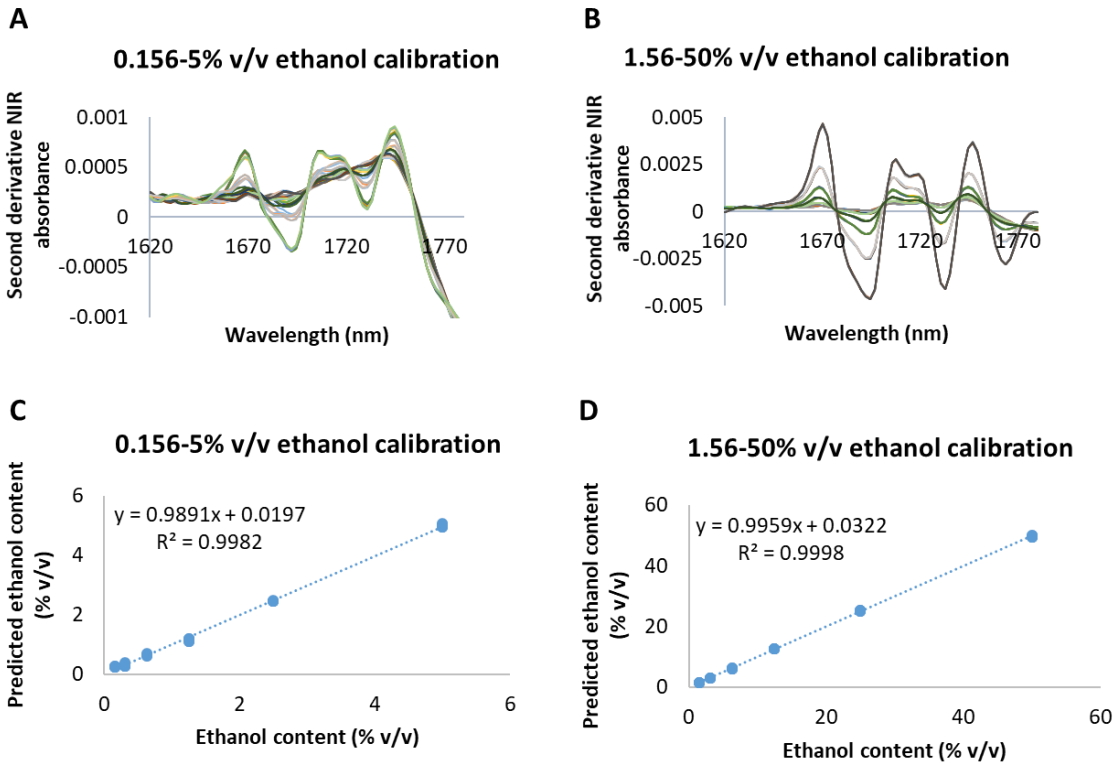

Figure 41. The content of ethanol in PBS/ethanol mixture was quantified by NIR spectroscopy in a probe setting. Second derivative NIR absorbance for A) Ethanol standards containing 0.156-5% v/v ethanol and B) Ethanol standards containing 1.56-50% v/v ethanol. Predicted ethanol content for C) Ethanol standards containing 0.156-5% v/v ethanol and D) Ethanol standards containing 1.56-50% v/v ethanol.

4.3.9.2. Ethanol quantification in the presence of liposomes using NIR spectroscopy

After confirming the NIR accuracy and precision in quantifying the ethanol content in an ethanol/PBS solution, we aimed to assess the ethanol content in the presence of the liposome dispersion in off-line and in-line settings. The results demonstrate the accuracy and precision of the NIR in detecting the ethanol content in very low concentrations in an off-line setting (i.e., 0.5% v/v ethanol in liposome dispersion, Figure 42A). In an in-line setting, the NIR device demonstrated sufficient accuracy and precision, which was tested by measuring the ethanol content in a liposome dispersion to which a known amount of ethanol was added (Figure 42B).

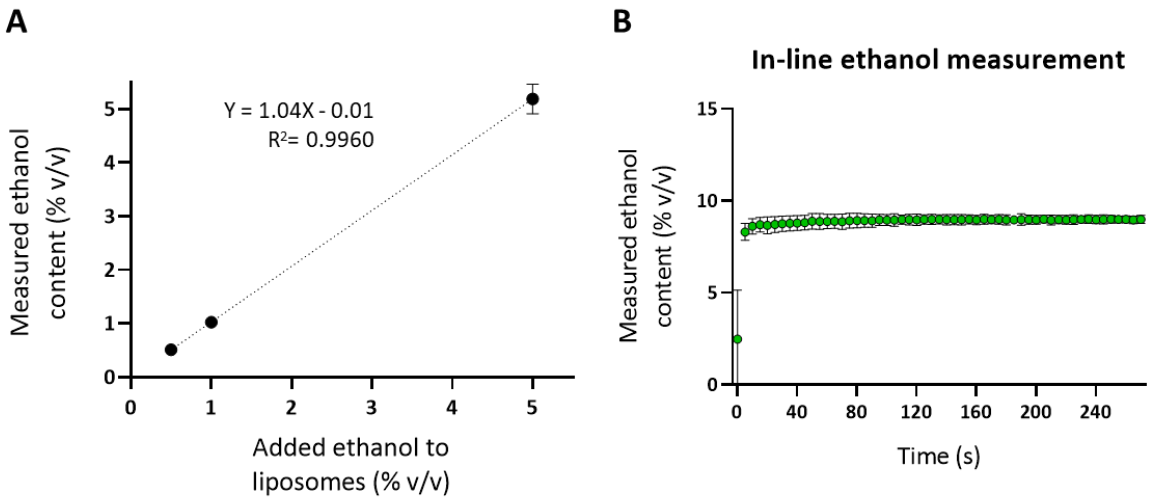

Figure 42. The content of ethanol in liposome dispersions was quantified by NIR spectroscopy. A) Off-line validation measurements of different ethanol contents in a liposome dispersion. B) In-line analysis and quantification of the ethanol content in an in-flow liposome dispersion with the pre-defined 10% v/v ethanol content. Liposomes were formed with 70 mM lipid in ethanol while the TFR was set at 62 mL min^{-1} (n=3). Reproduced from Ref. (Sheybanifard et al., 2023) with permission from the Royal Society of Chemistry.

4.3.9.3. Size and PDI quantification in an in-line setup using NFS device

Size and PDI were the next quality attributes of the liposomes that were quantified In-line. In-line real-time assessment of the quality attributes provides the opportunity for any required instant interventions and early correction of the parameters during CFM operation. Prior to in-line size and PDI measurements, a comparison was done between the two size determination devices: the standard Malvern DLS and the new NFS device. The outcome in terms of size and PDI of the same liposome dispersions in an off-line setup was compared (Figure 43, red circles present the off-line measurements of size and PDI). After preparation, particle size was fixed by diluting liposomal dispersions with PBS to eliminate the effect of the high ethanol environment on size growth. As shown in the Figure 43, the off-line measurements of the samples indicated a size of 85 ± 3 nm and a PDI of 0.23 ± 0.04 using the NFS device (mean and SD of three independent batches). Measuring the same samples in a Malvern DLS device, the recorded size was 71 ± 2 nm and the PDI was 0.09 ± 0.01 (mean and SD of three independent batches). The obtained size and PDI of the

liposomes from each device were comparable (yet not identical). Moreover, such a monodisperse sample revealed a PDI of less than 0.1 in standard DLS device and a PDI of below 0.25 in NFS instrument, emphasizing on the influence of the measurement device specifications (e.g., laser wavelength, etc.) on the obtained size and PDI.

Next, we prepared and measured the dispersions in an in-line setup. In the beginning of the measurements, the NFS indicated that the measurement criteria were not yet optimized (Figure 43, measurements in the blue area). Specifically in the first two batches, the size and PDI were larger than expected and/or fluctuating. Within this timeframe, the PDI measurements yielded values mostly above 0.35 and the sizes were larger than expected (in batch 1) and/or fluctuating (in batch 2). After 40 to 80 seconds (depending on the batch), the NFS software judged the measurement reliable and indicated that the criteria is met (Figure 43, measurements in the green areas). At this time, the recorded values were precise and accurate and the measurement was apparently stabilized, displaying a size of 82 ± 3 nm and a PDI of 0.22 ± 0.10 (mean and SD of three independent batches in that time frame). These values were in the range that was expected based on the previous off-line measurements in the vial configuration. From the time the syringe pumps were turned off to the time the dispersion flow stopped, the measurements were shown in a red area. Once the in-line measurements were finished, the remaining formulations in the flow cell were inspected in a follow up off-line measurement and we observed roughly similar size (83 ± 3 nm) and PDI (0.16 ± 0.03) results (mean and SD of three independent batches, Figure 43, orange triangles). The obtained results confirmed the precision and accuracy of the NFS device in the in-line assessment of the liposome size and PDI.

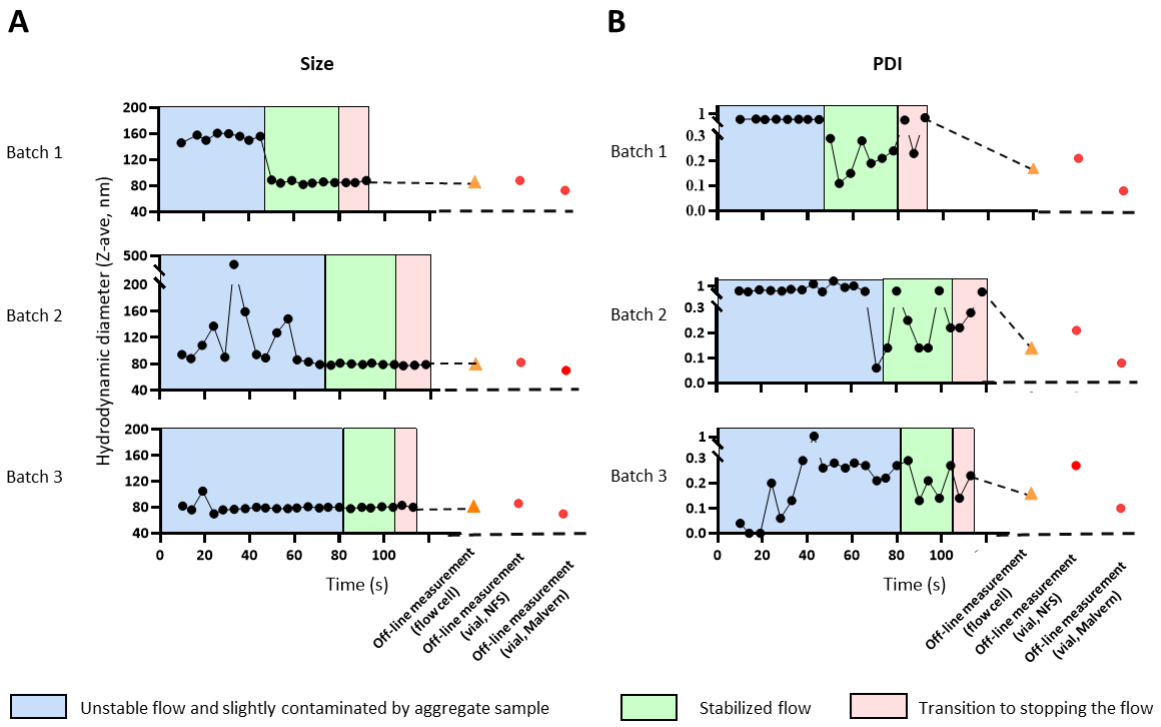

Figure 43. In-line and off-line quantification of liposome A) Hydrodynamic diameter and B) PDI using NanoFlowSizer. Blue areas refer to the time period in which the measurements were less reliable due to factors such as instability of the flow and/or formation of large (or aggregated) vesicles. Green areas refer to the time interval in which the measurements were reliable. Red areas refer to the time period in which the syringe pumps were turned off and consequently, the flow rate was decreased to zero. Prior to size and PDI measurements of the in-line and flow-cell module off-line samples (i.e., black circles and orange triangles respectively), one volume of the liposome dispersions were diluted with 4 volumes of PBS in an in-line setup. Liposomes were formed with 70 mM lipid in ethanol while the TFR was set at 62 mL min^{-1} (n=3). Reproduced from Ref. (Sheybanifard et al., 2023) with permission from the Royal Society of Chemistry.

5. Discussion

A major challenge in the development of therapeutic NP from bench to bedside is to ensure formulations are obtained with the desired critical quality attributes while their manufacturing method is translated from laboratory scale to industrial scale. To overcome this challenge, it is crucial to systematically evaluate and utilize composition and manufacturing process parameters as essential tools to control the critical quality attributes of therapeutic NP and to lay the groundwork for the development of an industrial-scale production setup.

Within the scope of the research work presented in this thesis, we evaluated formulation and manufacturing aspects of two prototypic nanoparticulate systems. Initially, we focused on evaluating the design and production aspects of polymeric micelles (PM), which critically depend on the physicochemical properties of their mPEG-*b*-p(HPMA-Bz) amphiphilic block copolymer building block. The production of the amphiphilic block copolymer used here was translated from a laboratory scale to industrial scale. In the second part of this thesis, we looked at the composition aspects and manufacturing method of another nanoparticle, namely liposomes, which less critically depends on the physicochemical properties of its main building block (i.e., the phospholipids) but more on the dispersion medium composition and on the actual process parameters during manufacturing. In this context we designed and evaluated a continuous flow manufacturing setup that allows for better controlled manufacturing and a smoother translation to clinical (and/or industrial) manufacturing.

5.1. Key design and production aspects of polymeric micelles based on mPEG-*b*-p(HPMA-Bz) amphiphilic block copolymer

Since 2013, amphiphilic block copolymers of methoxy poly(ethylene glycol)-b-(N-(2-benzoyloxypropyl) methacrylamide) (mPEG-*b*-p(HPMAm-Bz) have been successfully used to prepare Π electron-stabilized polymeric micelles for therapeutic purposes (Shi et al., 2013). As a consequence of the preclinical successes achieved with PM based on mPEG-*b*-p(HPMA-Bz) block copolymer and their expanding use in drug delivery field, developing a robust procedure to scale up the synthesis of the polymer is of great importance. In that

regard, free radical polymerization (FRP) is a feasible synthesis method (Bresseleers et al., 2019; Shi et al., 2015; Shi et al., 2013) in which a polymer is synthesized via a macroinitiator route using free radicals as the building blocks. However, large-scale polymer synthesis has multiple drawbacks such as increased viscosity and difficult heat and mass transfer that eventually result in low reproducibility and inefficient production.

Specifically for large-scale synthesis of mPEG-*b*-p(HPMA-Bz) block copolymer using FRP, in the process of mPEG-ABCPA-mPEG synthesis as the macroinitiator, incomplete esterification of ABCPA and mPEG may lead to the formation of mPEG−ABCPA or unreacted PEG and/or ABCPA. Thus, the presence of the aforementioned impurities in the macroinitiator results in a solution containing a mixture of mPEG-*b*-p(HPMA-Bz) block copolymer, unwanted p(HPMA-Bz) homopolymer, and unreacted PEG impurities. Moreover, defective coupling of macroinitiator (i.e., mPEG-ABCPA-mPEG) and the monomer (i.e., HPMA-Bz) can also result in the presence of each of the unreacted components in the final product.

The homopolymer (i.e., p(HPMA-Bz)) and the monomer (i.e., HPMA-Bz) impurities can eventually incorporate themselves into the micelle core and consequently increase the size of the micelles and decrease the capacity to encapsulate drugs (Bagheri et al., 2018). The presence of free PEG and macroinitiator, on the other hand, might result in inaccurate characterization of the polymer's properties such as its molecular weight (M_w) and may cause the measured M_w to deviate from its calculated value (Wilbon et al., 2013). Moreover, it can result in unwanted reactions with the target drug (Saraf et al., 2020). Therefore, it is essential to minimize the impurities of the block copolymer either during synthesis or post-modification through purification.

Here, we aimed to introduce a new step in the synthesis process to ensure sufficient purity of large-scale synthesized mPEG-*b*-p(HPMA-Bz) polymer (Bresseleers et al., 2019). We successfully established a purification protocol to detect and eliminate different classes of impurities. Previous experiments with PM made of the impure block copolymer demonstrated instability in particle size and drug retention. However, we did not observe substantial differences in the evaluated physicochemical characteristics between PM based

on the impure polymer and the purified polymer. Nevertheless, it is more desirable to use a polymer with the highest level of purity due to the potential drawbacks associated with the impure polymer as mentioned above.

As shown by this example, *in vivo* drug retention and physical stability of PM demands a comprehensive understanding of how process and composition parameters determine the critical quality attributes that ensure optimal PM performance *in vivo* and to carefully control these parameters. To shed more light on how composition parameters determine the main critical quality attributes, size and drug retention capacity of PM based on the mPEG-*b*-p(HPMA-Bz) block copolymer were evaluated. More specifically, we formulated and evaluated PM based on several lab-scale synthesized mPEG-*b*-p(HPMA-Bz) block copolymers (differing from each other in terms of hydrophobic block size) and loaded these PM with different quantities of paclitaxel (PTX) by changing the drug to polymer ratio.

Indeed, particle size plays a major role in the *in vivo* performance of PM (and therapeutic nanoparticles in general). Thus, it is crucial to specify the appropriate size range (Bae and Park, 2011). Previous studies have shown that PM size should be larger than 10 nm in order to evade renal filtration (Hoshyar et al., 2016) and smaller than 200 nm to allow for sterile filtration. PM in this size range can potentially improve circulation time and consequently, enhance the accumulation in the target site. In general, the target diameter of PM are aimed at 10-100 nm (Jones and Leroux, 1999; Yokoyama, 2011), while research has shown that sub 50 nm PM demonstrate superior tumor penetration (Cabral et al., 2011). During the research work presented in this thesis, we aimed at forming monodisperse PM with hydrodynamic diameters around and less than 50 nm using the $mPEG_{5k}$-*b*-p(HPMA-Bz) block copolymer.

In our studies, we found that there was no difference in cellular uptake (both in 2D and 3D microspheroid culture) between PM of different sizes. Nevertheless, 40 nm PM based on $mPEG_{5k}$-*b*-$p(HPMA\text{-}Bz)_{5k}$ showed superior penetration after 4 hours of incubation in our 3D cultured human hepatocellular tumor model at all depth layers. This is in agreement with earlier observations that showed the influence of the PM size on their tumor penetration (Cabral et al., 2011; Priwitaningrum et al., 2016). Intriguingly, although PM based on

$mPEG_{5k}$-*b*-p(HPMA-Bz)$_{3k}$ had a comparable size, the tissue penetration capacity appeared inferior. We hypothesize that the relatively poor penetration observed with $mPEG_{5k}$-*b*-p(HPMA-Bz)$_{3k}$ is a result of poor stability of these PM when they are incubated in biological media. This is understandable, since the critical micelle concentration can be expected to go up with smaller hydrophobic blocks in the copolymer.

Besides PM size, drug retention (which can also be expressed as drug release rate) is another key quality attribute of PM that is determined by multiple factors including PM core hydrophobicity, PM size, and the drug to polymer ratio (i.e., drug loading) (Yu et al., 2013). Drug release rate reflects the mass transfer of active drug over time and is dependent on the drug concentration (inside vs. outside of the drug delivery vehicle). After release in the blood circulation, many hydrophobic drug molecules tend to bind to proteins that are present in the blood stream. As an example, albumin is the major protein that captures PTX with high protein binding (more than 90%) (Eiseman et al., 1994; Kumar et al., 1993). Therefore, to assess the drug release rate from PM, we used albumin to solubilize the released fraction of PTX and better mimic the *in vivo* condition. We measured the fraction of PTX that was retained in the PM at a specific time point and calculated the released fraction using an indirect method.

Based on evaluation of the drug release rate as a function of polymer hydrophobicity, we showed that PM based on $mPEG_{5k}$-*b*-p(HPMA-Bz) block copolymer with longer hydrophobic block sizes (i.e., 10k and 17k) were more effective in retaining the drug during storage and released PTX at a slower rate compared to the PM based on the shorter hydrophobic block sizes. These findings are in line with observations from other researchers (Hussein and Youssry, 2018; Lin et al., 2003).

It was previously shown that using a centrifugation method, the PTX release of PM in PBS is approximately 30% of the initial encapsulated drug after 10 days (Shi et al., 2015). In our studies, we added polysorbate 80 micelles and albumin to the incubation buffer. Both additives can potentially interact with and capture PTX and consequently, better represent the drug release behavior in the biologic milieu and predict the *in vivo* release kinetics. Regardless of formulation type, we observed that between 36-69% of PTX is released in the

first four hours. The acceptability of a limited burst release is determined by the required time for PM to significantly accumulate in tumor site after administration using the EPR effect (Maeda et al., 2013). As it is shown in literature, both a drug release rate that is too slow or too rapid are suboptimal. A too slow drug release can translate to suboptimal pharmacological activity, and a too rapid drug release enhances clearance resulting in suboptimal drug accumulation at the site of interest (Yokoyama, 2014). Generally, researchers aim for a slow but sustained drug release profile. Ideally, the encapsulated drug should be retained in the PM during its residence time in the circulation and gets rapidly released upon entry into the target tissue. The latter is very crucial in order to avoid drug resistance (Deng et al., 2012). Since such a release behavior would be challenging to achieve in practice, a sweet spot must be found between maximal drug retention and release for each drug and formulation.

Another composition parameter that was evaluated during the research presented here was the PTX loading percentages (i.e., the drug to the polymer ratios). Our results demonstrated that increasing the drug to polymer ratio (i.e., around 15% w/w) leads to more PTX leakage over time and relatively low stability during storage. Nevertheless, the *in vitro* PTX release rate did not change upon changes in the drug to polymer ratio. Considering the benefits of formulating PM with high drug loading, we selected the highest drug loading percentage that showed promising storage stability (i.e., the 10% w/w) as the optimum.

5.2. Key design and production aspects of liposome dispersions

After identifying composition parameters such as the physicochemical characteristics of the polymer building block as well as the drug to polymer ratio as the main determinants of the critical quality attributes of the PM, we next focused more on liposomes and the main composition and manufacturing process parameters that control the liposome critical quality attributes.

To prepare the liposomes in the current thesis, we used an ethanolic lipid solution of DSPE-PEG-2000, EPC, and cholesterol. EPC (highly purified egg phosphatidylcholine) was selected as the main bilayer compartment of the liposomal particles. Owing to its low phase transition temperature, EPC does not require high temperatures in order to dissolve in

ethanol and form liposomes, making it a viable choice for screening and optimization purposes. The other bilayer component of liposomes was DSPE-PEG-2000, which improves the stability of the particles during storage and is responsible for their prolonged circulation upon i.v. injection. Lastly, the third bilayer component was cholesterol. Among many other benefits, cholesterol improves the packing of phospholipid molecules (Demel and De Kruyff, 1976), which results in better retention of the encapsulated drugs in the liposomes. For our lipid composition, we chose DSPE-PEG-2000, EPC, and cholesterol at a molar ratio of 5:60:35 respectively (Materials and methods section 3.5.1). It has previously been shown that incorporation of 5-7 mol % PEG-lipids results in maximum liposome stability (Baekmark et al., 1997), while a two to one ratio of PC versus cholesterol has been shown to improve the formulation stability and to achieve a controlled drug release, mainly owing to the effect of cholesterol at this molar ratio on enhancing the packing density of the phospholipid molecules (Briuglia et al., 2015).

To assess and control the critical quality attributes of liposome dispersions, multiple composition and manufacturing process parameters can be employed. During the studies presented in this thesis we observed that total flow rate (TFR), lipid concentration, ethanol concentration and residence time of the liposomes in high ethanol environment can critically influence the critical quality attributes of liposomes, namely size and PDI.

In line with what is observed in other studies (Carugo et al., 2016), we noted that decreasing lipid concentration and increasing TFR leads to liposomes with a smaller mean particle size. Regarding the effect of the lipid concentration on particle size, Yang et al. proposed a hypothesis arguing that decreasing the lipid concentration reduces the probability of merging of the freshly formed lipid bilayers, which in turn results in a smaller liposome size (Yang et al., 2012). Increasing TFR, on the other hand, affects the mixing of organic and aqueous streams. It was previously hypothesized that when the TFR is high, the two streams mix more rapidly and consequently phospholipid bilayers form, merge, and develop into liposomes more quickly. As a result, slow lipid bilayer merging is avoided, resulting in smaller and more monodisperse liposomes dispersion (Yanar et al., 2020).

By carefully changing the TFR and lipid concentration, we could obtain monodisperse liposomes with sizes varying between 80 to 150 nm (PDIs <0.25). At first glance, such a difference in size may not appear big. However, within this size range usually a striking difference in the *in vivo* performance of the liposomes is seen concerning their pharmacokinetics and organ distribution (Nagayasu et al., 1999). It is worth noting that within this range in which there is a 1.9 times increase in liposome diameter from 80 nm to 150 nm, an increase in drug encapsulating volume of up to 6.6 times can be expected (the volume calculated as a function of the diameter).

Ethanol content at the point of mixing is another composition parameter that affects liposome size and PDI. Our results show that once the ethanol content at the point of liposome formation is 50% v/v, monodisperse liposomes with small sizes are obtained. Both going up or down from 50% v/v ethanol content resulted in an increase in liposome size and PDI. Another advantage of liposome formation in such a high ethanol content is the fact that it allows for high lipid concentrations to be present at the point of liposome formation, leading to a relatively concentrated liposome dispersion. This, in turn, enhances the encapsulation efficiency of hydrophilic drugs that are encapsulated in the aqueous interior.

Indeed, previous studies already revealed the effect of composition and manufacturing process parameters such as lipid concentration, ethanol concentration, and TFR on liposome key quality attributes (Carugo et al., 2016; Costa et al., 2016). However, in the majority of these studies, relatively low concentrations of the lipid starting materials and organic solvent at the point of liposome formation were used (approximately between 5-25 mM and 10-25% v/v respectively) (Hood et al., 2014; Jo et al., 2020; Lim et al., 2014; Lim et al., 2020; Lou et al., 2019; Lv et al., 2021; Tiboni et al., 2021). This in turn limits the encapsulation efficiency of hydrophilic drugs in the liposome vesicles. More importantly, while performing our experiments, we discovered that the presence of high ethanol environment can be an influential manufacturing process parameter to control the liposome size and PDI as well. Our results show that liposome size increases with increasing the residence time of liposomal dispersion in a medium containing high percentages of ethanol. At 50% v/v ethanol, the maximum size growth was observed, confirming that 50% v/v is the optimum percentage to form the liposomes and fine-tune the size. Once a desired

particle size is obtained, the size can be effectively fixated by decreasing the ethanol percentage below a certain threshold (i.e., below 20% v/v) via simply diluting the sample with PBS.

The mechanism of particle growth is currently not fully understood. However, it is possibly a type of vesicle annealing that is hypothetically driven by an Ostwald ripening mechanism. In this mechanism, lipids diffuse through the dispersion medium facilitated by the high percentage of ethanol. Especially small liposomes tend to expel more phospholipids into the dispersion medium than the larger counterparts. Meanwhile, liposomes that are already large tend to more effectively take up the phospholipids and consequently, their size increases. However, besides Ostwald ripening, liposomal coalescence may also play a role.

After assessing the effect of composition and process parameters on the actual formation process of the liposomes as the first production step of the CFM setup, we investigated the subsequent liposome purification step using a tangential flow filtration (TFF). Purification of the liposomal dispersion is required at two levels; first, to remove any residual organic solvent and second, to remove any potential un-encapsulated drug.

TFF operates on the principle of repeated cycling the liposomal dispersion over a semipermeable membrane (Clutterbuck et al., 2017). Since multiple cycles are often required for sufficient purification, this process is not suitable for continuous flow manufacturing and is mainly used for bulk production. To incorporate it into the CFM setup, we attempted to improve the TFF performance to allow for single pass purification, and determined that the requirements included a low inlet pressure, a pressure evenly distributed over the entire filtration unit and a sufficiently large surface area of the filter membrane.

During the production of liposome dispersions, it is essential to control the critical quality attributes to ensure the overall quality of the final product. As a matter of fact, CFM allows for in-line and real-time evaluation of these quality attributes, which helps avoiding batch-to-batch variations and eventually, lowers the risk of batch failure. In-line quality control

enables instant interventions and thus, provides the opportunity of real-time correction if required (De Beer et al., 2011; Helal et al., 2019).

As part of the research work described in this thesis, an NIR instrument was used for in-line, real-time quantification of the ethanol content of a dispersion that runs through the CFM setup. Besides this, another ground-breaking new instrument, namely the NanoFlowSizer was used as an instrument enabling in-line and real-time quantification of size and PDI of the particles while they are in flow (depending on the type of flow cell, the flow can vary between 0 to >2,000 mL min^{-1}).

Quantification of ethanol content is essential for two reasons. First, a parenteral formulation to be used in clinic simply cannot contain more than 5,000 ppm (0.5%) ethanol (Group, 2019), and thus, the content of ethanol residues must be measured and limited. Second, different concentrations of ethanol in the aqueous medium of the dispersion result in different viscosity and refractive index values. Defining these two parameters is essential to obtain a reliable in-line size measurement from NFS. On the other hand, quantification of size and PDI is crucial due to their significant impact on the nanoparticle *in vivo* behavior (Bae and Park, 2011; Danaei et al., 2018).

Evaluating the liposome size with the NFS device in an off-line setup showed that the size and PDI of the liposome obtained with the NFS were comparable (yet not identical) to the values obtained from standard DLS. Nevertheless, monodisperse samples with only one particle population showed a PDI lower than 0.1 in standard DLS device and a PDI of below 0.25 in NFS instrument. Therefore, samples with PDIs equal and lower than these values (i.e., 0.1 and 0.25 for standard DLS and NFS respectively) were considered as desirable monodisperse dispersions.

The fact that the same particle size distribution results in different PDIs as measured with DLS and NFS arises from the fact that the PDI represents the relative variance of the scattering intensity-based size distribution. Size and wavelength are factors responsible for defining the scattering intensity. Therefore, different devices with different wavelengths of light (e.g., λ=633 nm for standard DLS vs. λ=1300 nm for the SR-DLS based NFS) might show different intensity-based size distribution (Z-ave) and PDI.

All in all, our experiments showed that combined with the in-line NIR instrument, the NFS instrument is perfectly suitable for in-line real-time size and PDI measurements as part of the CFM setup. Still, it is important to keep in mind that the stability of the NFS for in-line measurements as well as its data reliability and quality of the flow corrections that it calculates are all affected by flow instabilities and particle aggregates, both of which must be kept to a minimum.

5.3. Conclusions and outlook

Within the scope of the research work presented in this thesis, the production of two of the most advanced NP formulations in the field of nanomedicine was investigated and systematically evaluated regarding the effect of composition and manufacturing process on their critical quality attributes. Several aspects of synthesis and manufacturing were closely assessed with the aim of facilitating the translation to clinical production. The first part of the research work focused on polymeric micelles (PM) while the second part was dedicated to liposomes.

Regarding the critical quality attributes of PM, a key finding was that the quality of the block copolymer starting material is an important (composition) parameter. Therefore it is necessary to obtain and to work with the polymer with high level of purity. Proper purification protocols become even more important during scale up due to the inherent shortcomings associated with the large-scale production including increased preparation viscosity and difficulties in heat and mass transfer. Therefore, a purification protocol was established for purifying the large-scale synthesized block copolymer. Of note, it is indeed more desirable to optimize the large-scale synthesis of the polymer in a way that obviates the need for further post-modification processing (e.g., purification). Nevertheless, further investigations are required for introducing the purification protocol that was demonstrated in the current thesis into the scale-up manufacturing process.

During our experiments we also observed that the drug to polymer ratio as well as the hydrophobicity of the block copolymer building block play major roles in controlling the PM critical quality attributes. In our studies, we defined a drug to polymer ratio of 10% w/w as the optimum drug loading percentage that showed promising storage stability. Regarding

the hydrophobicity of the block copolymer, high *in vitro* stability and drug retention, and slow drug release were observed with PTX-loaded PM made of polymers with longer hydrophobic block sizes. On the other hand, superior *in vitro* tumor penetration was observed in PM based on polymers with shorter hydrophobic block sizes (i.e., $mPEG_{5k}$-*b*-$p(HPMA\text{-}Bz)_{5k}$). Future *in vivo* studies are required to determine the critical impact of drug release rate and tissue distribution on the antitumor efficacy of these PM. Furthermore, such studies assist specifying the PM characteristics that are crucial to obtain and control the optimal PM-based PTX nanomedicine.

In the second part of the studies performed within the scope of this thesis we focused on liposomes. We aimed at developing a CFM setup in order to better control the composition and manufacturing process parameters that are important for the critical quality attributes of liposomes. Eventually, utilizing these parameters may enable a novel end-to-end manufacturing line for liposomal drug production that can be operated in an automated and remote fashion. With the help of a millifluidic device, we could achieve relatively monodisperse liposomal particles and we could control their critical quality attributes such as mean size and polydispersity using several composition and manufacturing process parameters. These parameters include lipid concentration (as a composition parameter) as well as TFR and liposome incubation time in high ethanol environment (as manufacturing process parameters). There are yet other composition and manufacturing process parameters that should be explored in future studies, namely lipid composition, process temperature, flow rate ratios and aqueous medium composition (e.g., drug concentration, osmolarity, ionic strength). Moreover, during the studies presented in the current thesis, we mainly focused on size and PDI of liposomes as two critical quality attributes. Other liposome quality attributes such as drug retention and release require additional studies with drug-encapsulating liposomes.

Next, the possibility of using a single pass TFF to remove the residues of the organic solvent as well as integration of two in-line and real-time measuring instruments to assess the mean particle size (Z-ave), PDI and ethanol residues were evaluated. The obtained results confirm that careful fine-tuning of these techniques make them suitable for integration into the CFM setup, eventually allowing one all-encompassing, coherent system. Since the CFM

technique is a modular manufacturing setup, it enables the integration of other in-process analysis instruments as well. As an example, a Raman spectrometer probe could be explored as a means to quantify total lipid and drug content in-line.

Indeed, the in-line in-process analysis features that have been explored here can in the future become part of fully automated control of the process using feedback loops that tune and adjust the key process parameters. Eventually this allows for a simple scale-up by letting the system run in a remote-controlled fashion for the time needed to achieve the desired batch size. This comes with the further benefit of a minimized chance of batch failures. We are convinced that the CFM setup is not limited to manufacturing of liposomal drug products and that further exploration of its value for polymeric and lipid NP is warranted.

Concluding, we believe that the results presented in the current thesis and the lessons learnt can pave the way towards a more rational design, better production and easier scale-up of nanomedicinal drug products with the aim to foster their clinical translation and show their therapeutic value in patients.

6. Summary: Controlling Critical Quality Attributes of Therapeutic Nanoparticles Upon Scale-up Manufacturing (by Maryam Sheybanifard)

Polymeric micelles (PM) and liposomes are two leading nanoparticulate drug delivery systems. Despite numerous advantages, their clinical success is hampered by challenges related to maintaining the critical quality attributes while translating the manufacturing process from laboratory-scale to clinical and industrial scale. We argue that these challenges can be overcome by identifying and controlling the key composition and manufacturing process parameters that directly impact the nanoparticle critical quality attributes. We first explored this with PM and we next addressed liposomes.

Concerning PM, besides the quality of the block copolymer starting material in terms of purity, the length of the hydrophobic block appeared to be the primary parameter that determines PM critical quality attributes, including physical stability and drug release rate. Longer hydrophobic blocks led to better stability, while a shorter hydrophobic block led to a smaller particle size, which appeared preferable in tumor penetration capacity. Drug-to-polymer ratio was another parameter that was of key importance, and our studies helped find the maximum loading capacity of the micelles without jeopardizing drug retention and stability.

Regarding liposomes, the manufacturing method appeared crucial in controlling the quality attributes. Thus, a continuous flow manufacturing setup was developed to better control the composition and manufacturing process parameters. This approach may especially be suitable for scale-up and clinical production. We discovered that parameters like lipid concentration, total flow rate and residence time of liposomes in the high ethanol environment determined liposomes' final particle size and polydispersity, which we could measure in an in-line setting. This will enable a novel end-to-end manufacturing line for liposomes and also other NP that can be operated in an automated and remote fashion.

In conclusion, systematic evaluation and effective utilization of the key composition and manufacturing process parameters of PM and liposomes enables better control of their critical quality attributes, which will foster their scale up for clinical trials and for the market.

6. Zusammenfassung: Kontrolle kritischer Qualitätsmerkmale von therapeutischen Nanopartikeln in der Großproduktion (von Maryam Sheybanifard)

Polymermizellen (PM) und Liposomen sind zwei der meist genutzten nanopartikuläre Arzneimittelabgabesysteme. Trotz zahlreicher Vorteile wird ihr klinischer Erfolg oft durch Schwierigkeiten behindert, welche mit der Beibehaltung der kritischen Qualitätsmerkmale einhergehen, die während der Übertragung der Herstellungsmethode vom Labormaßstab auf den klinischen und industriellen Maßstab entstehen. Wir argumentieren, dass diese Herausforderungen durch die Identifizierung und Kontrolle der wichtigsten Parameter für die Zusammensetzung und den Herstellungsprozess, die sich direkt auf die kritischen Qualitätseigenschaften der Nanopartikel auswirken, überwunden werden können. Wir haben dies zunächst mit PM untersucht und uns dann mit Liposomen befasst.

Bei PM scheint neben der Reinheit des Blockcopolymer-Ausgangsmaterials, die Länge des hydrophoben Blocks der wichtigste Parameter zu sein, der die kritischen Qualitätseigenschaften von PM, wie die physikalische Stabilität und die Freisetzungsrate von Arzneimitteln, bestimmt. Ein längerer hydrophober Block führte zu einer besseren Stabilität und ein kürzerer hydrophober Block führte zu einer kleineren Partikelgröße, was für die Tumorpenetrationskapazität vorteilhaft erschien. Das Verhältnis von Wirkstoff zu Polymer war ein weiterer wichtiger Parameter, und unsere Studien trugen dazu bei, die maximale Beladungskapazität der Mizellen zu finden, ohne die Rückhaltung des Wirkstoffs und die Stabilität zu gefährden.

Bei den Liposomen erwies sich das Herstellungsverfahren selbst als entscheidend für die Kontrolle der Qualitätsmerkmale. Daher wurde ein kontinuierliches Herstellungsverfahren entwickelt, um die Zusammensetzung und die Parameter des Herstellungsprozesses besser kontrollieren zu können. Dieser Ansatz eignet sich besonders für eine Hochskalierung. Wir entdeckten, dass Parameter wie die Lipidkonzentration, die Gesamtdurchflussrate und die Verweilzeit der Liposomen in der Umgebung mit hohem Ethanolgehalt die letztendliche Partikelgröße und Polydispersität der Liposomen bestimmen, die wir in einem Inline-Versuchsaufbau gemessen haben. Dies wird letztendlich eine neuartige Ende-zu-Ende-Herstellungslinie für Liposomen und auch andere NP ermöglichen, die automatisiert und ferngesteuert betrieben werden kann.

Zusammenfassend lässt sich sagen, dass die systematische Bewertung und effektive Nutzung der wichtigsten Parameter für die Zusammensetzung und den Herstellungsprozess von PM- und Liposomendispersionen dazu beigetragen haben, ihre kritischen Qualitätsmerkmale zu kontrollieren, und dass sie die Hochskalierung für klinische Versuche und für den Markt fördern werden.

7. References

Abouelmagd, S.A., Sun, B., Chang, A.C., Ku, Y.J., Yeo, Y., 2015. Release kinetics study of poorly water-soluble drugs from nanoparticles: are we doing it right? Molecular Pharmaceutics 12, 997-1003.

Akbarzadeh, A., Rezaei-Sadabady, R., Davaran, S., Joo, S.W., Zarghami, N., Hanifehpour, Y., Samiei, M., Kouhi, M., Nejati-Koshki, K., 2013. Liposome: classification, preparation, and applications. Nanoscale Research Letters 8, 102.

Allison, G., Cain, Y.T., Cooney, C., Garcia, T., Bizjak, T.G., Holte, O., Jagota, N., Komas, B., Korakianiti, E., Kourti, D., Madurawe, R., Morefield, E., Montgomery, F., Nasr, M., Randolph, W., Robert, J.-L., Rudd, D., Zezza, D., 2015. Regulatory and Quality Considerations for Continuous Manufacturing. May 20–21, 2014 Continuous Manufacturing Symposium. Journal of Pharmaceutical Sciences 104, 803-812.

Almoustafa, H.A., Alshawsh, M.A., Chik, Z., 2017. Technical aspects of preparing PEG-PLGA nanoparticles as carrier for chemotherapeutic agents by nanoprecipitation method. International Journal of Pharmaceutics 533, 275-284.

Anselmo, A.C., Mitragotri, S., 2019. Nanoparticles in the clinic: An update. Bioengineering & Translational Medicine 4, e10143.

Anselmo, A.C., Mitragotri, S., 2021. Nanoparticles in the clinic: An update post COVID-19 vaccines. Bioengineering & Translational Medicine n/a, e10246.

Bader, H., Ringsdorf, H., Schmidt, B., 1984. Watersoluble polymers in medicine. Die Angewandte Makromolekulare Chemie 123, 457-485.

Bae, Y.H., Park, K., 2011. Targeted drug delivery to tumors: myths, reality and possibility. J Control Release 153, 198-205.

Baekmark, T.R., Pedersen, S., Jørgensen, K., Mouritsen, O.G., 1997. The effects of ethylene oxide containing lipopolymers and tri-block copolymers on lipid bilayers of dipalmitoylphosphatidylcholine. Biophysical Journal 73, 1479-1491.

Bagheri, M., Bresseleers, J., Varela-Moreira, A., Sandre, O., Meeuwissen, S.A., Schiffelers, R.M., Metselaar, J.M., van Nostrum, C.F., van Hest, J.C.M., Hennink, W.E., 2018. Effect of Formulation and Processing Parameters on the Size of mPEG-b-p(HPMA-Bz) Polymeric Micelles. Langmuir 34, 15495-15506.

Bangham, A.D., Horne, R.W., 1964. Negative staining of phospholipids and their structural modification by surface-active agents as observed in the electron microscope. Journal of Molecular Biology 8, 660-IN610.

Batzri, S., Korn, E.D., 1973. Single bilayer liposomes prepared without sonication. Biochimica et Biophysica Acta (BBA) - Biomembranes 298, 1015-1019.

Besseling, R., Damen, M., Wijgergangs, J., Hermes, M., Wynia, G., Gerich, A., 2019. New unique PAT method and instrument for real-time inline size characterization of concentrated, flowing nanosuspensions. European Journal of Pharmaceutical Sciences 133, 205-213.

Bodmeier, R., Huagang, C., 1990. Indomethacin polymeric nanosuspensions prepared by microfujidization. Journal of Controlled Release 12, 223-233.

Bozzuto, G., Molinari, A., 2015. Liposomes as nanomedical devices. Int J Nanomedicine 10, 975-999.

Bresseleers, J., Bagheri, M., Storm, G., Metselaar, J.M., Hennink, W.E., Meeuwissen, S.A., van Hest, J.C.M., 2019. Scale-Up of the Manufacturing Process To Produce Docetaxel-Loaded mPEG-b-p(HPMA-Bz) Block Copolymer Micelles for Pharmaceutical Applications. Organic Process Research & Development 23, 2707-2715.

Briuglia, M.-L., Rotella, C., McFarlane, A., Lamprou, D.A., 2015. Influence of cholesterol on liposome stability and on in vitro drug release. Drug Delivery and Translational Research 5, 231-242.

Bryant, S.J., Jafta, C.J., Atkin, R., Gradzielski, M., Warr, G.G., 2019. Catanionic and chain-packing effects on surfactant self-assembly in the ionic liquid ethylammonium nitrate. Journal of Colloid and Interface Science 540, 515-523.

Cabral, H., Matsumoto, Y., Mizuno, K., Chen, Q., Murakami, M., Kimura, M., Terada, Y., Kano, M., Miyazono, K., Uesaka, M., 2011. Accumulation of sub-100 nm polymeric micelles in poorly permeable tumours depends on size. Nature Nanotechnology 6, 815-823.

Carugo, D., Bottaro, E., Owen, J., Stride, E., Nastruzzi, C., 2016. Liposome production by microfluidics: potential and limiting factors. Scientific Reports 6, 25876.

Chen, Z., Han, J.Y., Shumate, L., Fedak, R., DeVoe, D.L., 2019. High Throughput Nanoliposome Formation Using 3D Printed Microfluidic Flow Focusing Chips. Advanced Materials Technologies 4, 1800511.

Cleeland, C.S., Bennett, G.J., Dantzer, R., Dougherty, P.M., Dunn, A.J., Meyers, C.A., Miller, A.H., Payne, R., Reuben, J.M., Wang, X.S., Lee, B.-N., 2003. Are the symptoms of cancer and cancer treatment due to a shared biologic mechanism? Cancer 97, 2919-2925.

Clutterbuck, A., Beckett, P., Lorenzi, R., Sengler, F., Bisschop, T., Haas, J., 2017. Single-Pass Tangential Flow Filtration (SPTFF) in Continuous Biomanufacturing, Continuous Biomanufacturing - Innovative Technologies and Methods, pp. 423-456.

Costa, A.P., Xu, X., Khan, M.A., Burgess, D.J., 2016. Liposome Formation Using a Coaxial Turbulent Jet in Co-Flow. Pharmaceutical Research 33, 404-416.

Danaei, M., Dehghankhold, M., Ataei, S., Hasanzadeh Davarani, F., Javanmard, R., Dokhani, A., Khorasani, S., Mozafari, M.R., 2018. Impact of Particle Size and Polydispersity Index on the Clinical Applications of Lipidic Nanocarrier Systems. Pharmaceutics 10, 57.

De Beer, T., Burggraeve, A., Fonteyne, M., Saerens, L., Remon, J.P., Vervaet, C., 2011. Near infrared and Raman spectroscopy for the in-process monitoring of pharmaceutical production processes. International Journal of Pharmaceutics 417, 32-47.

Delma, K.L., Lechanteur, A., Evrard, B., Semdé, R., Piel, G., 2021. Sterilization methods of liposomes: Drawbacks of conventional methods and perspectives. International Journal of Pharmaceutics 597, 120271.

Demel, R.A., De Kruyff, B., 1976. The function of sterols in membranes. Biochimica et Biophysica Acta (BBA) - Reviews on Biomembranes 457, 109-132.

Deng, C., Jiang, Y., Cheng, R., Meng, F., Zhong, Z., 2012. Biodegradable polymeric micelles for targeted and controlled anticancer drug delivery: Promises, progress and prospects. Nano Today 7, 467-480.

Deshpande, P.P., Biswas, S., Torchilin, V.P., 2013. Current trends in the use of liposomes for tumor targeting. Nanomedicine 8, 1509-1528.

DeVita, V.T., Chu, E., 2008. A History of Cancer Chemotherapy. Cancer Research 68, 8643.

Eiseman, J.L., Eddington, N.D., Leslie, J., MacAuley, C., Sentz, D.L., Zuhowski, M., Kujawa, J.M., Young, D., Egorin, M.J., 1994. Plasma pharmacokinetics and tissue distribution of paclitaxel in CD 2 F 1 mice. Cancer Chemotherapy and Pharmacology 34, 465-471.

EMA, 2019. Guideline on the sterilisation of the medicinal product, active substance, excipient and primary container. EMA/CHMP/CVMP/QWP/850374/2015, Accessed on 2nd Oct 2021.

Fang, J., Nakamura, H., Maeda, H., 2011. The EPR effect: Unique features of tumor blood vessels for drug delivery, factors involved, and limitations and augmentation of the effect. Advanced Drug Delivery Reviews 63, 136-151.

Fessi, H., Puisieux, F., Devissaguet, J.P., Ammoury, N., Benita, S., 1989. Nanocapsule formation by interfacial polymer deposition following solvent displacement. International Journal of Pharmaceutics 55, R1-R4.

Gagliardi, A., Giuliano, E., Eeda, V., Fresta, M., Bulotta, S., Awasthi, V., Cosco, D., 2021. Biodegradable polymeric nanoparticles for drug delivery to solid tumors. Frontiers in pharmacology 12, 17.

Gothwal, A., Khan, I., Gupta, U., 2016. Polymeric Micelles: Recent Advancements in the Delivery of Anticancer Drugs. Pharmaceutical Research 33, 18-39.

Greszta, D., Mardare, D., Matyjaszewski, K., 1994. " Living" radical polymerization. 1. Possibilities and limitations. Macromolecules 27, 638-644.

Group, I.E.W., 2019. ICH guideline Q3C (R6) on impurities: guideline for residual solvents Step 5. International Council for Harmonisation of Technical Requirements for Pharmaceuticals for Human Use (ICH) pp, 1-32.

Hamaguchi, T., Matsumura, Y., Suzuki, M., Shimizu, K., Goda, R., Nakamura, I., Nakatomi, I., Yokoyama, M., Kataoka, K., Kakizoe, T., 2005. NK105, a paclitaxel-incorporating micellar nanoparticle formulation, can extend in vivo antitumour activity and reduce the neurotoxicity of paclitaxel. British Journal of Cancer 92, 1240-1246.

Helal, N.A., Elnoweam, O., Eassa, H.A., Amer, A.M., Eltokhy, M.A., Helal, M.A., Fayyaz, H.A., Nounou, M.I., 2019. Integrated continuous manufacturing in pharmaceutical industry: current evolutionary steps toward revolutionary future. Pharmaceutical Patent Analyst 8, 139-161.

Hong, K., Zhang, H., Mays, J.W., Visser, A.E., Brazel, C.S., Holbrey, J.D., Reichert, W.M., Rogers, R.D., 2002. Conventional free radical polymerization in room temperature ionic liquids: a green approach to commodity polymers with practical advantages. Chemical communications, 1368-1369.

Hood, R.R., DeVoe, D.L., Atencia, J., Vreeland, W.N., Omiatek, D.M., 2014. A facile route to the synthesis of monodisperse nanoscale liposomes using 3D microfluidic hydrodynamic focusing in a concentric capillary array. Lab on a Chip 14, 2403-2409.

Hoshyar, N., Gray, S., Han, H., Bao, G., 2016. The effect of nanoparticle size on in vivo pharmacokinetics and cellular interaction. Nanomedicine 11, 673-692.

Hussein, Y.H., Youssry, M., 2018. Polymeric micelles of biodegradable diblock copolymers: Enhanced encapsulation of hydrophobic drugs. Materials 11, 688.

Ilare, J., Sponchioni, M., 2020. From batch to continuous free-radical polymerization: Recent advances and hurdles along the industrial transfer. Advances in Polymer Reaction Engineering 56, 229.

Israelachvili, J.N., Marčelja, S., Horn, R.G., 1980. Physical principles of membrane organization. Quarterly Reviews of Biophysics 13, 121-200.

Israelachvili, J.N., Mitchell, D.J., Ninham, B.W., 1976. Theory of self-assembly of hydrocarbon amphiphiles into micelles and bilayers. Journal of the Chemical Society, Faraday Transactions 2: Molecular and Chemical Physics 72, 1525-1568.

Jahn, A., Vreeland, W.N., Gaitan, M., Locascio, L.E., 2004. Controlled Vesicle Self-Assembly in Microfluidic Channels with Hydrodynamic Focusing. Journal of the American Chemical Society 126, 2674-2675.

Jain, K.K., 2008. Drug Delivery Systems - An Overview, in: Jain, K.K. (Ed.), Drug Delivery Systems. Humana Press, Totowa, NJ, pp. 1-50.

Jo, M., Park, K.-M., Park, J.-Y., Yu, H., Choi, S.J., Chang, P.-S., 2020. Microfluidic assembly of mono-dispersed liposome and its surface modification for enhancing the colloidal stability. Colloids and Surfaces A: Physicochemical and Engineering Aspects 586, 124202.

Jones, M.-C., Leroux, J.-C., 1999. Polymeric micelles–a new generation of colloidal drug carriers. European Journal of Pharmaceutics and Biopharmaceutics 48, 101-111.

Kastner, E., Kaur, R., Lowry, D., Moghaddam, B., Wilkinson, A., Perrie, Y., 2014. High-throughput manufacturing of size-tuned liposomes by a new microfluidics method using

enhanced statistical tools for characterization. International journal of pharmaceutics 477, 361-368.

Kesharwani, S.S., Kaur, S., Tummala, H., Sangamwar, A.T., 2019. Multifunctional approaches utilizing polymeric micelles to circumvent multidrug resistant tumors. Colloids and Surfaces B: Biointerfaces 173, 581-590.

Kim, T.-Y., Kim, D.-W., Chung, J.-Y., Shin, S.G., Kim, S.-C., Heo, D.S., Kim, N.K., Bang, Y.-J., 2004. Phase I and Pharmacokinetic Study of Genexol-PM, a Cremophor-Free, Polymeric Micelle-Formulated Paclitaxel, in Patients with Advanced Malignancies. Clinical Cancer Research 10, 3708.

Kumar, G., Walle, U., Bhalla, K., Walle, T., 1993. Binding of taxol to human plasma, albumin and alpha 1-acid glycoprotein. Research Communications in Chemical Pathology and Pharmacology 80, 337-344.

Lee, S., 2017. Modernizing the way drugs are made: a transition to continuous manufacturing. US FDA (Ed.).

Lee, S.L., O'Connor, T.F., Yang, X., Cruz, C.N., Chatterjee, S., Madurawe, R.D., Moore, C., Yu, L.X., Woodcock, J., 2015. Modernizing pharmaceutical manufacturing: from batch to continuous production. Journal of Pharmaceutical Innovation 10, 191-199.

Li, M.C., Hertz, R., Bergenstal, D.M., 1958. Therapy of Choriocarcinoma and Related Trophoblastic Tumors with Folic Acid and Purine Antagonists. New England Journal of Medicine 259, 66-74.

Lichtenberg, D., Ahyayauch, H., Alonso, A., Goñi, F.M., 2013. Detergent solubilization of lipid bilayers: a balance of driving forces. Trends in Biochemical Sciences 38, 85-93.

Lim, J.-M., Swami, A., Gilson, L.M., Chopra, S., Choi, S., Wu, J., Langer, R., Karnik, R., Farokhzad, O.C., 2014. Ultra-High Throughput Synthesis of Nanoparticles with Homogeneous Size Distribution Using a Coaxial Turbulent Jet Mixer. ACS Nano 8, 6056-6065.

Lim, S.W.Z., Wong, Y.S., Czarny, B., Venkatraman, S., 2020. Microfluidic-directed self-assembly of liposomes: Role of interdigitation. Journal of Colloid and Interface Science 578, 47-57.

Lin, W.-J., Juang, L.-W., Lin, C.-C., 2003. Stability and release performance of a series of pegylated copolymeric micelles. Pharmaceutical Research 20, 668-673.

Lin, W., Ma, G., Kampf, N., Yuan, Z., Chen, S., 2016. Development of Long-Circulating Zwitterionic Cross-Linked Micelles for Active-Targeted Drug Delivery. Biomacromolecules 17, 2010-2018.

Lou, G., Anderluzzi, G., Woods, S., Roberts, C.W., Perrie, Y., 2019. A novel microfluidic-based approach to formulate size-tuneable large unilamellar cationic liposomes: Formulation, cellular uptake and biodistribution investigations. European Journal of Pharmaceutics and Biopharmaceutics 143, 51-60.

Lu, Y., Park, K., 2013. Polymeric micelles and alternative nanonized delivery vehicles for poorly soluble drugs. International Journal of Pharmaceutics 453, 198-214.

Lv, S., Jing, R., Liu, X., Shi, H., Shi, Y., Wang, X., Zhao, X., Cao, K., Lv, Z., 2021. One-Step Microfluidic Fabrication of Multi-Responsive Liposomes for Targeted Delivery of Doxorubicin Synergism with Photothermal Effect. Int J Nanomedicine 16, 7759-7772.

Maeda, H., Nakamura, H., Fang, J., 2013. The EPR effect for macromolecular drug delivery to solid tumors: Improvement of tumor uptake, lowering of systemic toxicity, and distinct tumor imaging in vivo. Advanced Drug Delivery Reviews 65, 71-79.

Martínez Rivas, C.J., Tarhini, M., Badri, W., Miladi, K., Greige-Gerges, H., Nazari, Q.A., Galindo Rodríguez, S.A., Román, R.Á., Fessi, H., Elaissari, A., 2017. Nanoprecipitation process: From encapsulation to drug delivery. International Journal of Pharmaceutics 532, 66-81.

Maurer, E.I., Sharma, M., Schlager, J.J., Hussain, S.M., 2014. Systematic analysis of silver nanoparticle ionic dissolution by tangential flow filtration: toxicological implications. Nanotoxicology 8, 718-727.

Moad, G., Solomon, D.H., 2006. The chemistry of radical polymerization. Elsevier.

Nagayasu, A., Uchiyama, K., Kiwada, H., 1999. The size of liposomes: a factor which affects their targeting efficiency to tumors and therapeutic activity of liposomal antitumor drugs. Advanced Drug Delivery Reviews 40, 75-87.

Nasongkla, N., Bey, E., Ren, J., Ai, H., Khemtong, C., Guthi, J.S., Chin, S.-F., Sherry, A.D., Boothman, D.A., Gao, J., 2006. Multifunctional Polymeric Micelles as Cancer-Targeted, MRI-Ultrasensitive Drug Delivery Systems. Nano Letters 6, 2427-2430.

NCI, N.C.I., A to Z List of Cancer Drugs.

Patil, Y.P., Jadhav, S., 2014. Novel methods for liposome preparation. Chemistry and Physics of Lipids 177, 8-18.

Porfire, A., Achim, M., Barbalata, C., Rus, I., Tomuta, I., Cristea, C., 2019. Pharmaceutical development of liposomes using the QbD approach. Liposomes Adv. Perspect 2019, 1-20.

Pratten, M.K., Lloyd, J.B., Hörpel, G., Ringsdorf, H., 1985. Micelle-forming block copolymers: Pinocytosis by macrophages and interaction with model membranes. Die Makromolekulare Chemie 186, 725-733.

Priwitaningrum, D.L., Blondé, J.-B.G., Sridhar, A., van Baarlen, J., Hennink, W.E., Storm, G., Le Gac, S., Prakash, J., 2016. Tumor stroma-containing 3D spheroid arrays: A tool to study nanoparticle penetration. Journal of Controlled Release 244, 257-268.

Rao, J.P., Geckeler, K.E., 2011. Polymer nanoparticles: Preparation techniques and size-control parameters. Progress in Polymer Science 36, 887-913.

Reis, M.H., Leibfarth, F.A., Pitet, L.M., 2020. Polymerizations in Continuous Flow: Recent Advances in the Synthesis of Diverse Polymeric Materials. ACS Macro Letters 9, 123-133.

Rhee, M., Valencia, P.M., Rodriguez, M.I., Langer, R., Farokhzad, O.C., Karnik, R., 2011. Synthesis of Size-Tunable Polymeric Nanoparticles Enabled by 3D Hydrodynamic Flow Focusing in Single-Layer Microchannels. Advanced Materials 23, H79-H83.

Saraf, I., Modhave, D., Kushwah, V., Neshchadin, D., Gescheidt, G., Trausinger, G., Melchior, P., Magnes, C., Paudel, A., 2020. Feasibility of rapidly assessing reactive impurities mediated excipient incompatibility using a new method: A case study of famotidine-PEG system. Journal of Pharmaceutical and Biomedical Analysis 178, 112893.

Scholz, C., Iijima, M., Nagasaki, Y., Kataoka, K., 1995. A novel reactive polymeric micelle with aldehyde groups on its surface. Macromolecules 28, 7295-7297.

Shah, S., Dhawan, V., Holm, R., Nagarsenker, M.S., Perrie, Y., 2020. Liposomes: Advancements and innovation in the manufacturing process. Advanced Drug Delivery Reviews 154-155, 102-122.

Sheybanifard, M., Beztsinna, N., Bagheri, M., Buhl, E.M., Bresseleers, J., Varela-Moreira, A., Shi, Y., van Nostrum, C.F., van der Pluijm, G., Storm, G., Hennink, W.E., Lammers, T., Metselaar, J.M., 2020. Systematic evaluation of design features enables efficient selection of Π electron-stabilized polymeric micelles. International Journal of Pharmaceutics 584, 119409.

Sheybanifard, M., Guerzoni, L.P.B., Omidinia-Anarkoli, A., De Laporte, L., Buyel, J., Besseling, R., Damen, M., Gerich, A., Lammers, T., Metselaar, J.M., 2023. Liposome manufacturing under continuous flow conditions: towards a fully integrated set-up with in-line control of critical quality attributes. Lab on a Chip 23, 182-194.

Shi, Y., Luo, H.Q., Li, N.B., 2011. Determination of the critical premicelle concentration, first critical micelle concentration and second critical micelle concentration of surfactants by resonance Rayleigh scattering method without any probe. Spectrochimica Acta Part A: Molecular and Biomolecular Spectroscopy 78, 1403-1407.

Shi, Y., van der Meel, R., Theek, B., Oude Blenke, E., Pieters, E.H.E., Fens, M.H.A.M., Ehling, J., Schiffelers, R.M., Storm, G., van Nostrum, C.F., Lammers, T., Hennink, W.E., 2015. Complete Regression of Xenograft Tumors upon Targeted Delivery of Paclitaxel via Π–Π Stacking Stabilized Polymeric Micelles. ACS Nano 9, 3740-3752.

Shi, Y., van Steenbergen, M.J., Teunissen, E.A., Novo, L.s., Gradmann, S., Baldus, M., van Nostrum, C.F., Hennink, W.E., 2013. Π–Π Stacking Increases the Stability and Loading Capacity of Thermosensitive Polymeric Micelles for Chemotherapeutic Drugs. Biomacromolecules 14, 1826-1837.

Shiraishi, K., Yokoyama, M., 2013. Polymeric micelles possessing polyethyleneglycol as outer shell and their unique behaviors in accelerated blood clearance phenomenon. Biological and Pharmaceutical Bulletin 36, 878-882.

Soga, O., van Nostrum, C.F., Fens, M., Rijcken, C.J.F., Schiffelers, R.M., Storm, G., Hennink, W.E., 2005. Thermosensitive and biodegradable polymeric micelles for paclitaxel delivery. Journal of Controlled Release 103, 341-353.

Soga, O., van Nostrum, C.F., Ramzi, A., Visser, T., Soulimani, F., Frederik, P.M., Bomans, P.H.H., Hennink, W.E., 2004. Physicochemical Characterization of Degradable Thermosensitive Polymeric Micelles. Langmuir 20, 9388-9395.

Sung, H., Ferlay, J., Siegel, R.L., Laversanne, M., Soerjomataram, I., Jemal, A., Bray, F., 2021. Global Cancer Statistics 2020: GLOBOCAN Estimates of Incidence and Mortality Worldwide for 36 Cancers in 185 Countries. CA: A Cancer Journal for Clinicians 71, 209-249.

Talelli, M., Iman, M., Varkouhi, A.K., Rijcken, C.J.F., Schiffelers, R.M., Etrych, T., Ulbrich, K., van Nostrum, C.F., Lammers, T., Storm, G., Hennink, W.E., 2010. Core-crosslinked polymeric micelles with controlled release of covalently entrapped doxorubicin. Biomaterials 31, 7797-7804.

Tiboni, M., Tiboni, M., Pierro, A., Del Papa, M., Sparaventi, S., Cespi, M., Casettari, L., 2021. Microfluidics for nanomedicines manufacturing: An affordable and low-cost 3D printing approach. International Journal of Pharmaceutics 599, 120464.

Tomeh, M.A., Zhao, X., 2020. Recent Advances in Microfluidics for the Preparation of Drug and Gene Delivery Systems. Molecular Pharmaceutics 17, 4421-4434.

Torchilin, V.P., 2006. Micellar Nanocarriers: Pharmaceutical Perspectives. Pharmaceutical Research 24, 1.

Trietsch, S.J., Naumovska, E., Kurek, D., Setyawati, M.C., Vormann, M.K., Wilschut, K.J., Lanz, H.L., Nicolas, A., Ng, C.P., Joore, J., 2017. Membrane-free culture and real-time barrier integrity assessment of perfused intestinal epithelium tubes. Nature Communications 8, 262.

Valencia, P.M., Farokhzad, O.C., Karnik, R., Langer, R., 2012. Microfluidic technologies for accelerating the clinical translation of nanoparticles. Nature Nanotechnology 7, 623-629.

Wagner, A., Vorauer-Uhl, K., 2011. Liposome technology for industrial purposes. Journal of drug delivery 2011.

Wevers, N.R., Van Vught, R., Wilschut, K.J., Nicolas, A., Chiang, C., Lanz, H.L., Trietsch, S.J., Joore, J., Vulto, P., 2016. High-throughput compound evaluation on 3D networks of neurons and glia in a microfluidic platform. Scientific Reports 6, 38856.

Wilbon, P.A., Chu, F., Tang, C., 2013. Progress in Renewable Polymers from Natural Terpenes, Terpenoids, and Rosin. Macromolecular Rapid Communications 34, 8-37.

Worsham, R.D., Thomas, V., Farid, S.S., 2019. Potential of Continuous Manufacturing for Liposomal Drug Products. Biotechnology Journal 14, 1700740.

Yanar, F., Mosayyebi, A., Nastruzzi, C., Carugo, D., Zhang, X., 2020. Continuous-Flow Production of Liposomes with a Millireactor under Varying Fluidic Conditions. Pharmaceutics 12, 1001.

Yang, K., Delaney, J.T., Schubert, U.S., Fahr, A., 2012. Fast high-throughput screening of temoporfin-loaded liposomal formulations prepared by ethanol injection method. Journal of Liposome Research 22, 31-41.

Yokoyama, M., 2011. Clinical applications of polymeric micelle carrier systems in chemotherapy and image diagnosis of solid tumors. Journal of Experimental & Clinical Medicine 3, 151-158.

Yokoyama, M., 2014. Polymeric micelles as drug carriers: their lights and shadows. Journal of drug targeting 22, 576-583.

Yoo, H.S., Park, T.G., 2001. Biodegradable polymeric micelles composed of doxorubicin conjugated PLGA–PEG block copolymer. Journal of Controlled Release 70, 63-70.

Yu, H., Xia, D., Zhu, Q., Zhu, C., Chen, D., Gan, Y., 2013. Supersaturated polymeric micelles for oral cyclosporine A delivery. European Journal of Pharmaceutics and Biopharmaceutics 85, 1325-1336.

Yu, K., Eisenberg, A., 1996. Multiple Morphologies in Aqueous Solutions of Aggregates of Polystyrene-block-poly(ethylene oxide) Diblock Copolymers. Macromolecules 29, 6359-6361.

Zhang, L., Liu, W., Lin, L., Chen, D., Stenzel, M.H., 2008. Degradable Disulfide Core-Cross-Linked Micelles as a Drug Delivery System Prepared from Vinyl Functionalized Nucleosides via the RAFT Process. Biomacromolecules 9, 3321-3331.

Zook, J.M., Vreeland, W.N., 2010. Effects of temperature, acyl chain length, and flow-rate ratio on liposome formation and size in a microfluidic hydrodynamic focusing device. Soft matter 6, 1352-1360.

8. Appendix

8.1. List of original publications

Sheybanifard, M*., Beztsinna, N*., Bagheri, M., Buhl, E.M., Bresseleers, J., Varela-Moreira, A., Shi, Y., van Nostrum C.F., van der Pluijm, G., Storm, G., Hennink, W.E., Lammers, T., & Metselaar J.M. Systematic evaluation of design features enables efficient selection of Π electron-stabilized polymeric micelles. ***International journal of pharmaceutics.*** 2020 Jun 30;584:119409. (*These authors contributed equally).

Sheybanifard, M, Guerzoni L.P.B., Omidinia-Anarkoli, A., De Laporte, L., Buyel, J.F., Besseling, R., Damen, M., Gerich, A., Lammers, T., & Metselaar J.M. Liposome manufacturing under continuous flow conditions: towards a fully integrated set-up with in-line control of critical quality attributes. ***Lab on a Chip***. 2023;23(1):182-94.

8.2. Acknowledgements

"This book has ended but the story goes on"
-- Saadi Shirazi, A.D. 1210-1291

Now that I think about my PhD journey, I know for sure that I would have not been here without the support of many people. So, I want to express my gratitude and thank them all.

First and foremost, I would like to express my gratitude to my PhD supervisor, **Dr. Josbert M Metselaar**. **Bart**, it is indeed difficult to describe how grateful l am to have you as my mentor. I sincerely appreciate your long-standing support prior and during my PhD journey. I am grateful for each and every comment/feedback/remark you shared with me as they helped me grow scientifically. I particularly enjoyed our scientific (and non-scientific) discussions that we had all around the globe, in Utrecht, Enschede, Aachen, and even in Vancouver. Besides a prominent scientific growth, you also helped me broaden my view of life and improve my critical thinking. Thank you for everything! I have repeatedly mentioned to everyone (and I will continue to do so) how fortunate and lucky I am to have you as my mentor, supervisor and also friend.

I would like to express my appreciation to **Prof. Twan Lammers**. **Twan**, thank you for being an inspiring example of an excellent scientist. I am sincerely grateful for all your guidance and support and for providing me the opportunity to not only be part of your group, but also to go for new adventures and explore science in other companies and research groups.

I would also take this opportunity to thank **Prof. Fabian Kiessling**, the director of the institute of Experimental Molecular Imaging (ExMI), RWTH, Aachen. Thank you very much for all your helpful suggestions and feedbacks along the way.

I am glad that I had my dear friends and colleagues at ExMI around me. Thank you all for being friendly and supportive during this challenging period. Apart from the scientific input that I received nearly every day from you, I could easily rely on you during the occasional catastrophic moments :D. Specifically, **Jasmin** (Groß), You are truly a breeze of fresh air! I was so hesitant to join my first ExMI "Lab Out" in 2019 but joining that event was one of my best decisions as it started our wonderful friendship. I am sorry for all my monologues during our lunch times :D. I want you to know how much I love you and I wish you and Felix lots of success and happiness in your professional and personal lives. My dear ChemLab friends: **Marek, Alec, Quim, Zaheer, Tarun, Sara, Shiva and Armin**. The friendly (and welcoming) environment that we had in the Chemistry Lab is apparent from many collaborations running in the lab. I enjoyed our (non)scientific discussions, from the polymeric micelles all the way to the liposomes! **Marek**, thank you for all your help during my time at ExMI, you are truly an amazing lab manager! **Quim**, I enjoyed a lot working with you and learned a lot from our discussions and meetings. I wish you all the best. **Sara**, I want to specifically thank you for your comments and suggestions on my thesis, they helped me improving it a lot. I wish you success in your PhD and beyond. **Armin**, it is wonderful to get to know you and become your friend. I enjoyed our fruitful discussions (in Persian!) and all the gifts from Iran :D. In addition, I want to thank you for all your helps during these years and wish you success in your future endeavors. To all my friends and colleagues in the office

area, **Anshu, Asmaa, Elena, Alessandro**, **Ilaria**, thank you for being there for me and I wish you success and happiness.

I would also like to take the opportunity to express my appreciation to my past supervisors, **Dr. Wigard Kloosterman, Dr. Alessio Marcozzi, Dr. Nataliia Beztsinna, Prof. Wim Hennik, Prof. Gert storm,** and **Prof. Jai Prakash**. **Nataliia,** from the moment in the interview that you asked me about "how to calculate the encapsulation efficiency" the learning curve never came to a steady state. I continue to learn from you how to be a good scientist and even more importantly, a better human being. I wish you and your family all the happiness and success.

I spend a wonderful part of my PhD doing research visits in the Netherlands and in Canada. For that I am grateful to all the supervisors, friends, and colleagues both in Oss, specifically **Dr. Rut Besseling, Ad Gerich, Michiel Damen, Frando van der Pas, Dr. Carl Schuurmans** and in Vancouver, specifically **Prof. Pieter Cullis, Dr. Genc Basha, Dr. Dominik Witzigmann**, **Tania, Karen, Madelaine, Jerry, Yao, Rein, Miffy, Fariba, Arash and Harrison.** I cannot thank you enough, I really felt home there. This level of hospitality and openness is not common and could not be realized without you!

To all my Iranian friends **Mahnaz, Arash, Mahsa, Azin,** and **Shafigh.** You all showed me that it is possible to have a life while doing a PhD. **Mahnaz,** you are a true friend, and you are always there in my sad and happy moments. I am grateful to have you in my life. **Mahsa**, thank you for sharing your experience and expertise in polymeric micelles with me. Being at UIPS was much more pleasant with your presence. **Azin,** thank you for being a caring friend during my time in Vancouver. I wish you all the happiness in the world.

Last but not least, fulfilling my PhD mission was not possible without the love, support and sacrifices of my beloved family. Therefore, I feel obliged to heartedly express my gratefulness toward them. Firstly, **Dad,** you are my hero, inspiration, and pride. The one who encouraged me to follow this path, and without your sacrifices, I would have never been able to be where I am today. I love you with all my heart. **Mom,** although I am far away from you, I always felt your unconditional love in my heart. You taught me to be strong, independent, and kind and I am eternally in your debt. My lovely sister, **Farnaz** and brother, **Reza,** we are three souls in three bodies :D. I love you guys so much and I am the luckiest to have you both. And finally, to my dear **Amin!** The role you played in my life cannot be expressed in words. Before we met, I thought I was living a great life. But I know it now, it was just an illusion of happiness. I am the luckiest woman in this planet who has the most amazing partner by herself. Your selfless, loving spirit is something that I have never seen before. Thank you for tolerating all my bitterness in these years, thank you for helping me on each and every step of my life (including my PhD), for all the inconvenient journeys that you took for me (literally and figuratively), and for your absolute love and support. "I love you for all the times I have not lived…, I love you for loving" (Paul Éluard).

تو را به خاطر دوست داشتن دوست می دارم، تو را به جای همهٔ روزگارانی که نمی زیسته ام دوست می دارم.

8.3. Eklärung zür Datenaufbewahrung

Affidavit according to § 5 (1) for Data Retention

Hiermit erkläre ich, dass die dieser Dissertation zu Grunde liegenden Originaldaten (I hereby declare that the original data forming the basis of this doctoral thesis are stored) am Institut für Experimentelle Molekulare Bildgebung des Universitätsklinikums RWTH Aachen hinterlegt sind.

8.4. Erklärung über den Eigenanteil

Affidavit according to § 5(1) § 11 (3) 12 of the doctoral studies regulations

I, Maryam Sheybanifard, hereby declare on oath that I independently collected and prepared the following results portrayed in the dissertation "Controlling Critical Quality Attributes of Therapeutic Nanoparticles Upon Scale-up Manufacturing". I had the following assistance with completing the dissertation. These are listed in the acknowledgments:

Names ↓	Study supervision	Study design/conception	Lab-scale polymer synthesis	Large-scale polymer synthesis	Polymer purification	Micelles formation and characterization	Micelles uptake and penetration	TEM Imaging	Production of the Millifluidic device	Liposome formation and characterization	In-line quantification of the liposomes	Interpretation of data evaluation	Data evaluation	Statistical evaluation
M.Sheybanifard		30			80	65		40	15	100	70	35	30	30
J.Pena			15		15	15						5		
A.Azadkhah-Shalmani			25		5								10	
N.Beztsinna	4	5				20	100							15
M.Bagheri			20	34										
M.Buhl								60						
J. Bresseleers			20	33										
A.Varela-Moreira			20	33										
Y.Shi		5										2		
C.F.van Nostrum	2													
G.van der Pluijm		5												
G.Storm	2	5												
W.E.Hennink	2	5												
L.P.B. Guerzoni									40					
A.Omidinia-Anarkoli									40			3	3	
L.De Laporte									5					
J.F.Buyel												5	7	20
R.Besseling												10	10	
M. Damen											20			
A. Gerich											10			
T.Lammers	25	20										15	15	15
J.Metselaar	65	25										25	25	20
Sum (%)	100	100	100	100	100	100	100	100	100	100	100	100	100	100

_____

Signature of the doctoral candidate,
(Maryam Sheybanifard)

As the supervisor of the above dissertation, I confirm the statements of Maryam Sheybanifard.

_____

Signature of the doctoral supervisor
(Josbert M Metselaar)

8.5. Curriculum vitae

Maryam Sheybanifard

PERSONAL INFORMATION

Birthplace: Kazeroon, Iran,
Birth date: December 1, 1989
Address: De Heugden 307, 6411 DW, Heerlen, the Netherlands.
Phone: +31 (0) 6 144 88322
Email: msheybanifar@ukaachen.de, sheybani.s@gmail.com

RESEARCH INTERESTS

- Drug delivery systems
  - Lipid nanoparticles for gene delivery
  - Liposomal dispersion for drug delivery
  - Polymeric Nano carriers for drug delivery
  - Continuous flow manufacturing of nanoparticles
- Gene Editing and molecular biology
  - SiRNA and mRNA encapsulation in nanoparticles
  - CRISPR/Cas9 for gene editing

EDUCATION

Doctor of theoretical medicine (Dr.rer.medic)
Department of Nanomedicine and Theranostics, Institute for Experimental Molecular Imaging, Faculty of Medicine, RWTH Aachen University, Aachen, Germany (March 2019 - present)
Thesis title: "*Controlling Critical Quality Attributes of Therapeutic Nanoparticles Upon Scale-up Manufacturing"*
Supervisors: Dr. Josbert M Metselaar (jmetselaar@ukaachen.de), Prof. Dr. Twan Lammers (tlammers@ukaachen.de)

Professional doctorate in pharmacy (PharmD)
Faculty of Pharmacy, Tabriz University of Medical Sciences, Tabriz, Iran (2008-2014).
Thesis Title: "*Evaluating of the breast cancer risk factors in patients who refer to Namazi hospital of Shiraz"*.
Advisor: Dr. Mohammad Sattari (GhandforoushM@tbzmed.ac.ir).
GPA: 8/10

OCCUPATION

Doctor of theoretical medicine (Dr.rer.medic)
Department of Nanomedicine and Theranostics, Institute for Experimental Molecular Imaging, Faculty of Medicine, RWTH Aachen University, Aachen, Germany, supported by the German Research Foundation (Deutsche Forschungsgemeinschaft; DFG) in the framework of the Research Training Group 2375 "Tumor-targeted Drug Delivery" (March 2019 - present).
Visiting researcher
Life Sciences Institute, Department of Biochemistry & Molecular Biology, University of British Columbia (UBC), Vancouver, Canada (February 2022 – July 2022)
Visiting researcher
InProcess-LSP company, Oss, the Netherlands (May 2021 – June 2021)
Junior researcher
Targeted Therapeutics group, Department of Biomaterial Science and Technology (BST), Faculty of Science and Technology (TNW), Twente University, the Netherlands (April 2018 - September2018)
Guest researcher

Utrecht Institute for Pharmaceutical Sciences (UIPS), Department of Pharmaceutics, Utrecht University, the Netherlands (Aug 2017 – March 2018)
Guest researcher
Department of Medical Genetics, University Medical Center, Utrecht, the Netherlands (Oct 2016 - Jun 2017)
Clinical pharmacist
Amir Oncology Hospital, Shiraz, Iran (Jun 2014 - Jan 2016).

RESEARCH PROJECTS

- Induction/ inhibition of apoptosis in hepatocytes in HCC model (2022-present)
- Continuous-flow manufacturing of actively targeted drug delivery systems (2019-present)
- Design and evaluation of novel peptide formulations (2018)
- Encapsulation of hydrophobic drugs in polymeric pi-pi stacking micelles (2017-2018)
- Inducing structural variations in human cells using CRISPR/Cas9 system (2016-2017)

PROFESSIONAL SKILLS

- Laboratory expertise in Pharmaceutics:
  - LNP formulation preparation
  - Polymeric micelle preparation
  - Liposome preparation
  - Millfluidics and continuous manufacturing
  - Storage-stability evaluation
  - HPLC
  - Dynamic light scattering (DLS, size analyzer)
  - Zetasizer
  - Fluorescence spectroscopy

- Laboratory expertise in Genetics:
  - Cell culture
  - PCR, RNA extraction and DNA synthesis
  - Flow cytometry
  - Gene editing (CRISPR/Cas9)
  - Nucleic acid quantitation
  - Gel electrophoresis
  - Molecular cloning
  - Experience with confocal microscopy

PUBLICATIONS

- **Sheybanifard, M.**,…Lammers, T., & Metselaar, J. M. " Liposome manufacturing under continuous flow conditions: towards a fully integrated set-up with in-line control of critical quality attributes". Lab on a Chip. 2023;23(1):182-94.
- **Sheybanifard, M.**, Beztsinna, N., ... Storm, G., Hennink, W. E., Lammers, T., & Metselaar, J. M. "Systematic evaluation of design features enables efficient selection of Π electron-stabilized polymeric micelles". International Journal of Pharmaceutics (2020): 119409.

LANGUAGE SKILLS

- **English**: Fluent (C1), IELTS 7.5 (overall)
- **Persian**: Native
- **Dutch**: Elementary